UNIVERSITÉ DE **RENNES 1**

UNIVERSITE BRETAGNE LOIRE

THÈSE / UNIVERSITÉ DE RENNES 1
sous le sceau de l'Université Bretagne Loire

pour le grade de

DOCTEUR DE L'UNIVERSITÉ DE RENNES 1

Mention : Sciences de la Terre

Ecole doctorale Sciences de la Matière

Daniel JARA HEREDIA

Préparée à l'unité de recherche Géosciences Rennes
(UMR CNRS 6118)
OSUR Observatoire des Sciences de l'Univers de Rennes

Improvement of the numerical capacities of simulation tools for reactive transport modeling in porous media.

Thèse soutenue à Rennes le 12 Juin 2017 :

devant le jury composé de :

Michel KERN
Chercheur, Inria Rocquencourt / *rapporteur*
Benoit NOETINGER
Directeur Expert, IFPEN/ *rapporteur*
Jocelyne ERHEL
Directrice de recherche, Inria Rennes / *examinateur*
Benoit COCHEPIN
Ingénieur, Andra / *examinateur*
Jean-Raynald DE DREUZY
Directeur de recherche, Université Rennes 1/ *directeur de thèse*

ABSTRACT

Reactive transport modeling in porous media involves the simulation of several physico-chemical processes: flow of fluid phases, transport of species, heat transport, chemical reactions between species in the same phase or in different phases. The resolution of the system of equations that describes the problem can be obtained by a fully coupled approach or by a decoupled approach. Decoupled approaches can simplify the system of equations by breaking down the problem into smaller parts that are easier to handle. Each of the smaller parts can be solved with suitable integration techniques. The decoupling techniques might be non-iterative (operator splitting methods) or iterative (fixed-point iteration), having each its advantages and disadvantages. Non-iterative approaches have an error associated with the separation of the coupled effects, and iterative approaches might have problems to converge.

In this thesis, we develop an open-source code written in MATLAB (https://github.com/TReacLab/TReacLab) in order to model the problematic of concrete atmospheric carbonation for an intermediate-level long-lived nuclear waste package in a deep geological repository. The code uses a decoupled approach. Classical operator splitting approaches, such as sequential, alternating or Strang splitting, and less classical splitting approaches, such as additive or symmetrically weighted splitting, have been implemented. Besides, two iterative approaches based on an specific formulation (SIA CC, and SIA TC) have also been implemented. The code has been interfaced in a generic way with different transport solvers (COMSOL, pdepe MATLAB, FVTool, FD scripts) and geochemical solvers (iPhreeqc, PhreeqcRM). In order to validate the implementation of the different approaches, a series of classical benchmarks in the field of reactive transport have been solved successfully and compared with analytical and external numerical solutions. Since the associated error due to the combination of operator splitting and numerical techniques may be complex to assess, we explore the existing mathematical tools used to evaluate it. Finally, we frame the atmospheric carbonation problem and run preliminary simulations, stating the relevant problems and future steps to follow.

RESUME

La modélisation du transport réactif dans les milieux poreux implique la simulation de plusieurs processus physico-chimiques : écoulement de phases fluides, transport de chaleur, réactions chimiques entre espèces en phases identiques ou différentes. La résolution du système d'équations qui décrit le problème peut être obtenue par une approche soit totalement couplée soit découplée. Les approches découplées simplifient le système d'équations en décomposant le problème sous-parties plus faciles à gérer. Chacune de ces sous-parties peut être résolue avec des techniques d'intégration appropriées. Les techniques de découplage peuvent être non-itératives (operator splitting methods) ou itératives (fixed-point iteration), chacunes ayant des avantages et des inconvénients. Les approches non-iteratives génèrent une erreur associée à la séparation des sous-parties couplées, et les approaches itératives peuvent présenter des problèmes de convergence.

Dans cette thèse, nous développons un code sous licence libre en langage MATLAB (https://github.com/TReacLab/TReacLab) dédie à la modélisation du la problématique de la carbonatation atmosphérique du béton, dans le cadre du stockage de déchets de moyenne activité et longue vie en couche géologique profonde. Le code propose un ensemble d'approche découplée : classique, comme les approches de fractionnement séquentiel, alternatif ou Strang, et moins classique, comme les approches de fractionnement additif ou par répartition symétrique. En outre, deux approches itératives basées sur une formulation spécifique (SIA CC et SIA TC) ont également été implémentées. Le code été interfacé de manière générique avec différents solveurs de transport (COMSOL, pdepe MATLAB, FVTool, FD scripts) et géochimiques (iPhreeqc, PhreeqcRM). Afin de valider l'implémentations des différentes approches, plusieurs bancs d'essais classiques dans le domaine du transport réactif ont été utilises avec succès. L'erreur associée à la combinaison du fractionnement de l'opérateur et des techniques numériques étant complexe à évaluer, nous explorons les outils mathématiques existants permettant de l'estimer. Enfin, nous structurons le problème de la carbonatation atmosphérique et présentons des simulations préliminaires, en détaillant les problèmes pertinents et les étapes futures à suivre.

List of Contents

List of Figures

List of Tables

CHAPTER 1: INTRODUCTION

I INTRODUCTION

Hydro-chemical numerical simulations are important to assess the safety of disposal systems for radioactive waste and spent nuclear fuel in deep geological repositories. They study the different coupled effects between fluid transport (single- and multi-phase) and the chemical reactions (homogeneous and heterogeneous), and to predict the future hydro-chemical states over time for the system under study. This field of science is known as reactive transport modeling and has been applied successfully in different areas such as water treatment (Langergraber and Šimůnek, 2012), mining industry (Amos *et al.*, 2004), or geothermal energy (Bozau and van Berk, 2013). Nuclear waste agencies are interested in the potential of reactive transport modeling to capture the non linear behavior of aqueous components as a consequence of chemical reactions such as complex aqueous speciation and kinetically controlled dissolution or precipitation processes.

The thesis is organized into two main sections. The first one is devoted to the development of a tool that can help to model and gain a deeper insight in the different problems related to nuclear waste from the point of view of reactive transport modeling in porous media. The second part frames the problematic of the atmospheric carbonation in the nuclear waste storage context by using the developed tool.

I.1 Context of the thesis

In France, "L'Agence Nationale pour la gestion des Déchets RadioActifs" (ANDRA[1]) is responsible for managing the nuclear waste. The radiological risk of the nuclear waste is assessed by two parameters: a) the activity level and b) the half-life, originating several categories of nuclear waste. The activity level is divided into very low, low, intermediate and high, while the half-life category is divided into very short-lived (less than 100 days), short-lived (less than 31 years) and long-lived radionuclides (more than 31 years). Two of these categories are of special interest: the high-level waste (HLW) and the intermediate-level long-lived waste (ILW-LL). The first one represents around 0.2% of the volume and 96% of the radioactivity of the nuclear waste and the second around 3% and 4% respectively (Dupuis and Gonnot, 2013).

---

[1] www.andra.fr

The storage of HLW and ILW-LL are planned to be stored in the CIGEO[2] (Centre industriel de stockage géologique) project during their lifespan which is around thousands of years (Figure I.1). CIGEO is a deep geological repository which will be located between Meuse and Haute-Marne in the eastern part of the Paris Basin, with a depth of roughly 500 meters, and it will cover around 15 km^2. The volume of waste estimated to be stored in the geological disposal facility is of 10000 m^3 for HLW and 70000 m^3 for ILW-LL.
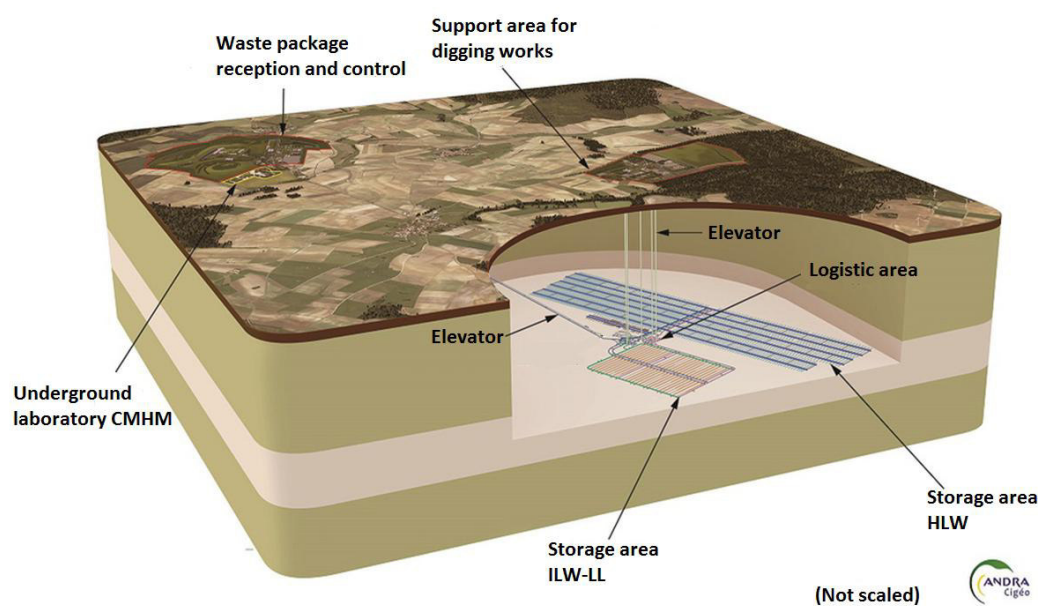
Figure I.1: Schematic diagram of the main facilities of the CIGEO project[2] which geological formation is composed mainly of argillaceous rocks, specifically Callovo-Oxfordian clay.

I.1.1 Repository Safety

A set of basic safety rules have been defined by the "Autorité de Sûreté Nucléaire" (ASN) (ANDRA, 2005a; ASN, 2008) setting the main objectives for the repository such as the absence of seismic risks in the long term, confinement properties for radioactive substances, and rock suitable to underground excavations. The target is to preserve the environment and human beings from risks associated with nuclear waste. Consequently, the following functions must be fulfilled:

---

[2] www.cigéo.com

- Preventing water circulation because it can degrade waste packages and migration of radionuclides into the environment;
- Limiting the release of radioactive substances by the package and immobilizing them in the repository as long as possible;
- Delaying and reducing the migration of radioactive substances beyond the repository or geological layer.

In order to complete such functions a passive engineered barrier system is designed comprising a variety of sub-systems: canister, buffer, backfill, and so on. The main purpose of such systems is to delay as much as possible the release of radionuclides from the waste to the host rock. Consequently, ANDRA and homologues institution of other countries (e.g. SKB) facing similar problems have developed R&D programs to study the behavior of rocks and radionuclides in order to assess the design of future repositories. Among these studies is possible to find problems related to the migration of radionuclides such as uranium through the host rock using experiments or numerical simulations (Dittrich and Reimus, 2015; Pfingsten, 2014; Xiong *et al.*, 2015). Studies focused on HLW which will be confined in a vitrified glass either in contact with a bentonite buffer or with the host rock. Consequently, the evolution of the dissolution of the vitrified glass has been estimated through numerical and experimental simulations (Debure *et al.*, 2013), and also the interaction between the glass and bentonite, and between the glass and the host rock through numerical simulations (Ngo *et al.*, 2014). Numerical experiences have also contributed to give insights on the geochemical evolution of the HLW, engineered barriers and host rock through the several thousand of years (Trotignon *et al.*, 2007; Yang *et al.*, 2008), in some cases taking into account possible climate change scenarios (Nasir *et al.*, 2014; Spycher *et al.*, 2003), or comparing with analogous natural sites (Chen *et al.*, 2015; Martin *et al.*, 2016). Since many of these studies have been carried out using or relying on numerical simulations and no analytical solutions exist, code intercomparison work has also been performed in order to compare codes results (Marty *et al.*, 2015; Xie *et al.*, 2015).

Here we aim on solving numerical simulations about the effects of atmospheric carbonation process over concrete in a nuclear waste context.

I.1.2 Description of the problem: Atmospheric carbonation

ILW-LL is proposed to be conditioned in cylinders of bitumen or concrete according to the type of waste which includes metals (fuel claddings), effluent treatment sludges and nuclear plant operating equipment. The primary ILW-LL package will be placed in a high-performance reinforced concrete container (Figure I.2), containing from 1 to 4 primary packages (ANDRA, 2005a; ANDRA, 2005b).
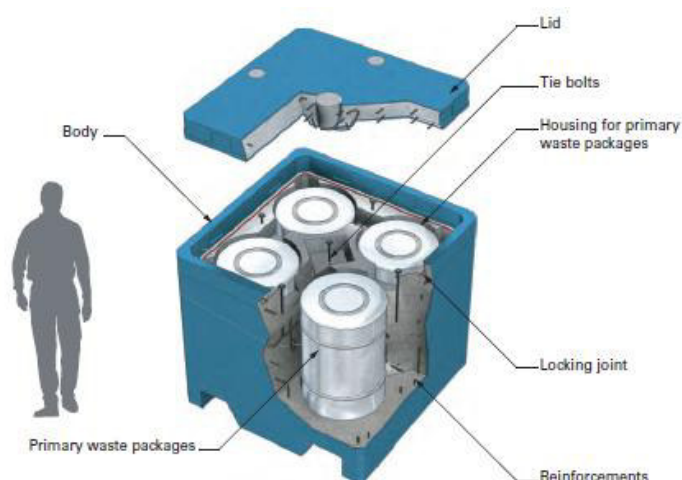
Figure I.2: Disposal container for intermediate-level long-lived waste (ILW-LL) containing four primary waste packages (ANDRA, 2005b).

The disposal containers of ILW-LL are planned to be placed in vaults which will be ventilated during the operation period (up to 150 years). Ventilation is required to guarantee operating safety, evacuate radioactive gas such as hydrogen produced by radiolysis, and residual heat from the waste. One of the consequences of the vault ventilation is that it will desaturate the disposal container, leading to a physico-chemical process known as concrete atmospheric carbonation (Thouvenot *et al.*, 2013).

The atmospheric carbonation process is summarized as follows:

1. The carbon dioxide (CO_2) diffuses into the concrete and dissolves into the pore solution:

$$CO_{2(g)} \rightleftarrows CO_{2(aq)}. \qquad (I.1)$$

2. The water molecules react with CO_2 to form carbonic acid (H_2CO_3):

$$CO_{2(aq)} + H_2O \rightleftarrows H_2CO_3. \tag{I.2}$$

3. H_2CO_3 dissociates as bicarbonate (HCO_3^-), also called hydrogen carbonate, and carbonate (CO_3^{2-}) ions according to the pH of the solution (Figure I.3). The dissociation releases H^+ ions, leading to a pH drop:

$$H_2CO_3 \rightleftarrows H^+ + HCO_3^-, \tag{I.3}$$

$$HCO_3^- \rightleftarrows H^+ + CO_3^{2-}. \tag{I.4}$$

4. The principal hydration products (Table I-1) of the concrete, particularly portlandite ($Ca(OH)_2$), dissolve in order to buffer the decrease of the pH level and maintain the equilibrium of the solution. Furthermore, the dissolution of portlandite releases Ca^{2+} ions which reacts with CO_3^{2-} in the pore solution, precipitating as calcite ($CaCO_3$).

$$Ca(OH)_2 \rightleftarrows Ca^{2+} + 2\,OH^- \tag{I.5}$$

$$Ca^{2+} + CO_3^{2-} \rightleftarrows CaCO_{3(s)} \tag{I.6}$$
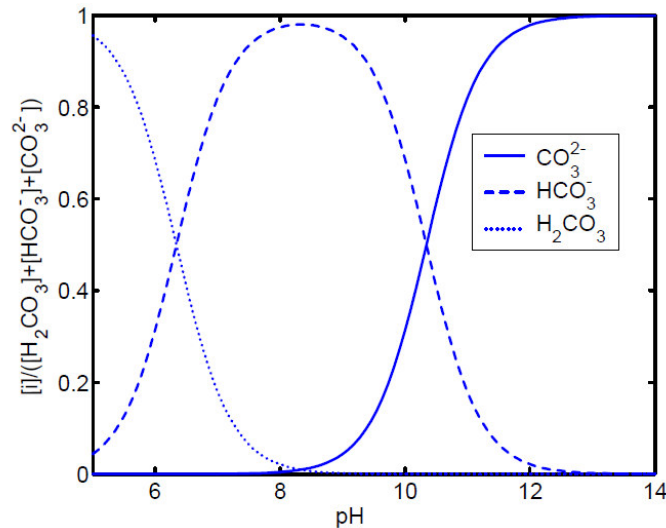
Figure I.3: Molar fraction of the chemical species H_2CO_3, HCO_3^-, and CO_3^{2-} respect pH at 20°C and equilibrium (Thiery, 2006).

6

Families of hydration products	Calcium silicate hydrate (e.g. CSH), Calcium hydroxide (e.g. portlandite), Afm (e.g. Monocarboaluminate), and AFt (e.g. Ettringite)

Table I-1: Families of concrete hydration products.

At first glance, the carbonation process might not seem harmful for the concrete. Generally, even a decrease in porosity can be expected because the carbonation products usually have higher molar volume than their reactants (Glasser *et al.*, 2008). Nevertheless, the decrease in alkalinity turns out to be an issue for the reinforcing steel bars of the concrete, and thus for the concrete structure. Normally, the pore solution in concrete has an alkaline environment with a pH between 12.5 and 13.5 in order to maintain the corrosion of the reinforcing steel bars in a range of very low rates. At such high pH a thin passive oxide layer forms on the steel and slows down the corrosion. If the passive layer is destroyed, for example due to the decrease of pH owing to atmospheric carbonation, corrosion occurs and might result in a failure of the structure (Zhang, 2016). Therefore, assessing the depth of the carbonation front is a main mean for evaluating the safety of the concrete package for ILW-LL (Figure I.4).
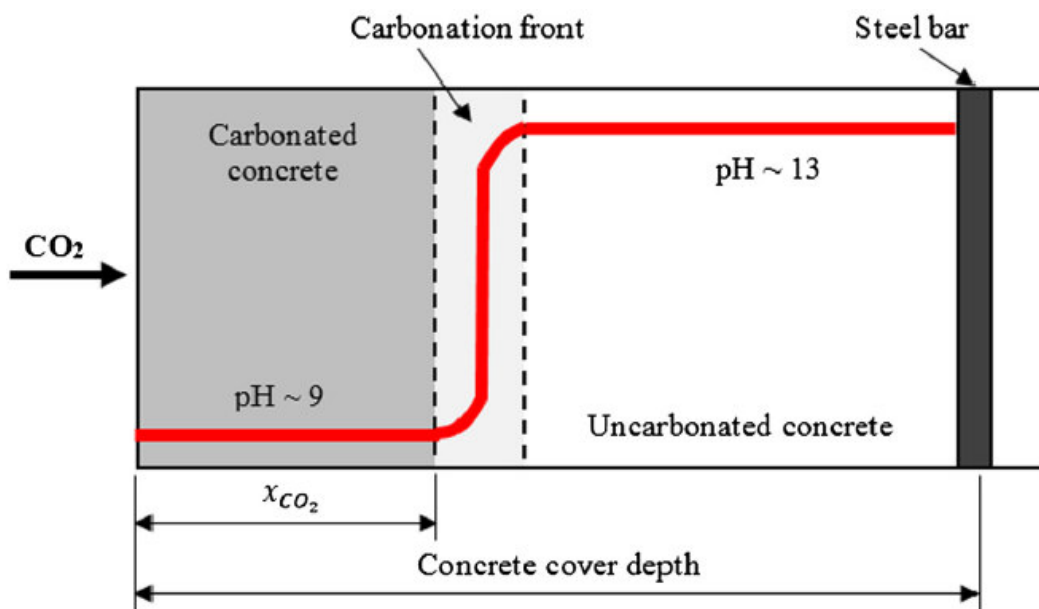
Figure I.4: Carbonation front in a simplified 1D model sketch. Three zones from left to right can be observed: a fully carbonated concrete with a pH around 9, a transition area where the carbonation process is occurring and an uncarbonated area with a pH around 13 (Ta et al., 2016).

Experimental studies of the carbonation process give an insight of the phenomenon in the concrete package (Duprat *et al.*, 2014; Ekolu, 2016; Shi *et al.*, 2016; Thiery *et al.*, 2007), but due to the long time scale of the waste confinement, detailed numerical studies of the physico-chemical processes are necessary in order to assess the safety of the disposal containers.

I.2   State-of-the-art: Reactive transport modeling

I.2.1 Mathematical model

Before any simulation, a conceptualization of the reality must be carried out. Mathematical models are tools that can help to conceptualize such reality. According to the hypothesis and assumptions that are taken, different models with their own intrinsic difficulties and simplicities arise. Comparisons between the results of the mathematical model and reality will determine the validity of the model (Hassan, 2004). Two main processes have to be modeled in terms of reactive transport: species transport and chemical reactions. The selection of laws, therefore the system of equations, are subject to the working scale.

I.2.1.1 Spatial scale

Here we work at a mesoscopic scale, where transport and reactions are described by macroscale equations based on a continuum formulation. The properties of the porous media such as porosity and density, are averaged over a control volume known as Representative Elementary Volume (REV) (Figure I.5) (Bear, 1972). REV works under the following assumptions (Steefel *et al.*, 2005):

- REV is large enough to have a meaningful average but small enough to assume that the volume of the REV is infinitesimal.
- All existing phases coexist at a single point in space and are well-mixed.
- Heterogeneous reactions are distributed homogeneously throughout the REV.
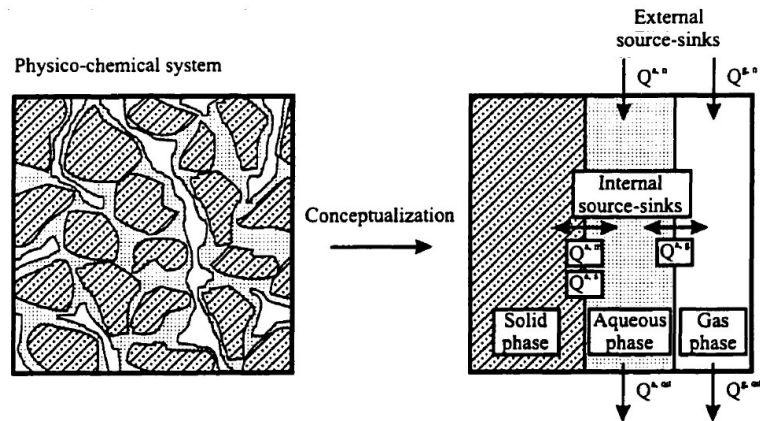
Figure I.5: Conceptualization of the REV with three phases: solid, liquid, gas. Liquid and gas are mobile. Heterogeneous reactions are given between liquid and solid, and between liquid and gas (Mayer, 1999).

These assumptions cannot be freely implemented at other scales, since they might not represent the reality properly. For instance, at a microscopic scale the non-uniform distribution of the heterogeneous reactions must be captured to explain micro-scales gradients of concentration. The assumptions of average concentration has been criticized since they do not properly capture the process in the pore scale (Dentz *et al.*, 2011; Gramling *et al.*, 2002), but the bridges between scales must still be constructed (Frippiat and Holeyman, 2008). Therefore, these assumptions are useful to explain the processes occurring in the porous media.

I.2.1.2 Transport and reaction operators

The introduction of a fluid out of equilibrium into an equilibrium system by a transport force is fundamentally the reason for reactions. Transport can be viewed as the sum of different fluxes passing through a unit area per unit time. The governing equations describing the transport phenomena are partial differential equations (PDE) such as:

$$\frac{\partial c_i}{\partial t} = L_i(c_i) + F_i(c_1, c_2, \dots, c_m), \qquad\qquad i = 1, 2, \dots, m \qquad (I.7)$$

where c_i is the concentration corresponding to the species i (ML^{-3}), $L_i(\ )$ is the transport operator related to the species i (ML^{-3}T^{-1}), and $F_i(c_1, c_2, \dots, c_m)$ is the reaction operator (ML^{-3}T^{-1}).

9

Transport

The transport operator is composed by an advection and diffusion-dispersion term, and is given by:

$$L(*) = \nabla(D\nabla * -v *), \qquad (I.8)$$

where v is the velocity vector (LT^{-1}) and D the diffusion-dispersion tensor (L^{2}T^{-1}) (Bear, 1972; Scheidegger, 1954).

Advection

The advection is the translation in space of a substance by bulk motion. In the reactive transport field, advection has been usually modeled by applying Darcy's law. Darcy discovered that there was a relationship between the flow rate of a liquid flowing through a porous media and the gradient of pressures (Darcy, 1856). Later, a mathematical expressions were derived from the Navier-Stokes equation (Hubbert, 1957; Whitaker, 1986) which corroborates the relationship of Darcy. Darcy's law for single phase flow is given by:

$$v = -\frac{K_s}{\mu}(\nabla p - \rho g), \qquad (I.9)$$

where K_s is the absolute (or intrinsic) permeability tensor (L^2) which is a characteristic property of the solid matrix, μ is the dynamic viscosity (MT^{-1}L^{-1}), g is the gravity vector (LT^{-2}), p is the pressure (MT^{-2}L^{-1}), ρ is density of the α phase (ML^{-3}), and v is the volumetric fluid velocity (LT^{-1}). Darcy law might not be the first option if the fluid in the porous media is fast, since the pressure drops induced by inertial effects are not well capture by Darcy's law (Veyskarami *et al.*, 2016).

Diffusion

Diffusion is the concentration flux induced by concentration gradients. It has usually been modeled by application of Fick's law (Fick, 1855):

$$\frac{\partial C}{\partial t} = \nabla D_D \nabla c, \qquad (I.10)$$

where D_D is the molecular diffusion (L^2T^{-1}). In porous media, the molecular diffusion of equation (I.10) is replaced by an effective diffusion. It is derived from the molecular diffusion to take into account the influence of the geometry of the porous media:

$$D_e = \theta \cdot \tau \cdot D_D, \qquad\qquad (I.11)$$

where D_e is the effective diffusion coefficient (L^2T^{-1}), τ is the tortuosity of the porous media (-), and θ is the liquid volume fraction (-). Application of Fick's law might be controversial in some situations, such as in the case where the solution is not diluted and is charged (Steefel and Maher, 2009). Diffusion is species dependent, but in some cases it can be considered equal to all the species in the same phases. For example, in advection-dominated case.

Dispersion

Hydrodynamical dispersion is caused by the fact that groundwater must flow around solid particles (porous medium). Consequently, the diverging path of water will cause variations in velocity within pore channels leading to solute spreading, such mechanical mixing is called dispersion. The dispersion tensor is normally calculated from the velocity field of the fluid v, for instance in a 1D case:

$$D_D = \sigma \cdot v, \qquad\qquad (I.12)$$

where σ is the dispersivity (L), and D_D the dispersion tensor (L^2T^{-1}). The sum of the dispersion and diffusion turns out to give the dispersion-diffusion tensor.

The dispersion-diffusion tensor can be estimated from a Fickian dispersion or a non-Fickian dispersion. The first has a dispersivity which is spatial-dependent (Burnett and Frind, 1987), whereas the second might depend on time (Zoua *et al.*, 1996) or other parameters.

This section has introduced basic transport fluxes, but other forces can have a significant role. For instance, geochemical reactions have an impact on flow properties such as viscosity and density (Abriola and Pinder, 1985; Wissmeier and Barry, 2008), also they can modified the porosity of the solid matrix due to precipitation/dissolution processes, affecting the permeability parameter (Cochepin *et al.*, 2008; Dobson *et al.*, 2003; Poonoosamy *et al.*, 2015).

Chemistry

Chemical reactions transform a set of chemical substances (reactants) into another (products). They are modeled using fundamentally two mathematical descriptions: equilibrium reactions through the Local Equilibrium Assumption (LEA) (Thompson, 1959) and kinetic reactions. The first one is represented by algebraic equations (AEs) and the second one by Ordinary Differential Equations (ODEs) (Rubin, 1983). Reactions that occur in the same phase are known as homogeneous reactions, whereas reactions that involve mass transfer between different phases are known as heterogeneous reactions. Some of the most common reactions that can be found are (Merkel *et al.*, 2005):

- Aqueous complexation (Speciation).
- Redox processes.
- Dissolution/Precipitation.
- Surface complexation.
- Gas-liquid interactions.

The choice of whether to model a reaction as kinetic or equilibrium is given by its characteristic time scale. In Steefel and Maher (2009) it is stated that if the Damköhler number is significantly larger than one, the reaction which is taking place is faster than the transport time scale, hence the hypotheses of the equilibrium approach is assumed valid. For example, reactions such as aqueous complexation are extremely fast, hence they are usually modeled as equilibrium reactions. Other reactions, like rusting, are slow, therefore a kinetic approach would be more appropriate.

Equilibrium reactions

The equilibrium state is the most stable state of a chemical system for a given set of state variables such as temperature (T), pressure (P), and compositional constraints. The chemical state is defined by the total Gibbs free energy (G), and its differential changes with the progress variable ξ which is the number of moles of a reactant normalized to the stoichiometric coefficient (Nordstrom, 2004):

$$\left(\frac{\partial G}{\partial \xi}\right)_{P,T} = 0. \tag{I.13}$$

12

Any perturbation in the system will force equation (I.13) to be different than 0. Consequently, after a perturbation the new minimum in the free-energy curve must be found so as to know the new equilibrium state. There are two main approaches to solve the problem: a) The equilibrium constant approach (Brinkley 1947; Morel and Morgan, 1972) based on the ion association theory (Bjerrum, 1926) and the free-energy minimization approach (Van Zeggeren and Storey, 2011; White et al., 1958) based on the mixed electrolyte theory (Reilly et al., 1971). Both approaches employ mass-balance and mass-action laws. They are related by:

$$\Delta_r G^0 = RTlnK, \hspace{3cm} (I.14)$$

where R is the universal gas constant ($L^2T^{-2}\Theta^{-1}$), T is the absolute temperature (Θ), K is the equilibrium constant, and G is Gibbs free energy of the reaction (ML^2T^{-2}).

Although both approaches should give the same results, their implemented solution might differ. Thus, the free-energy minimization approach uses a minimization procedure which is not mathematically equivalent to find the roots of a set of nonlinear algebraic equations, which is the method used by the equilibrium constant approach (Press *et al.*, 2007). Furthermore, the free energy minimization approach relaxes the equilibrium states of the system while keeping the mass balance fixed. Mass is gradually adjusted until the equilibrium of the system is achieved. On the other hand, the equilibrium constant approach relaxes the mass balance while keeping the equilibrium constant fixed. So, during the iterations of the numerical technique the mass balance is gradually adjusted until the specified convergence is reached. If there are large mass balance violations, the problem does not converge (Steefel and MacQuarrie, 1996).

Mass action law

Chemical equilibrium reactions can be mathematical described by a mass balance equation such as:

$$\sum_{i=1}^{Ne} s_{ij} c_i \leftrightharpoons 0, \hspace{3cm} i = 1, ..., N_e \hspace{1cm} (I.15)$$

where s_{ij} is the stoichiometric coefficient of species i for the j reaction. The number of products and reactant varies according to the reaction in consideration. Note that the equation

is reversible. Each equilibrium reaction gives rise to a mass action law (Waage and Guldberg, 1986) as:

$$K_J = \prod_{j=1}^{Ne} \langle c_i \rangle^{s_{ij}}$$

(I.16)

where K_J is the equilibrium constant of the reaction j, which depends on temperature and pressure. Notice that $\langle \ \rangle$ is the ion activity and not the concentration, unless the solution is diluted. Because of the interaction among charged ions, there is a deviation from the ideal behavior of the solution, therefore the concentration must be corrected by the activity. The activity is an ion-specific correction factor:

$$\langle C \rangle = \gamma_c C,$$

(I.17)

being γ_c the activity coefficient of the species C. The activity coefficient is a function of the ionic strength, and is comprised between 0 and 1. Therefore, the activity is smaller or equal to the concentration. The activity coefficient might be calculated by the use of different equations depending on its ionic strength, e.g. Debye–Hückel, Davies, and Pitzer (Appelo and Postma, 2004).

Kinetic reactions

Kinetics reactions study the rate of chemical reactions and the factors that affect the rate. They are represented with ordinary differential equations and usually they are defined as (Parkhurst and Appelo, 1999):

$$\frac{dc_i}{dt} = \alpha_{i,k} R_k,$$

(I.18)

where R_k is the reaction rate (MT^{-1}L^{-3}), and $\alpha_{i,k}$ is the stoichiometric coefficient of species i.

I.2.2 Numerical approaches

The numerical resolution of the system of equations arising from a reactive transport problem (PDE) can be achieved by several numerical methods: finite difference method, finite element method (Sun and Sun, 2013), mixed finite element method (Mosé *et al.*, 1994), random walk method (Prickett *et al.*, 1981), or modified method of characteristics (Russell

and Wheeler, 1983). A table with some methods can be found in Besnard (2004). Here we do not focus on the numerical methods but rather on the numerical approach.

In the field of reactive transport two main approaches exist: operator splitting or global implicit approach. The operator splitting follows a "divide and conquer" strategy by decoupling the system (Holden *et al.*, 2010), and then solving each part of the governing equations separately (Engesgaard and Kipp, 1992). On the other hand, global implicit approach solves simultaneously the governing equations of transport and chemistry leading to a fully coupled system (de Dieuleveult and Erhel, 2010). Both methods have their advantages and drawbacks. Operator splitting can be easily implemented, it can use existing geochemical or nonreactive transport software (Parkhurst *et al.*, 2004), each operator can be solved with the most suitable technique. Unfortunately, the decoupling of operators leads, in general, to the splitting error (Carrayrou *et al.*, 2004). Iterative approaches might be used to reduce such error, but convergence problems might arise (Samper *et al.*, 2000). On the other hand, global implicit approaches are more difficult to implement due to larger and more complex systems and require more computational resources, however they are more robust and accurate (Saaltink *et al.*, 2000).

During several decades the only plausible scheme to solve a large set of equations was the operator splitting approach (Yeh and Tripathi, 1989). Once the computational power of computers increased, studies have shown the benefits of the global implicit approaches (Fahs *et al.*, 2008; Saaltink *et al.*, 2001). Nowadays, thanks to more refined numerical formulations (Hoffmann *et al.*, 2012; Molins *et al.*, 2004), high performance computation (Glenn *et al.*, 2007; Hoffmann *et al.*, 2010), and new numerical schemes (Hammond *et al.*, 2005), the gap between the efficiency of global implicit and operator splitting seems to be closed (Carrayrou *et al.*, 2010).

I.2.3 Codes

The number of reactive transport codes in literature is large. Tables describing some of these codes can be found in Carrayrou *et al.* (2010), Steefel *et al.* (2015), Sedighi (2011), and Lee *et al.* (2011). The codes are based on two of the previous strategies although each one has its own particularities. For instance, Crunchflow (Steefel, 2009) and MIN3P (Mayer, 2000) are two codes that use global implicit approach but the amount of physical phenomena that

they can reproduce is not the same, since Richards' equation for unsaturated soil can be solved in MIN3P but not in Crunchflow. Also, Crunchflow is not parallelized, contrary to MIN3P. Nevertheless, Crunchflow can also work using splitting operator approaches and MIN3P cannot. Other codes with similar strategies (operator splitting approach) are HP1 (Jacques and Šimůnek, 2005) and PHT3D (Appelo and Rolle, 2010), but each one has its own features. HP1 discretizates its space using finite element method, whereas PHT3D uses finite volume method as well as a modified method of characteristics.

The difference between codes do not only reside on its computational efficiency, numerical techniques or implemented phenomena. The distribution policy of each software can also differ. Software like OpenGeoSys (Kolditz *et al.*, 2012) and PFLOTRAN (Lichtner *et al.*, 2015) are open source making it available to everyone, while others such as Hytec (van der Lee *et al.*, 2003) and Toughreact (Xu *et al.*, 2011) are commercial software.

In general, all the software tend to embed the transport and chemical operators which may difficult the application of new numerical methods and schemes. In order to gain flexibility, we propose an object-oriented approach using operator splitting techniques in a generic form, allowing users to develop new decoupled schemes and to plug their different transport and chemistry solvers in an open source environment.

I.3   Objectives and issues

The motivation of this thesis arises from the problematic of modeling atmospheric carbonation on a concrete overpack for ILW-LL by applying operator splitting methods in the field of reactive transport modeling. Simulation of carbonation process can be found in the literature but they are rather simplified systems (Bary and Mügler, 2006). These simplified problems help to understand main key parameters such as the role of the aggregates in the carbonation process (Ruan and Pan, 2012), the width of the carbonation front associated to the characteristic time of the chemical reactions of carbonation and to the characteristic time of the CO_2 diffusion (Thiery *et al.*, 2007), the impact of the carbonated zones in the moisture, and the transport of gaseous CO_2 and calcium ions (Bary and Sellier, 2004). Although, complex chemical system which might help to understand the detailed chemical evolution of the solid matrix are rather scarce (Trotignon *et al.*, 2011). Rather than focus only in the physical and chemical process, we analyze operator splitting approaches in practical cases by

solving each physico-chemical phenomena with different solvers such as COMSOL and PHREEQC. To find about new possible approaches to solving the carbonation process.

However, the separation of process in order to solve the system of interest might lead to an error, since the approach usually decouples non-linear systems (Carrayrou *et al.*, 2004; Simpson and Landman, 2008). Therefore a series of questions arise, such as: What are the tools to understand the operator splitting error? What are the consequence derived from using different numerical approaches? What limitations arise from operator splitting approach and from the application of different solvers? And the limiting factors in simulating the carbonation process by operator splitting techniques? To answer this questions, we implement a generic operator splitting into a code by using object-oriented programming in order to couple different solvers of transport and chemistry.

The use of object-oriented programming allows to keep separate processes and to quickly develop and try new implementations. This separation gives the possibility of explore new operator splitting algorithms and coupled different solvers in practical cases.

CHAPTER 2: DEVELOPMENT OF TREACLAB

II. DEVELOPMENT OF TReacLab

The following section presents the submitted article which can be read in section II.1, extra benchmarks (section II.2), extra information of the used codes by TReacLab (section II.3) and operator splitting concepts related to the article (section II.4). In the article, we illustrate the different operator splitting methods implemented in the object-oriented code TReacLab: sequential splitting (Geiser, 2009), alternating additive splitting (Faragó *et al.*, 2008a; Faragó *et al.*, 2008b), Strang (Strang, 1968) and symmetrically weighted splitting (Csomós *et al.*, 2005), and also the two sequential iterative approaches: SIA TC and SIA CC (de Dieuleveult *et al.*, 2009). The schemes are consistent and performances are consistent with the references, which are mainly analytical solutions and numerical results of the PHREEQC software. Furthermore, we illustrate the easiness and flexibility of plugging new solvers into TReacLab, from commercial software like COMSOL, to open source software like iPhreeqc. Assuming that the reactive transport problem is well-posed, there is a consistent decomposition of operators and each operator is solved with sufficient accuracy. We would expect to get the better results with sequential iterative approaches providing that convergence is reached, followed by the second-order operator splitting: alternating, Strang and symmetrically weighted splitting, and finally the first-order splitting: sequential and additive splitting. If the operators of chemistry and transport commute, which is usually not the case, operator splitting might be as accurate as sequential iterative approaches. In terms of computation speed, non-iterative approaches are faster, since for each time step there is no need to iterate (Samper *et al.*, 2009).

II.1 Article

TReacLab: an object-oriented implementation of non-intrusive operator splitting methods to couple independent transport and geochemical software

TReacLab: an object-oriented implementation of non-intrusive operator splitting methods to couple independent transport and geochemical software

Daniel Jara[1], Jean-Raynald de Dreuzy[1], Benoit Cochepin[2]

[1]Géosciences Rennes, UMR CNRS 6118, Campus de Beaulieu, University of Rennes 1, Rennes, France

[2]ANDRA, 1/7 Rue Jean Monnet, 92298 Châtenay-Malabry, France

Abstract

Reactive transport modeling contributes to understand geophysical and geochemical processes in subsurface environments. Operator splitting methods have been proposed as non-intrusive coupling techniques that optimize the use of existing chemistry and transport codes. In this spirit, we propose a coupler relying on external geochemical and transport codes with appropriate operator segmentation that enables possible developments of additional splitting methods. We provide a free and accessible object-oriented implementation in TReacLab developed in the MATLAB environment. TReacLab contains classical coupling methods, template interfaces and calling functions for two classical transport and reactive software (PHREEQC and COMSOL). We illustrate and test the approach on three classical benchmarks with equilibrium and kinetically-controlled, and homogeneous and heterogeneous reactions. We show that full decoupling to the implementation level has a cost in terms of accuracy compared to more integrated and optimized codes. Use of fully decoupled implementations like TReacLab are still justified for coupling independent transport and chemical software at a minimal development effort but should be systematically and carefully assessed.

Keywords: Porous media; Reactive transport; Operator splitting; Object-oriented programming.

Corresponding author: daniel.jara-heredia@univ-rennes1.fr

1. Introduction

The fate of chemical species in geological media results from the interaction of physical transport and chemical reactivity (Steefel *et al.*, 2005). Understanding how they interact

requires field and laboratory studies as well as numerical models. Numerical models are especially important for building predictive scenarios where experiments are limited spatially and temporally, as in long-term nuclear waste disposal assessment (Marty *et al.*, 2014; Thouvenot *et al.*, 2013; Trotignon *et al.*, 2007). On the physical transport side, extensive work in applied mathematics and computational science has provided widely-used software for single and multi-phase flows as well as transport of chemical species such as MODFLOW (McDonald and Harbaugh, 1988), MT3DMS (Zheng and Wang, 1999), HYDRUS (Kool and Van Genuchten, 1991), COMSOL (COMSOL, 2010), FEFLOW (Diersch, 1996), MRST (Lie, 2014), and TOUGH2 (Pruess *et al.*, 1999). On the chemistry side, geochemical software have implemented a wide range of chemical functions and reactions, including equilibrium aqueous speciation, equilibrium mineral dissolution/precipitation, gas phase exchange, ion exchange, redox reactions, and kinetic reactions. Some of these software are PHREEQC (Parkhurst and Appelo, 1999), GEMS (Kulik *et al.*, 2013), CHEPROO (Bea *et al.*, 2009), MINTEQ (Peterson *et al.*, 1987), CHESS (Van der Lee, 2002), and Geochemist's Workbench (Bethke, 2007).

To combine physical and chemical reactivity, couplers have been developed between transport and geochemical codes such as PHAST for coupling HST3D and PHREEQC (Parkhurst *et al.*, 2004), HP1 for HYDRUS and PHREEQC (Šimůnek *et al.*, 2006), PHT3D for MT3DMS and PHREEQC (Prommer *et al.*, 1999), HYTEC for RT1D/R2D2/METIS and CHESS (van der Lee *et al.*, 2003), OpenGeoSys-GEMS (Kulik *et al.*, 2013) and iCP for COMSOL and PHREEQC (Nardi *et al.*, 2014). Most of the previous cited codes have embedded the coupling method with the geochemical and transport methods to enhance global performance and reliability. Here, in order to gain flexibility, we propose in our code TReacLab a complementary development in the form of an ensemble of Operator Splitting methods (OS) with a generic set of interfaces to transport and reaction operators. TReacLab is designed as an open toolbox where additional OS techniques can be implemented and benchmarked. Other transport and geochemical codes may also be used at the minimal cost of developing the necessary interfaces. TReacLab is written in MATLAB based on a series of abstract classes using object-oriented programming (Commend and Zimmermann, 2001; Register, 2007; Rouson *et al.*, 2011).

After recalling in section 2 the reactive transport and OS formalism used, we present in section 3 our OS implementation. We especially show how to implement alternative OS

methods and how to connect other transport and geochemical codes. Methods are assessed and discussed on the basis of 3 benchmarks in section 4.

2. Numerical model

2.1. Reactive transport equation

The reactive transport equation can be written in a general way as (Saaltink *et al.*, 1998):

$$\frac{\partial c}{\partial t} = ML(c) + S_e^t r_e + S_k^t r_k + Q, \tag{1}$$

where c is the vector of concentrations for N_s chemical species in the system. M is a diagonal matrix that specifies whether a species is mobile or immobile. Its diagonal elements are 1 or 0 accordingly. S_k^t and S_e^t are the transposed stoichiometric matrix for kinetic and equilibrium reactions, respectively. r_e and r_k ($ML^{-3}T^{-1}$) are the reaction rates of the N_e equilibrium and N_k kinetic reactions, respectively. Q is the external sink/source term ($ML^{-3}T^{-1}$). L is the transport operator ($ML^{-3}T^{-1}$), which includes advection and diffusion. In the following, we consider only single-phase flow:

$$L(c) = \nabla \cdot [\mathbf{D}\nabla c - \boldsymbol{v}c]. \tag{2}$$

$\mathbf{D}$ (L^2T^{-1}) is the effective dispersion-diffusion tensor (Bear, 1972). The velocity $\boldsymbol{v}$ (LT^{-1}) is computed in a pre-processing phase, which can be decoupled from the reactive transport problem as long as hydraulic properties are not modified by the chemical reactivity. The chemical system can be generically written with the N_e equilibrium reactions:

$$\emptyset_e(c) = 0, \tag{3}$$

and kinetically-controlled reactions:

$$r_k = \emptyset_k(c). \tag{4}$$

The reactive transport problem is thus made up of the N_s mass balance equation (1) and of the $N_e + N_k$ equilibrium and kinetic equations (3) and (4). Its unknowns are the concentrations c and the reaction rates r_e and r_k.

Components u are generally introduced when considering equilibrium reactions (Saaltink *et al.*, 2011):

$$u = Uc, \qquad (5)$$

where U is the component matrix (Fang *et al.*, 2003; Friedly and Rubin, 1992; Hoffmann *et al.*, 2012; Kräutle and Knabner, 2005; Steefel *et al.*, 2005). They are N_s - N_e linear combinations of chemical species that are not modified by equilibrium reactions (Molins *et al.*, 2004; Morel and Hering, 1993):

$$US_e^t r_e = 0. \qquad (6)$$

The component matrix is not unique. However, its application to equation (1) always leads to a system without the equilibrium rates but with the components u (Molins *et al.*, 2004; Saaltink *et al.*, 1998):

$$\frac{\partial u}{\partial t} = UML(c) + US_k^t r_k + UQ. \qquad (7)$$

The reactive transport problem is then made up of the $2N_s$ - N_e + N_k equations (3-5) and (7) for the same number of unknowns u, c and r_k.

2.2. Usual first-order sequential non-iterative and iterative approaches

We solve the reactive transport problem (3-5) and (7) first with classical sequential non-iterative approach, separating the transport operator from the chemical operator. The transport operator modifies the concentration of the component by the advective and dispersive processes of equation (2) applied to the concentration of the mobile species:

$$\frac{\partial u}{\partial t} = ML(u) + UQ. \qquad (8)$$

The chemical operator is simply derived from the set of equations (3-6) without the transport term:

$$\frac{\partial u}{\partial t} = US_k^t r_k$$
$$r_k = \emptyset_k(c)$$
$$u = Uc \qquad (9)$$
$$\emptyset_e(c) = 0.$$

This is still a system of $2N_s - N_e + N_k$ equations for the same number of unknowns. With an explicit integration of temporal derivatives (herein, we assume forward Euler), the solution at time step $n+1$ can be obtained from the solution at time step n, with the following successive application of the transport and chemical operators in a sequential approach:

$$u^* = u_n + \Delta t\big(UML(c_n)\big) + \int_{t_n}^{t_{n+1}} UQ(t)dt$$

$$\begin{cases} u^* = Uc_{n+1} \\ \emptyset_e(c_{n+1}) = 0 \end{cases} \tag{10}$$

$$r_{k_{n+1}} = \emptyset_k(c_{n+1})$$

$$u_{n+1} = u^* + \Delta t US_k^t r_{k_{n+1}}$$

In this formulation, the transport operator is directly applied to the solute concentration and modifies the components u. In the cases where there are only equilibrium reactions ($N_k = 0$), it is equivalent to the TC formulation of de Dieuleveult and Erhel (2010).

When the stability conditions of the explicit integration are too much constraining, implicit schemes should be used instead within a sequential iterative approach (Carrayrou *et al.*, 2004; de Dieuleveult and Erhel, 2010; Yeh and Tripathi, 1989):

$$u_{n+1} = u_n + \Delta t\big[ML(u_{n+1}) + S_k^t r_{k_{n+1}}\big] + \int_{t_n}^{t_{n+1}} UQ(t)dt$$

$$\begin{cases} u_{n+1} = Uc_{n+1} \\ \emptyset_e(c_{n+1}) = 0 \end{cases} \tag{11}$$

$$r_{k_{n+1}} = \emptyset_k(c_{n+1}).$$

Classical Picard's method have been extensively used to solve such kind of problems:

$$u_{n+1}^{k+1} = u_n + \Delta t\big[ML\big(u_{n+1}^{k+1}\big) + S_k^t r_{k_{n+1}}^k\big] + \int_{t_n}^{t_{n+1}} UQdt$$

$$\begin{cases} u_{n+1}^{k+1} = Uc_{n+1}^{k+1} \\ \emptyset_e\big(c_{n+1}^{k+1}\big) = 0 \end{cases} \tag{12}$$

$$r_{k_{n+1}}^{k+1} = \emptyset_k\big(c_{n+1}^{k+1}\big),$$

where k is the index of the Picard iteration method instantiated by:

$$u_{n+1}^{k=1} = u_n$$

$$r_{k\,n+1}^{k=1} = r_{k\,n}.$$

(13)

This formulation with the associated Picard method is a generalization of the CC formulation and algorithm of de Dieuleveult and Erhel (2010) with kinetic reaction terms.

We recall the necessity to check the consistency of the temporal integration scheme with the Operator Splitting method chosen. With this decomposition, explicit first-order scheme naturally leads to sequential non-iterative approach. The implicit first-order scheme requires a sequential iterative approach. Other choices are possible and might reduce errors depending on the chemical system (Barry *et al.*, 1996). As it should be possible to test and benchmark them at a reduced development cost, we use a generic decoupling formalism that can be used to implement a broad range of schemes.

2.3. Generic operator splitting implementation

The reactive transport system can be generically split in two operators. Using the formalism of Gasda *et al.* (2011), equation (1) can be written as:

$$\begin{cases} \frac{\partial c}{\partial t} = \mathcal{L}_1 c + \mathcal{L}_2 c, \\ \emptyset_e(c) = 0 \end{cases} \qquad c(t = 0) = c_0, \qquad 0 \le t \le T, \qquad (14)$$

with:

$$\mathcal{L}_1 = ML + Q, \qquad (15)$$

$$\mathcal{L}_2 = S_e^t r_e + S_k^t r_k, \quad \text{with} \quad \emptyset_e(c) = 0 \qquad (16)$$

with $\mathcal{L}_1$ as transport operator and $\mathcal{L}_2$ as chemical operator. Other decomposition are possible, e.g. the transport operator can be subdivided into an advection and a diffusion-dispersion operator (Clement *et al.*, 1998), or one operator might contain advection-reaction and the other diffusion (Liu and Ewing, 2005). Each operator will be solved separately for a splitting time step $\Delta t = t^{n+1} - t^n$ using adapted numerical methods.

The generic operator splitting methods implemented into the Toolbox are the sequential splitting, additive splitting, Strang splitting, symetrically weighted splitting, and alternating method (Appendix A). Assuming exact integration of the operators, the first two have a first-order temporal truncation error, and the three following a second-order one (Hundsdorfer

and Verwer, 2013). Since the operators are usually solved using numerical methods, the global order of such approaches might be modified because of the order of the numerical methods used for each operator (Barry *et al.*, 1996; Csomós and Faragó, 2008). The alternating splitting increases the order of the sequential splitting if the time steps are small enough (Simpson and Landman, 2008; Valocchi and Malmstead, 1992).

3. Operator splitting implementation and software organization

We provide in TReacLab an object-oriented toolbox for the non-intrusive operator splitting methods of the previous section. TReacLab is organized along three main components for coupling transport and reactivity, and proceeds in three pre-processing, processing and post-processing phases (Figure 1). These three components correspond to the three well-identified coupler, transport and chemistry classes. The three classes are fully segmented and exchange information through interfaces. Segmentation ensures that any of the three coupler, transport and chemistry classes can be replaced without modifications of any of the two other ones. The solution of the reactive transport problem eventually consists in the temporal integration of equations (15) and (16) with the chosen OS technique, which iteratively calls transport and geochemical solvers through interfaces (Figure 1, middle row). This is the core of the simulation that we identify as the processing phase. It is highly generic and does not require at run time any further specification of transport, reactivity and coupler methods. Standard error management techniques are used to stop the algorithm when any of the integration method of the three classes fails, stopping the running process and returning adapted error messages.
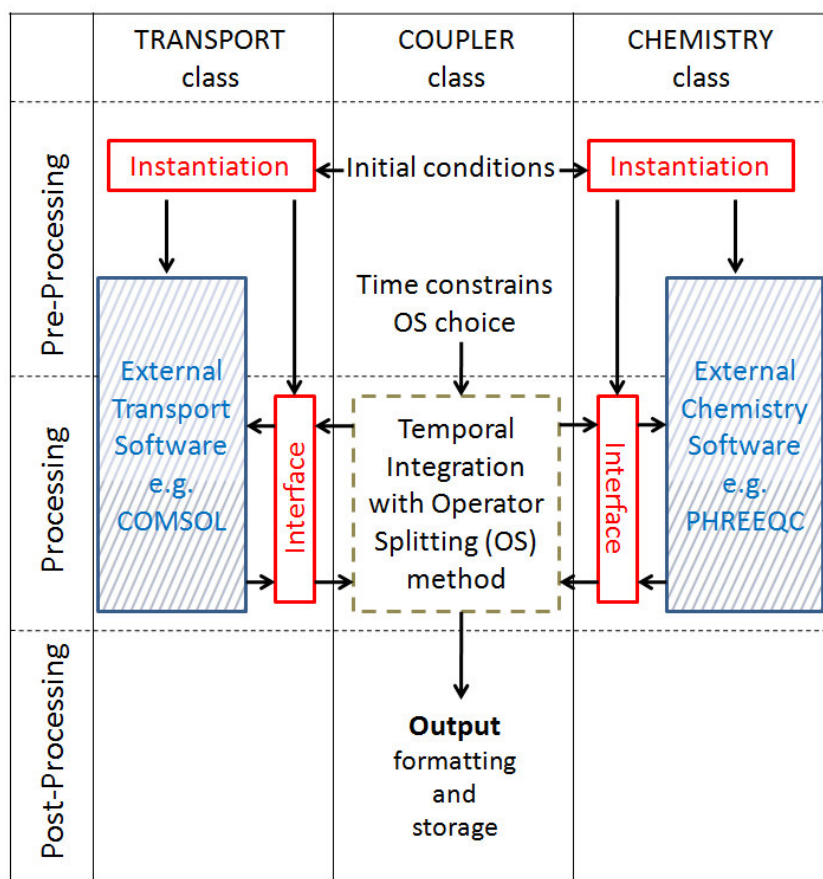
Figure 1: General software organization of TReacLab with the three coupler, transport and chemistry classes in columns, and the three pre-processing, processing, and post-processing phases in rows. Generic components represented in black are the organization and the coupler class. External software for transport and chemistry are represented in blue with hatched line (cannot be modified). Red boxes highlight the instantiation and interface methods that must be developed when connecting new transport or chemistry software.

The processing phase can be highly generic because all specifications of the coupler, transport, and chemistry classes are performed in a pre-processing phase (Figure 1, first row). The pre-processing phase consists in the instantiation of the coupler, transport and chemical classes, in the preparation of the interfaces that will transfer information and in the specifications of the initial conditions. As detailed in Appendix B, instantiations are highly code dependent. Instantiation can be done externally for example with the definition of a transport or chemical problem through the graphical user interface of software like COMSOL or PHREEQC. It can alternatively be done internally by a method within TReacLab specifying the inputs and parameters to existing interfaces like IPhreeqc (Charlton and Parkhurst, 2011), PhreeqcRM (Parkhurst and Wissmeier, 2015), or COMSOL livelink

(COMSOL, 2010). Even when instantiation is complex, it remains independent for each of the three classes. Cross-dependencies and feedback between transport and reactivity like density-driven flows with reacting species are not supported at this stage, although they may be important in some applications like CO_2 sequestration (Abarca *et al.*, 2013). Differences in diffusion coefficients between chemical species can however be introduced as long as they are well specified in the instantiation phase of the transport class.

Pre-processing phase specifies the initial conditions and transfers them to the coupler in charge of starting the numerical integration. Post-processing is generic and only consists in formatting and storing output concentrations and solver performances (Figure 1, bottom row). Specifications are all restricted to the instantiation of the software and interface in the pre-processing phase while processing and post-processing remain fully generic. Connections between specific algorithms and generic structures are done by interfaces. Appendix B provides a detailed description of the transport and chemistry classes, defining the interfaces to the external codes.

4. Examples and benchmarks

The three following examples validate the methods and illustrate the implementation presented in sections 2 and 3. The three of them are based on a 1D hydraulically homogeneous system with steady-state flow and uniform dispersion (equation (2)). They remain simple enough on the transport side to be compared systematically with well-established PHREEQC simulations. Even though the first objective of the simulations is to check the consistency of the methods developed with the results given by analytical solutions or equivalent PHREEQC simulations, we have performed a systematic convergence analysis to evaluate the relative performance of the different coupling methods.

The three examples display evolving degrees of complexity both in terms of chemical systems and in terms of software called for transport and reactivity, software versions are given in Table 1. The first example is a single-species transport with first-order decay. The transport solver is COMSOL and the chemical solver is a simple analytical solution. This example is used to assess the different coupling algorithms implemented and to check the implementation of the interface with COMSOL. The second example is an equilibrium precipitation/dissolution chemical system in a 1D hydraulically homogeneous system. Chemical solver is IPhreeqc. Several solvers have been compared for the transport solver,

both to check IPhreeqc interface implementation and to evaluate the effect of the transport solver. The third example is the most advanced in terms of chemistry and software. Chemical reactions are partly in equilibrium and partly kinetically controlled. They involve precipitation and dissolution reactions. The chemical code is PhreeqcRM. It is used in combination with COMSOL as transport solver. These three test cases have been chosen to check the implementation and assess the coupling methods developed. They are also simple enough from the development point of view to be taken as starting points to model more advanced chemical systems and transport conditions.

Software	Version
MATLAB	R2013b
COMSOL	4.3b
PHREEQC	3.3.7
IPhreeqc	3.3.7
PhreeqcRM	3.3.9

Table 1: Software versions.

4.1. Single-species transport with first-order decay

A single-species transport with first-order decay using different OS methods is compared to an analytical solution (Van Genuchten and Alves, 1982). The reactive transport system contains a single solute species of concentration c :

$$\frac{\partial c}{\partial t} = L(c) - kc, \tag{17}$$

where L is given by equation (2). Equation (17) can straightforwardly be separated into transport and chemistry operators corresponding to the two right-hand side terms.

At time 0, the solute concentration is 0 in the domain ($c(x, t=0) = 0$). The concentration at the left boundary is constant and equal to 1 mol/m^3 ($c(x = 0, t) = 1$ mol/m^3). The boundary condition on the right side of the domain is a perfectly absorbing ($c(x = x_{max}, t) = 0$).

Parameters are derived from Steefel and MacQuarrie (1996) and given in Table 2. The solver for transport is COMSOL and an analytical solution is used for the decay. Solute concentration progressively invades the domain from the left boundary with a smooth profile resulting from the combination of dispersion and decay (Figure 2). Second-order methods

perform much better than first-order methods as expected. Errors are more pronounced at the inlet boundary condition on the left side of the domain where the concentration is higher (Steefel and MacQuarrie, 1996; Valocchi and Malmstead, 1992). The sequential splitting method with the transport operator performed first overestimates the amount of reaction for the whole domain since it considers that all incoming concentration is getting in without decay for the full first time step. If the sequence of operators is exchanged, namely first chemistry is solved, and then transport is solved, the amount of reaction is underestimated. The second-order alternating splitting, which alternates between transport-chemistry and chemistry-transport steps, shows strong improvement with compensations between overestimation in the first application of the chemical operator and underestimation in the second application of the chemical operator (Simpson and Landman, 2008; Valocchi and Malmstead, 1992).

Parameter	Value
v [m/y]	100
D [m^2/y]	20
k [y^{-1}]	100
$x_{\max}$ [m]	6
Δx [m]	0.4
Δt [y]	$4 \cdot 10^{-3}$

Table 2: Parameters for the single-species transport with first-order decay benchmark. v is the velocity, D is the dispersion coefficient, k is the decay rate, x_{max} is the length of the 1D column, Δx is the grid size, and Δt is the time step.
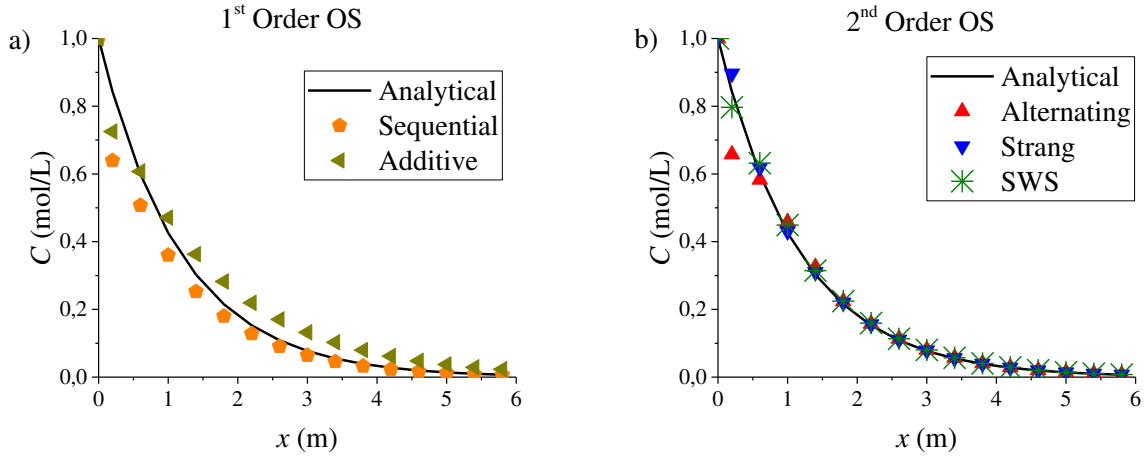
Figure 2: Comparison of first- and second-order OS for the single-species transport with first-order decay at t = 0.5 y. Parameters are given in Table 2. Analytical solution is derived from Van Genuchten and Alves (1982).

The error at time $t = 0.5$ y is taken as the quadratic difference over the domain of the analytical and numerical solutions c_A and c_N:

$$\|e\|_2 = \sqrt{\sum_{i=1}^{N_x}\left(c_A^i(t) - c_N^i(t)\right)^2}. \tag{18}$$

$\|e\|_2$ gives additional information on the performances of the different OS methods (Table 3). Overall, second order methods are significantly more accurate than first order methods for $\Delta t = 4\ 10^{-3}$y (first line of Table 3). For the smaller time step $\Delta t = 4\ 10^{-4}$y (last line of Table 3), first- and second-order methods display similar accuracies. In this case, the dominant error comes from the integration scheme of the temporal operator for transport rather than from the operator splitting as it has also been reported in similar tests (Csomós and Faragó, 2008; Gasda *et al.*, 2011). When reducing the time step Δt, first-order splitting methods might become as relevant as second-order methods.

Δt (y)	1st order		2nd order		
	Additive	Sequential	Alternating OS	Strang	SWS
4·10^{-3}	0.206	0.242	0.190	0.058	0.063
2·10^{-3}	0.105	0.108	0.067	0.032	0.024
4·10^{-4}	0.027	0.003	0.019	0.021	0.021

Table 3: Error $\|e\|_2$ of equation (18) for the single-species transport with first-order decay with different OS methods and splitting time steps.

4.2. Calcite dissolution

Calcite dissolution and dolomite formation has become a classical benchmark for reactive transport problems with sharp precipitation/dissolution fronts (Beyer *et al.*, 2012; Engesgaard and Kipp, 1992; Prommer *et al.*, 1999). Progressive introduction of magnesium calcium in a domain at equilibrium between calcium carbonate in solution and calcite ($CaCO_3$) dissolves the calcite and precipitates dolomite ($CaMg(CO_3)_2$). This chemical system has been modeled with the physical and chemical parameters given by Table 4 and Table 5. Chemical concentrations are initially homogeneous. At the initial time ($t = 0$), the chemical system is destabilized with the introduction of magnesium instead of calcium at the upper boundary condition ($x = 0$), inducing the dissolution/precipitation process. The boundary condition at the downstream limit (x_{max}) is a simple outflow of the solutes.

Here, we show how transport solvers can be applied and validate our interface to IPhreeqc. IPhreeqc performs the computation of components, aqueous speciation, precipitation and dissolution reactions (Charlton and Parkhurst, 2011). The database used is 'NAPSI_290502(260802).dat'. Transport is solved either with COMSOL Multiphysics (COMSOL, 2012), with a finite difference spatial discretization and forward Euler time integration, derived from built-in pdepe function of MATLAB (Skeel and Berzins, 1990). Transport and chemistry are coupled through the simple sequential approach of equations (A.1)-(A.3). PHREEQC is independently run as 1D reactive transport solver to provide a reference solution.

Parameter	Value
v [m/s]	10^{-5}
D [m^2/s]	$6.7 \ 10^{-8}$
x_{max} [m]	0.25
Δx [m]	0.01
Δt [s]	50

Table 4: Physical parameters for the calcite dissolution benchmark. v is the average velocity, D is the dispersion coefficient, x_{max} is the maximum length of the column, Δx is the grid size, and Δt is the time step.

Chemical Component and Species	Initial value	Boundary value at x=0
Ca [mol/L]	$1.23 \ 10^{-4}$	0
C [mol/L]	$1.23 \ 10^{-4}$	0
Cl [mol/L]	0	$2 \ 10^{-3}$
Mg [mol/L]	0	10^{-3}
pH [-]	9.91	7
Calcite [mol/L]	$2 \ 10^{-4}$	-
Dolomite [mol/L]	0	-

Table 5: Calcite dissolution benchmark initial and boundary values for aqueous components and mineral species. In PHREEQC, components are called elements.

Figure 3 and Figure 4 display aqueous and mineral equivalent concentrations at time $t = 10^4$ s. As magnesium and chloride get in the domain (Figure 3b and Figure 3d), calcite progressively dissolves and is replaced by dolomite as expected (Figure 4). Some of the calcium remains in solution and is flushed out (Figure 3a and Figure 3c). Because of the subsequent absence of calcium in solution, dolomite dissolves again with some increase of carbon in solution (Figure 3a and Figure 3c). The three different transport solvers give the same tendency as the reference PHREEQC solution. COMSOL is closer to the reference value, followed by the pdepe solver of MATLAB. The better performance of the coupling of IPhreeqc and COMSOL with respect to the other software couplings is likely coming from the more accurate time integration scheme of COMSOL for transport in comparison to the other solver.
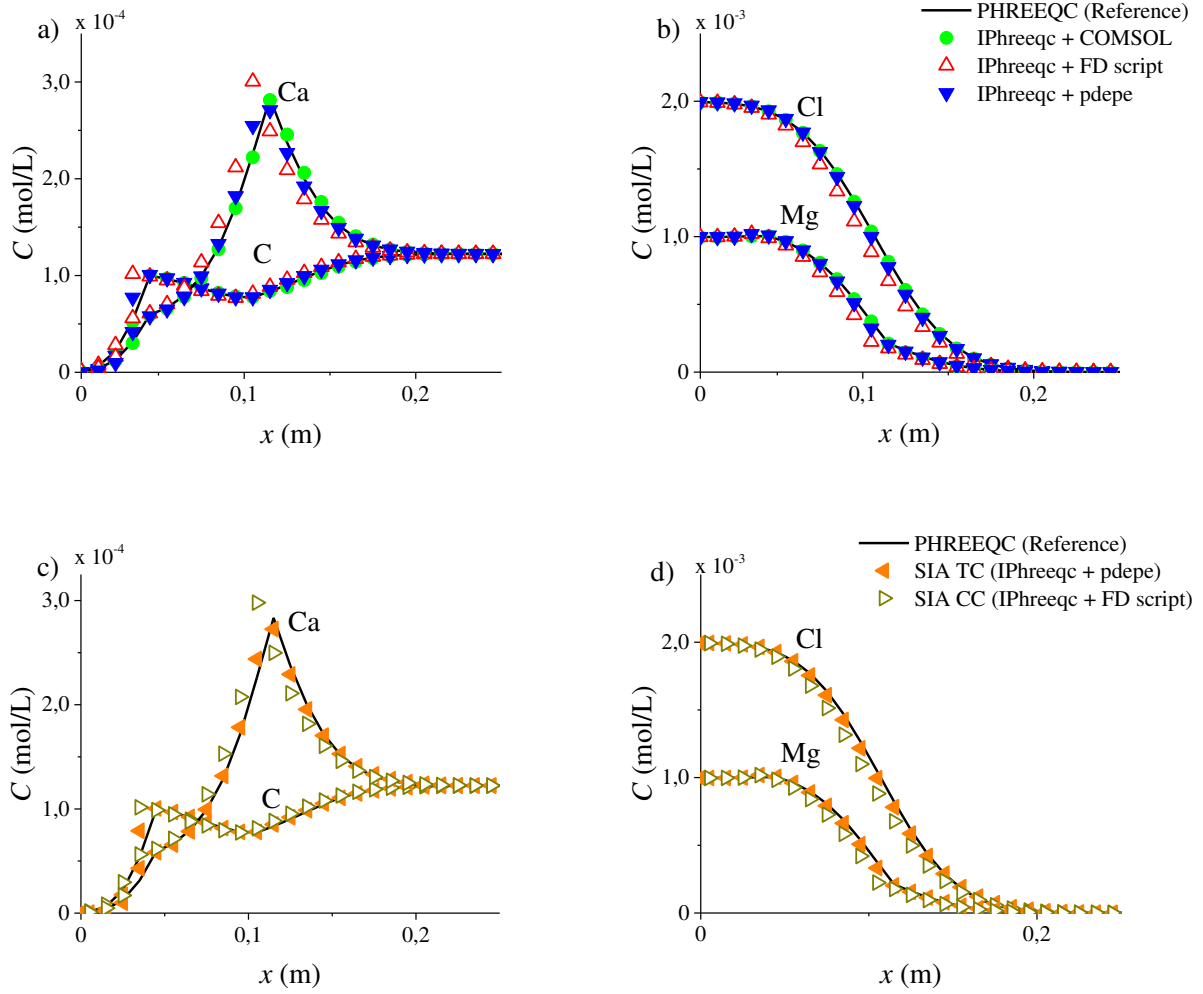
Figure 3: Aqueous concentration profiles at time t = 10⁴s.
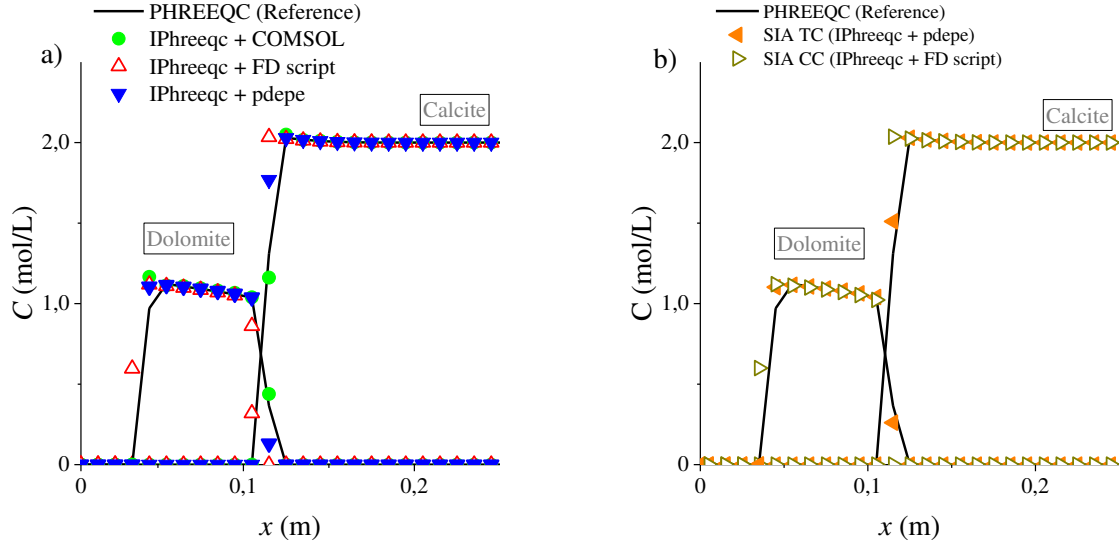
Figure 4: Dolomite and calcite equivalent concentration profiles with open and filled symbols respectively at time t = 10⁴ s.

Although COMSOL leads to more accurate results, it is more than one order of magnitude slower than the two other transport methods (Table 6). We checked that this large difference in performances does not come from the numerical method but from the large time required for COMSOL to start and stop when called numerous times externally. While this might not be an issue for large transport problems for which limitations will rather come from transport operator, it is a constrain for smaller tests and benchmarks.

Software Coupling	Time
IPhreeqc + COMSOL	668 s
IPhreeqc + FD script	24 s
IPhreeqc + pdepe	40 s

Table 6: Time performance for the calcite dissolution benchmark using a sequential operator splitting.

The error $\|e\|_2$ of equation (18) has been computed at time $t = 2.78$ h for the component "C" ($C = HCO_3^- + CO_3^{-2} + CaCO_3 + MgCO_3 + MgHCO_3^+ + CaHCO_3^+ + CO_2$) using the results of PHREEQC as reference. $\|e\|_2$ displays almost systematic convergence trends for sequential non-iterative approach (SNIA) with relatively more accurate second-order methods for $\Delta t = 1000$ s than for $\Delta t = 50$ s (Table 7). Whatever the coupling method, the agreement

with PHREEQC is overall good. Although COMSOL uses, as default, implicit time integration schemes for solving the transport equation instead of the required explicit method, it still compares well with PHREEQC. Indeed, the sequential non iterative method requires an explicit time integration for transport (equation (10)). It is not the case for COMSOL which uses (as default) a backward differentiation formula temporal integration scheme, which order varies with the internal time step adaptation (COMSOL, 2012). It thus introduces an additional error in the coupling scheme (de Dieuleveult *et al.*, 2009). However, by using such highly stable and accurate temporal integrations,, it enhances the robustness of the transport scheme.

For sequential iterative approaches (SIA), the time step reduction does not lead to more accuracy likely because of their different approximations to the SNIA approach of PHREEQC. To check that SIA methods have a monotonous convergence trend, we have computed their relative error $\|g\|_2$ using as reference the same method but with the smallest time step ($\Delta t = 50$ s) (equation (19)).

$$\|g\|_2 = \sqrt{\sum_{i=1}^{N_x}\left(c_N^i(t) - c_N^i(t, \Delta t = 50\ s)\right)^2}. \tag{19}$$

Table 8 shows indeed systematic decreasing trend of $\|g\|_2$ for Δt equal to 500s, 250s and 100s.

Δt (s)	1st order		2nd order			SIA	
	Additive	**Sequential**	**Alternating OS**	**Strang**	**SWS**	**TC**	**CC**
1000	$6.12 \; 10^{-5}$	$4.83 \; 10^{-5}$	$2.30 \; 10^{-5}$	$1.32 \; 10^{-5}$	$2.67 \; 10^{-5}$	X	X
500	$2.96 \; 10^{-5}$	$3.17 \; 10^{-5}$	$1.32 \; 10^{-5}$	$2.22 \; 10^{-5}$	$2.84 \; 10^{-5}$	$2.75 \; 10^{-5}$	$5.01 \; 10^{-5}$
50	$4.25 \; 10^{-6}$	$4.93 \; 10^{-6}$	$5.10 \; 10^{-6}$	$5.23 \; 10^{-6}$	$4.52 \; 10^{-6}$	$2.59 \; 10^{-5}$	$4.95 \; 10^{-5}$

Table 7: Error $\|e\|_2$ of equation (18) for the component C with different OS methods and splitting time steps for the calcite dissolution benchmark taking PHREEQC as reference.

Δt (s)	TC	CC
500	$1.79 \; 10^{-5}$	$9.86 \; 10^{-5}$
250	$1.76 \; 10^{-5}$	$9.07 \; 10^{-5}$
100	$1.43 \; 10^{-5}$	$6.56 \; 10^{-5}$

Table 8: Error $\|g\|_2$ of equation (19) for the component C with SIA TC and CC methods of equations (10) and (12)(10)(10) taking the results of the same methods with $\Delta t = 50$ s as reference.

4.3. Mixed equilibrium-kinetic system

We simulate the progressive increase of dissolved species in an atmospheric water infiltrating a granitic bedrock. This test case is derived from Nardi *et al.* (2014). The hydraulic properties of the system are found in Table 9. The infiltrating water has much lower concentrations of dissolved species than the resident water. It interacts with five minerals (Table 10). It is in equilibrium with calcite. The four other minerals k-feldspar, illite, albite and pyrite are subject to kinetically controlled dissolution with rates ranging from 10^{-13} to 10^{-11} mol/s. All parameters and rate laws of the simulation are provided in the PHREEQC file of iCP (Nardi *et al.*, 2014). The infiltrating water is quickly dissolving calcite to maintain equilibrium, increasing both the concentration of calcium and the pH of the solution. Other minerals also dissolve and increase the concentrations of Al and K in solution, however at a much slower rate because of the kinetic control of the reactions. pH is eventually buffered by the dissolution of illite and pyrite.

Parameter	Value
v [m/s]	$2.78 \cdot 10^{-6}$ m/s
D [m/s]	$5.55 \cdot 10^{-9}$ m^2/s
x_{max} [m]	0.08 m
Δx [m]	10^{-3} m
Δt [s]	720 s

Table 9: Parameters for mixed equilibrium-kinetic benchmark. v is the average velocity, D is the dispersion coefficient, x_{max} is the maximum length of the column, Δx is the grid size, and Δt is the splitting time.

Chemical Component and Species	Initial value	Boundary value
Ca [mol/L]	$1.4 \cdot 10^{-3}$	$3 \cdot 10^{-4}$
C [mol/L]	$4.9 \cdot 10^{-3}$	$1.9 \cdot 10^{-4}$
Cl [mol/L]	$1.1 \cdot 10^{-2}$	$9 \cdot 10^{-4}$
Mg [mol/L]	$7.4 \cdot 10^{-4}$	$2 \cdot 10^{-4}$
Mn [mol/L]	$3.4 \cdot 10^{-6}$	0
S [mol/L]	$9.6 \cdot 10^{-4}$	$4.8 \cdot 10^{-4}$
Na [mol/L]	$1.3 \cdot 10^{-2}$	$3 \cdot 10^{-4}$
K [mol/L]	$2.5 \cdot 10^{-4}$	$7.1 \cdot 10^{-4}$
Fe [mol/L]	$7.2 \cdot 10^{-6}$	$5.4 \cdot 10^{-5}$
Sr [mol/L]	0	$6.8 \cdot 10^{-7}$
Si [mol/L]	$2 \cdot 10^{-4}$	$2.5 \cdot 10^{-6}$
Al [mol/L]	$5.1 \cdot 10^{-9}$	10^{-8}
P [mol/L]	$3.8 \cdot 10^{-6}$	0
Br [mol/L]	$1.7 \cdot 10^{-5}$	0
F [mol/L]	$3.1 \cdot 10^{-5}$	$1.6 \cdot 10^{-5}$
pH [-]	7.5144	7.3
pe [-]	-3.0836	13.6
Calcite [mol/L]	6.065	-
K-feldspar [mol/L]	00.239	-
Illite [mol/L]	0.144	-
Albite [mol/L]	0.289	-
Pyrite [mol/L]	1.17	-

Table 10: Aqueous components and mineral species for mixed equilibrium-kinetic benchmark.

To simulate this set of reactions, we have chosen PhreeqcRM to assess the flexibility of TReaCLab. Transport is simulated with COMSOL to benefit from the accurate transport solver, it uses a variable order (between 1 and 5) backward differentiation formula. In the presence of both kinetically controlled and equilibrium reactions, both the quality of the transport and reactive integrations and coupling issues may be critical. We choose a simple sequential OS method with the successive integration of transport and reactivity. The results

obtained by the coupling of COMSOL and PhreeqcRM are highly close to the reference solution given by PHREEQC alone for the dissolved species and kinetically dissolving minerals (Figure 5). The time step of the coupled PhreeqcRM and COMSOL integration has been taken smaller than the characteristic mesh scale transport time and reactive time at least for the kinetical reaction to ensure accurate integrations. The most difficult quantity to get accurately is the calcium concentration because calcite is at equilibrium. The time step must be reduced to recover a steeper reactive front (Figure 6).

The comparison with PHREEQC provided by the error $\|e\|_2$ of equation (18) on the component "Al" shows overall small values compared to the mean "Al" component value of the order of 10^{-8} but no systematic convergence trends (Table 11). The transport methods have different approximations and cannot be directly compared by taking PHREEQC as reference. When taking the discretized Strang methods with $\Delta t = 90$ s as reference (Table 12), convergence trends become more systematic as for the SIA methods in the calcite dissolution benchmark.

This more advanced test shows that the computational load should be well balanced between the coupler, transport and chemistry methods. While coupling is the critical component in cases of equilibrium reactions and may even require highly integrated coupling strategies like global implicit methods (Hoffmann *et al.*, 2010; Saaltink *et al.*, 2001), it is not the case for kinetically controlled reactions. In this case of mixed equilibrium kinetic reaction, elementary coupling and accurate transport and reactive solvers can be efficient with small enough time steps. Evaluation of the quality of the resolution should thus systematically be assessed either by comparison with existing test cases in similar transport or reactive cases, by application of different coupling transport or reactive methods, or by proper convergence analysis.
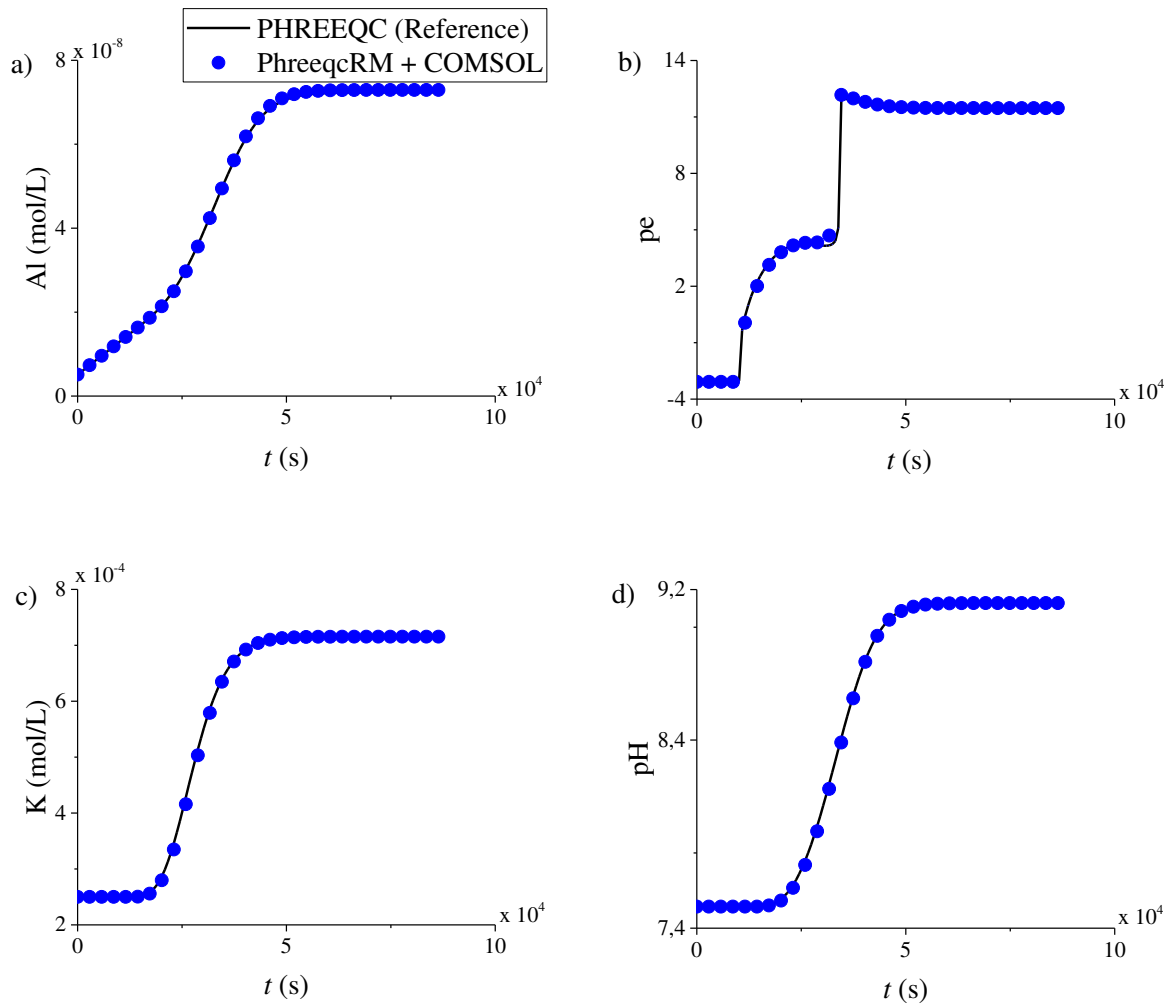
Figure 5: Comparison of results between the coupling of PhreeqcRM and COMSOL and PHREEQC observed for the mixed equilibrium-kinetic benchmark at the output of the column.
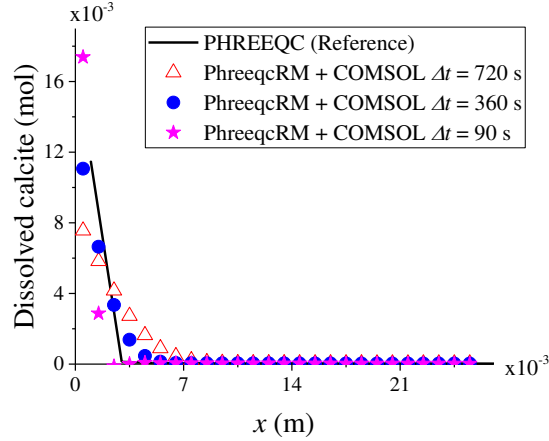
Figure 6: Quantity of dissolved calcite with PhreeqcRM and COMSOL for two different splitting time steps Δt = 720 s, 360 s and 90 s. PHREEQC independently is used as reference.

Δt (s)	1st order		2nd order		
	Additive	**Sequential**	**Alternating OS**	**Strang**	**SWS**
720	$3.56\ 10^{-9}$	$9.93\ 10^{-10}$	$3.06\ 10^{-9}$	$3.17\ 10^{-9}$	$3.20\ 10^{-9}$
360	$5.66\ 10^{-9}$	$3.87\ 10^{-9}$	$5.15\ 10^{-9}$	$5.22\ 10^{-9}$	$5.18\ 10^{-9}$
90	$3.51\ 10^{-9}$	$3.06\ 10^{-9}$	$3.40\ 10^{-9}$	$4.54\ 10^{-9}$	$3.40\ 10^{-9}$

Table 11: Error $\|e\|_2$ of equation (18) for the "Al" component with different OS methods and splitting time steps for mixed equilibrium-kinetic benchmark taking PHREEQC as reference.

Δt (s)	1st order		2nd order		
	Additive	**Sequential**	**Alternating OS**	**Strang**	**SWS**
720	$1.70\ 10^{-9}$	$7.14\ 10^{-9}$	$6.29\ 10^{-9}$	$6.16\ 10^{-9}$	$6.35\ 10^{-9}$
360	$2.89\ 10^{-9}$	$3.04\ 10^{-9}$	$4.32\ 10^{-9}$	$3.90\ 10^{-9}$	$4.36\ 10^{-9}$
90	$2.91\ 10^{-9}$	$3.38\ 10^{-9}$	$3.51\ 10^{-9}$	0	$3.51\ 10^{-9}$

Table 12: Error $\|e\|_2$ of equation (18) for the "Al" component with different OS methods and splitting time steps for mixed equilibrium-kinetic benchmark taking Strang method with Δt = 90 s as reference.

5. Discussion

As shown by many previous studies and by the three examples of the previous section, reactive transport problems can be solved by a wide diversity of transport, chemistry, and operator splitting methods. No method is currently accepted as systematically more accurate and efficient than any other. The systematic comparison of the implemented couplings with PHREEQC however shows that the full segmentation of the implementation has a cost in accuracy. Integration of the transport and chemistry operators in PHREEQC using more appropriate splitting with advection-reaction on one side and diffusion-reaction on the other side leads to better resolution of chemical fronts as shown in the second and third cases (Parkhurst and Appelo, 1999).It is not only the integration but also the successive improvements of the methods that lead to significantly more accurate schemes. While results are less accurate with TReacLab, they remain however close displaying the same overall behavior both on solute and mineral concentrations. The interest of fully segmented reactive transport implementations like in TReacLab is not motivated by the accuracy and should not be used when other more integrated and optimized software are appropriate and freely available.

Despite their lower accuracy, fully segmented implementations may be useful in situations where flexibility is essential. It is the case when extensive modeling work has been performed in independent software environments for transport or chemistry, and extensions to reactive transport problems are required. Transport and chemistry solvers are then imposed and should be coupled with as few specific developments as possible. For example, COMSOL and PHREEQC have been interfaced here and in several other works because of their complementarity (Nardi *et al.*, 2014; Nasir *et al.*, 2014; Wissmeier and Barry, 2011). It is possible to specify advanced geometrical configurations in COMSOL through a convenient graphical user interface (Azad *et al.*, 2016). PHREEQC provides advanced capacities for modeling complex geochemical systems with extensive database of reactions (Charlton and Parkhurst, 2011; Parkhurst and Wissmeier, 2015). In such cases, building the structure of the model may be the first and dominant issue in developing simulation capacities. That is when codes like TReacLab can provide practical bridges for reactive transport systems. The examples of section 4 however shows that they must be used with great care. Especially, the called software may have different temporal integration schemes than the explicit and implicit methods required by the SNIA and SIA coupling methods as discussed for the higher-order schemes of COMSOL in section 4.2. Using codes like COMSOL may enhance robustness at a

certain cost of accuracy. Thus, implementation capacity does not guarantee validity. Validity must be carefully checked and argued with other comparable cases or with appropriate convergence analysis.

Another targeted use of TReacLab concerns the development and test of new coupling methods or strategies. Operator splitting can be performed with various methods including for example adaptative time stepping (Belfort *et al.*, 2007; Gasda *et al.*, 2011). Other fully coupled global implicit strategies may also be more widely tested with finite difference computations of the Jacobian of the chemical operator (Amir and Kern, 2010). TReacLab may then be used as a platform where interfaces to chemical and transport operators are available and have been tested and documented for other coupling methods.

These applications are possible because TReacLab is a fully free and open software that can be directly accessed and downloaded (https://github.com/TReacLab/TReacLab). The free and open use of TReacLab has been dominant in its development and in the choices made for its organization. The repository is thus providing two main directories with sources and examples respectively. Sources are organized in four main categories for chemistry, transport, coupler and utilitaries. At the root of the chemistry, transport and coupler directories are the virtual classes as main entries. Examples of instantiations are provided in the subdirectories. Additional developments may take advantage of the documented examples provided at the different levels of the software.

6. Conclusion

We provide in the TReacLab code a fully segmented implementation of the coupling of independent geochemical and transport software. Coupling is based on a general expression of the split-operator strategy with a set of classical methods. TReacLab should facilitate the development of reactive transport simulation capacities for independent reactive and transport software. Systematic comparison to the well-established PHREEQC model for uniform 1D reactive transport cases shows that full decoupling at the implementation level has a cost in accuracy. Sharp dissolution fronts of thermodynamically controlled reactions especially are generally smoothed. Steeper fronts might be recovered with smaller splitting time steps at larger computational costs. Beyond the implementation and the simulation capacity, consistency and validity of the numerical models should be systematically assessed. TReacLab can be freely accessed and used to promote the development of coupling methods

and to provide additional modeling capacity for reactive transport coupling in geological media.

Appendix A: Implemented operator splitting methods

We detail the mathematical formulation for the sequential splitting (Geiser, 2009) :

$$\frac{\partial c^1}{\partial t} = \mathcal{L}_1 c^1, \qquad c^1(x, t^n) = c(x, t^n), \qquad t^n \leq t \leq t^{n+1}, \qquad (A.1)$$

$$\frac{\partial c^2}{\partial t} = \mathcal{L}_2 c^2, \qquad c^2(x, t^n) = c^1(x, t^{n+1}), \qquad t^n \leq t \leq t^{n+1}, \qquad (A.2)$$

$$c(x, t^{n+1}) = c^2(x, t^{n+1}), \qquad (A.3)$$

the additive splitting (Faragó *et al.*, 2008a; Faragó *et al.*, 2008b) :

$$\frac{\partial c^1}{\partial t} = \mathcal{L}_1 c^1, \qquad c^1(x, t^n) = c(x, t^n), \qquad t^n \leq t \leq t^{n+1}, \qquad (A.4)$$

$$\frac{\partial c^2}{\partial t} = \mathcal{L}_2 c^2, \qquad c^2(x, t^n) = c(x, t^n), \qquad t^n \leq t \leq t^{n+1}, \qquad (A.5)$$

$$c(x, t^{n+1}) = c^1(x, t^{n+1}) + c^2(x, t^{n+1}) - c(x, t^n), \qquad (A.6)$$

the Strang splitting (Strang, 1968) :

$$\frac{\partial c^1}{\partial t} = \mathcal{L}_1 c^1, \qquad c^1(x, t^n) = c(x, t^n), \qquad t^n \leq t \leq t^{n+1/2}, \qquad (A.7)$$

$$\frac{\partial c^2}{\partial t} = \mathcal{L}_2 c^2, \qquad c^2(x, t^n) = c^1\left(x, t^{n+1/2}\right), \qquad t^n \leq t \leq t^{n+1}, \qquad (A.8)$$

$$\frac{\partial c^1}{\partial t} = \mathcal{L}_1 c^1, \qquad c^1\left(x, t^{n+1/2}\right) = c(x, t^{n+1}), \qquad t^{n+1/2} \leq t \leq t^{n+1}, \qquad (A.9)$$

$$c(x, t^{n+1}) = c^1(x, t^{n+1}), \qquad (A.10)$$

46

and the symmetrically weighted splitting (SWS) (Csomós *et al.*, 2005) :

$$\frac{\partial c^1}{\partial t} = \mathcal{L}_1 c^1, \qquad c^1(x, t^n) = c(x, t^n), \qquad t^n \leq t \leq t^{n+1}, \qquad \text{(A.11)}$$

$$\frac{\partial c^2}{\partial t} = \mathcal{L}_2 c^2, \qquad c^2(x, t^n) = c^1(x, t^{n+1}), \qquad t^n \leq t \leq t^{n+1}, \qquad \text{(A.12)}$$

$$\frac{\partial c^{2*}}{\partial t} = \mathcal{L}_2 c^{2*}, \qquad c^{2*}(x, t^n) = c(x, t^n), \qquad t^n \leq t \leq t^{n+1}, \qquad \text{(A.13)}$$

$$\frac{\partial c^{1*}}{\partial t} = \mathcal{L}_1 c^{1*}, \qquad c^{1*}(x, t^n) = c^{2*}(x, t^{n+1}), \qquad t^n \leq t \leq t^{n+1}, \qquad \text{(A.14)}$$

$$c(x, t^{n+1}) = \frac{c^2(x, t^{n+1}) + c^{1*}(x, t^{n+1})}{2}. \qquad \text{(A.15)}$$

The alternating splitting algorithm (Valocchi and Malmstead, 1992) is based on a sequential splitting. It is defined by two successive splitting time steps with a permutation of the operator sequence between the splitting time steps.

Appendix B: Complementary notes on software organization

We successively describe the general toolbox organization, the coupler, transport and chemistry classes. We practically show how operator splitting methods can be introduced and how other transport and geochemical codes can be connected.

B.1 Coupling methods

The coupler is at the center of TReacLab as it performs the temporal integration and calls the transport and chemistry solvers through the OS algorithm. In the pre-processing phase, it gets the initial conditions and the temporal constrains of the integration. It is also in charge of storing the required results before formatting and outputting them in the post-processing phase. Because the coupler is at the core of the toolbox, its methods remain highly generic. Interactions with the transport and chemistry solvers are also fully generic thanks to template interfaces calling external software and managing the exchange of information. Calling external software relies on the so-called Solve_Engine method for both transport and chemistry software. Solve_Engine takes as inputs the concentration data and the time step over which the integration must be performed. It returns the updated concentrations, a flag to check the success of the integration and an error message in case of failure to activate and inform the error management procedure mentioned in the former section. The coupler is based on a fixed structure of concentration data. Whatever the structure of concentrations in the

transport and chemical codes, the structure of concentrations within the coupler is always the same. It consists in a matrix with in columns chemical species and in rows the position within the domain (Figure B.1). The size of the matrix is equal to the number of cells times the number of chemical species and components passed through the coupler. Chemical species include solutes and fixed species. As this is the sole link between the chemical code and the coupler also in charge of temporary results storage for the post-processing, it must transfer all quantities necessary for the algorithm and for the later extraction. The format of the matrix is set in the pre-processing phase and it is fixed for the whole simulation. TReacLab does not support yet any modification of species number to transfer between codes. Even if some solute species are absent over some time of the simulation, they will be transferred. This choice does not limit the capacity of the software as long as the chemical system is known from the beginning but might have some consequences on its performance in cases where solute composition strongly evolves. The choice of generality and flexibility, here like in other places, has a cost in efficiency. All modifications of concentration format are eventually performed in the interfaces between the coupler and the transport and chemistry solvers (Figure 1).

		Mobile components/Species		Fixed components/Species	
		C	Mg	Calcite	Dolomite
	1	$2 \cdot 10^{-4}$	$7 \cdot 10^{-2}$	0.7	2
	2	$1 \cdot 10^{-4}$	$8 \cdot 10^{-2}$	0.6	2.1
	...	...	...	...	...
	n	$1 \cdot 10^{-4}$	$9 \cdot 10^{-2}$	0.6	3

Figure B.1: Concentration format internal to the coupler class. To ensure generality, this structure of concentration is always the same and does not depend on the external transport and chemistry software. Species concentration are given in columns and are passed to the transport software as such. Concentrations at given locations are stored in rows with both mobile and fixed species. They are transferred either line per line or globally to the chemistry software. Fixed species are transferred from the chemistry code to the coupler to enable their possible use in the post-processing phase for results and outputs.

Thanks to the template methods calling the transport and chemical solvers and to the generic concentration format, operator splitting methods can be simply implemented. These are not more than a combination of simple calls of solvers passing and updating concentration information. Several sequential non-iterative techniques have thus been implemented, as detailed in section 2.3.

Specifications of the coupler are thus the name of the coupling method necessary to switch to the corresponding method in the coupler class, the temporal constrains of the integration and a vector of additional parameters. Temporal constrains of the integration are not only the initial and final times of the integration but also the times at which the solution must be stored. All time related parameters are stored into a time class. Additional parameters may be tolerances for example when using sequential iterative approaches. Instantiation of the coupler class thus consists in providing the identifier of the chosen coupling technique, the time constrains in the

time class (initial time, final time, time to save the results, OS time step) and the additional parameters possibly needed by the algorithm.

B.2 Geochemical solver

Geochemical codes widely differ by their principles, the type of reactivity they consider and their input/output formats and parameters. We propose to normalize some of their interface to simplify exchanges with the coupler. In any case of equilibrium or kinetic reactions or of a mixed combination of them, geochemical codes steadily take concentrations, reaction constants, rate parameters, reaction times, as inputs and return output concentrations. All specifications linked to the choice of components, primary and secondary species should be set in the geochemical code or in the interface so that the geochemical solver does not have to be modified and the coupler remains generic. Whether components are used or not, the definition of the chemical system is not unique. Even when components are used, several alternative and reliable definitions can be chosen (Fang *et al.*, 2003; Hoffmann *et al.*, 2012; Molins *et al.*, 2004). Numerical and conceptual consistencies between the transport and chemical systems should thus be ensured externally before any implementation.

While solute concentrations are instantiated by the coupler and systematically passed to the geochemical solver, equilibrium and kinetic constants are considered as constant. They are defined once for all in the pre-processing phase. For example in PHREEQC, chemical reactions and constants are already defined in databases like 'Phreeqc.dat' or 'llnl.dat'. Initialization of mineral quantities is done at the beginning of the simulation when setting the initial conditions through the coupler. The interface between the coupler and the geochemical solver is made up of the Solve_Engine that calls the geochemical solver and the methods that modify the concentration format. By default, the geochemical solver is instantiated and stored for each of the nodes of the computational grid for the whole domain of the simulation. Any data that are not passed to the coupler is, in general, kept in the instances of the geochemical code. Another option is provided by software that allow simultaneous computations for several independent batches like it is for example the case of PHREEQC. In such cases only one instance of the geochemical solver is necessary. Exchanges of data between the coupler and the geochemical solver are defined in the pre-processing phase and remain fixed for the whole duration of the simulation. It is precisely at this stage that components are derived through the algebraic operations of equation (5) and passed to the coupler. The coupler does not manage the transformation of concentration and species but just their transfer between the

transport and geochemical solvers. The use of components does not fundamentally change the calling sequence of the geochemical operator but modifies its interface to the coupler. Components may be specified by the geochemical code like in PHREEQC or by the user in the pre-processing phase by loading the matrix of U (equation (5)). In this latter case, components are defined by the user in the pre-processing phase and are computed by the interface that adapts the information to be passed through the coupler to the transport solver.

Connection of a new geochemical code requires essentially four operations. First, a new daughter class of the template chemistry class must be defined. It can be built up using, as template, one of the examples provided and described in the section 4. Second, an interface must be created to filter the required information given from the coupler to the Solve_Engine method. Third, an instantiation procedure should be provided whether it is internal or external to TReacLab. Fourth, the template Solve_Engine calling function of the geochemical solver must be written and optionally tested before being effectively used in reactive transport problems.

B.3 Transport solver

Despite the diversity of the transport mechanisms and numerical schemes to solve them, we provide here a basic interface designed mostly to address transport in a generic way. As previously stated, this approach assumes that transport parameters are not modified by the species concentration. This absence of feedback currently precludes density driven flows as well as permeability and porosity modifications due to precipitation or dissolution. TReacLab might be extended in this direction on the basis of slow evolutions of porosity or density. The transport operator relies on concentration independent parameters. We detail in the following the interaction between the coupler and the transport classes with the exchange of data and the instantiation of the transport solver. We will conclude this section with the development required to connect other transport codes.

While geochemical codes operate on species concentration on a given computational node, transport codes operate on a given species concentration over all the domain. In terms of data structure, each of the columns of the concentration array are successively transferred to the geochemical code and each of the rows (or linear combinations of rows) are given to the transport code (Figure B.1). The transport operator is thus iteratively called for each of the species or components explicitly specified in the interface between the coupler and the transport solver (Figure 1). The time range over which temporal integration should be

performed and the identifiers of the transported species are also transferred to the transport solver. Species identification is essential when considering species sensitive diffusion coefficient. The transport solver returns the updated concentration field at the final time of the time range, an indicator of success or failure of the integration and a message to document algorithm failures. The basic exchange of concentrations with the imposed integration times are the sole requirements for the coupler to proceed.

All other parameters of the transport code should be set in the pre-processing phase, which may become an important part of the eventual reactive transport code. In fact it does not cover only the flow and transport parameters but more broadly the full structure of the domain, of the computational grid, and of the boundary conditions. As for the geochemical code, the transport code can be instantiated internally or externally. In case of internal definition, it should contain at least the flow and transport properties, the morphology of the domain and the structure of the computational grid (coordinates of the computational nodes). A default set of classes is provided for 1D problems as templates for the morphology (domain definitions), the computational grid (identification and coordinates of nodes and edges), the boundary conditions (nature and values for boundary conditions) and the hydraulic and transport properties. We recall as also said in section 2.2 that some operator splitting techniques might impose limitations on the transport solver in terms of integration scheme or in terms of time step (de Dieuleveult *et al.*, 2009). Both the OS technique and the transport integration should be chosen consistent.

Operations on the transport class are thus decomposed between the pre-processing and the processing phases. Specifications of the operator with all necessary parameters is performed in the pre-processing phase. Only generic exchanges of concentrations are needed in the processing phase. Additional information would generally be needed externally to identify the location of the computational nodes. More advanced information from the definition of the domain, parameters and boundary conditions will be generally defined in the transport code rather than in TReacLab. For example, Comsol or Modflow have their own grid definitions. They are complete and efficient. It may be straightforwardly extracted and cross-referenced with the results of TReacLab as long as the cell numbers correspond, a basic but necessary requirement. This choice is motivated by both the generality and the simplicity of TReacLab. It also highlights that TReacLab remains a coupler that transfers information and does not process in any way the relation of concentrations between cells like a transport operator does.

The methodological choice of handling the spatial dimension of the problem within the transport operator is not only operational. It is also ensuring the capacity to connect a wide range of transport codes with their own logic and structure. For example, the multi-physics software COMSOL has its own mesh generator methods and internal structures that should not be duplicated in TReacLab but interfaced. Connecting other codes would thus require reduced work as long as they can already be called from the same environment of development (here MATLAB) on a discretized time basis. More in details, any new transport code would require: 1) the development of the main calling function Solve_Engine to call it from the coupler 2) the adaptation of the concentration format in the interface methods that match the concentrations to the internal data structure of the external code, 3) the instantiation of the transport class and 4) the access to the coordinates of the computational nodes for outputs purposes. As for the geochemical code, implementation of the interface should be checked before any full reactive transport coupling. This can be completed within TReacLab by using an idle process instead of the geochemical code.

REFERENCES

Abarca, E., Nardi, A., Grandia, F., Molinero, J., 2013. Feedback between reactive transport and convective flow during CO2 migration in a saline aquifer, EGU General Assembly Conference Abstracts, p. 7707.

Amir, L., Kern, M., 2010. A global method for coupling transport with chemistry in heterogeneous porous media. Computational Geosciences 14, 465-481.

Azad, V.J., Li, C., Verba, C., Ideker, J.H., Isgor, O.B., 2016. A COMSOL–GEMS interface for modeling coupled reactive-transport geochemical processes. Computers & Geosciences 92, 79-89.

Barry, D.A., Miller, C.T., Culligan-Hensley, P.J., 1996. Temporal discretisation errors in non-iterative split-operator approaches to solving chemical reaction/groundwater transport models. Journal of Contaminant Hydrology 22, 1-17.

Bea, S.A., Carrera, J., Ayora, C., Batlle, F., Saaltink, M.W., 2009. CHEPROO: A Fortran 90 object-oriented module to solve chemical processes in Earth Science models. Computers & Geosciences 35, 1098-1112.

Bear, J., 1972. Dynamics of fluids in porous media. Elsevier, New York.

Belfort, B., Carrayrou, J., Lehmann, F., 2007. Implementation of Richardson extrapolation in an efficient adaptive time stepping method: applications to reactive transport and unsaturated flow in porous media. Transport in Porous Media 69, 123-138.

Bethke, C.M., 2007. Geochemical and biogeochemical reaction modeling. Cambridge University Press.

Beyer, C., Li, D., De Lucia, M., Kühn, M., Bauer, S., 2012. Modelling CO2-induced fluid–rock interactions in the Altensalzwedel gas reservoir. Part II: coupled reactive transport simulation. Environmental Earth Sciences 67, 573-588.

Carrayrou, J., Mosé, R., Behra, P., 2004. Operator-splitting procedures for reactive transport and comparison of mass balance errors. Journal of Contaminant Hydrology 68, 239-268.

Charlton, S.R., Parkhurst, D.L., 2011. Modules based on the geochemical model PHREEQC for use in scripting and programming languages. Computers & Geosciences 37, 1653-1663.

Clement, T.P., Sun, Y., Hooker, B.S., Petersen, J.N., 1998. Modeling Multispecies Reactive Transport in Ground Water. Ground Water Monitoring & Remediation 18, 79-92.

Commend, S., Zimmermann, T., 2001. Object-oriented nonlinear finite element programming: a primer. Advances in Engineering Software 32, 611-628.

COMSOL, A., 2010. COMSOL Multiphysics-LiveLink for Matlab User's Guide, comsol 4.1 edition.

COMSOL, A., 2012. 4.3 User's Guide. Comsol.

Csomós, P., Faragó, I., 2008. Error analysis of the numerical solution of split differential equations. Mathematical and Computer Modelling 48, 1090-1106.

Csomós, P., Faragó, I., Havasi, Á., 2005. Weighted sequential splittings and their analysis. Computers & Mathematics with Applications 50, 1017-1031.

de Dieuleveult, C., Erhel, J., 2010. A global approach to reactive transport: application to the MoMas benchmark. Computational Geosciences 14, 451-464.

de Dieuleveult, C., Erhel, J., Kern, M., 2009. A global strategy for solving reactive transport equations. Journal of Computational Physics 228, 6395-6410.

Diersch, H.-J.G., 1996. Interactive, graphics-based finite-element simulation system FEFLOW for modeling groundwater flow, contaminant mass and heat transport processes. WASY Institute for Water Resource Planning and System Research Ltd., Berlin, Germany.

Engesgaard, P., Kipp, K.L., 1992. A geochemical transport model for redox-controlled movement of mineral fronts in groundwater flow systems: A case of nitrate removal by oxidation of pyrite. Water Resources Research 28, 2829-2843.

Fang, Y., Yeh, G.-T., Burgos, W.D., 2003. A general paradigm to model reaction-based biogeochemical processes in batch systems. Water Resources Research 39, 1083.

Faragó, I., Gnandt, B., Havasi, Á., 2008a. Additive and iterative operator splitting methods and their numerical investigation. Computers & Mathematics with Applications 55, 2266-2279.

Faragó, I., Thomsen, P.G., Zlatev, Z., 2008b. On the additive splitting procedures and their computer realization. Applied Mathematical Modelling 32, 1552-1569.

Friedly, J.C., Rubin, J., 1992. Solute transport with multiple equilibrium-controlled or kinetically controlled chemical reactions. Water Resources Research 28, 1935-1953.

Gasda, S.E., Farthing, M.W., Kees, C.E., Miller, C.T., 2011. Adaptive split-operator methods for modeling transport phenomena in porous medium systems. Advances in Water Resources 34, 1268-1282.

Geiser, J., 2009. Decomposition methods for differential equations: theory and applications. CRC Press.

Hoffmann, J., Kräutle, S., Knabner, P., 2010. A parallel global-implicit 2-D solver for reactive transport problems in porous media based on a reduction scheme and its application to the MoMaS benchmark problem. Computational Geosciences 14, 421-433.

Hoffmann, J., Kräutle, S., Knabner, P., 2012. A general reduction scheme for reactive transport in porous media. Computational Geosciences 16, 1081-1099.

Hundsdorfer, W., Verwer, J.G., 2013. Numerical solution of time-dependent advection-diffusion-reaction equations. Springer Science & Business Media.

Kool, J., Van Genuchten, M.T., 1991. Hydrus: One-dimensional Variably Saturated Flow and Transport Model, Including Hysteresis and Root Water Uptake; Version 3.3. US Salinity Laboratory.

Kräutle, S., Knabner, P., 2005. A new numerical reduction scheme for fully coupled multicomponent transport-reaction problems in porous media. Water Resources Research 41, W09414.

Kulik, D.A., Wagner, T., Dmytrieva, S.V., Kosakowski, G., Hingerl, F.F., Chudnenko, K.V., Berner, U.R., 2013. GEM-Selektor geochemical modeling package: revised algorithm and GEMS3K numerical kernel for coupled simulation codes. Computational Geosciences 17, 1-24.

Lie, K., 2014. An introduction to reservoir simulation using MATLAB: User guide for the Matlab reservoir simulation toolbox (MRST), SINTEF ICT, Department of Applied Mathematics, Oslo, Norway.

Liu, J., Ewing, R.E., 2005. An Operator Splitting Method for Nonlinear Reactive Transport Equations and Its Implementation Based on DLL and COM, In: Zhang, W., Tong, W., Chen, Z., Glowinski, R. (Eds.), Current Trends in High Performance Computing and Its Applications: Proceedings of the International Conference on High Performance

Computing and Applications, August 8–10, 2004, Shanghai, P.R. China. Springer Berlin Heidelberg, Berlin, Heidelberg, pp. 93-102.

Marty, N.C.M., Munier, I., Gaucher, E.C., Tournassat, C., Gaboreau, S., Vong, C.Q., Giffaut, E., Cochepin, B., Claret, F., 2014. Simulation of Cement/Clay Interactions: Feedback on the Increasing Complexity of Modelling Strategies. Transport in Porous Media 104, 385-405.

McDonald, M.G., Harbaugh, A.W., 1988. A modular three-dimensional finite-difference ground-water flow model, In: Survey, U.S.G. (Ed.), Denver, Colorado.

Molins, S., Carrera, J., Ayora, C., Saaltink, M.W., 2004. A formulation for decoupling components in reactive transport problems. Water Resources Research 40, W10301.

Morel, F.M., Hering, J.G., 1993. Principles and applications of aquatic chemistry. John Wiley & Sons.

Nardi, A., Idiart, A., Trinchero, P., de Vries, L.M., Molinero, J., 2014. Interface COMSOL-PHREEQC (iCP), an efficient numerical framework for the solution of coupled multiphysics and geochemistry. Computers & Geosciences 69, 10-21.

Nasir, O., Fall, M., Evgin, E., 2014. A simulator for modeling of porosity and permeability changes in near field sedimentary host rocks for nuclear waste under climate change influences. Tunnelling and Underground Space Technology 42, 122-135.

Parkhurst, D.L., Appelo, C., 1999. User's guide to PHREEQC (Version 2): A computer program for speciation, batch-reaction, one-dimensional transport, and inverse geochemical calculations.

Parkhurst, D.L., Kipp, K.L., Engesgaard, P., Charlton, S.R., 2004. PHAST, a program for simulating ground-waterflow, solute transport, and multicomponent geochemical reactions. USGS Techniques and Methods 6, A8.

Parkhurst, D.L., Wissmeier, L., 2015. PhreeqcRM: A reaction module for transport simulators based on the geochemical model PHREEQC. Advances in Water Resources 83, 176-189.

Peterson, S., Hostetler, C., Deutsch, W., Cowan, C., 1987. MINTEQ user's manual. Pacific Northwest Lab., Richland, WA (USA); Nuclear Regulatory Commission, Washington, DC (USA). Div. of Waste Management.

Prommer, H., Davis, G., Barry, D., 1999. PHT3D—A three-dimensional biogeochemical transport model for modelling natural and enhanced remediation. Contaminated Site Remediation: Challenges Posed by Urban and Industrial Contaminants. Centre for Groundwater Studies, Fremantle, Western Australia, 351-358.

Pruess, K., Oldenburg, C., Moridis, G., 1999. TOUGH2 user's guide version 2. Lawrence Berkeley National Laboratory.

Register, A.H., 2007. A guide to MATLAB object-oriented programming. CRC Press.

Rouson, D., Xia, J., Xu, X., 2011. Scientific software design: the object-oriented way. Cambridge University Press.

Saaltink, M.W., Ayora, C., Carrera, J., 1998. A mathematical formulation for reactive transport that eliminates mineral concentrations. Water Resources Research 34, 1649-1656.

Saaltink, M.W., Carrera, J., Ayora, C., 2001. On the behavior of approaches to simulate reactive transport. Journal of Contaminant Hydrology 48, 213-235.

Saaltink, M.W., Yakirevich, A., Carrera, J., Ayora, C., 2011. Fluid flow, solute and heat transport equations. Geochemical Modeling of Groundwater, Vadose and Geothermal Systems, 83.

Simpson, M.J., Landman, K.A., 2008. Theoretical analysis and physical interpretation of temporal truncation errors in operator split algorithms. Mathematics and Computers in Simulation 77, 9-21.

Šimůnek, J., Jacques, D., Van Genuchten, M.T., Mallants, D., 2006. Multicomponent geochemical transport modeling using HYDRUS-1D and HP1. J. Am. Water Resour. Assoc 42, 1537-1547.

Skeel, R.D., Berzins, M., 1990. A method for the spatial discretization of parabolic equations in one space variable. SIAM journal on scientific and statistical computing 11, 1-32.

Steefel, C.I., DePaolo, D.J., Lichtner, P.C., 2005. Reactive transport modeling: An essential tool and a new research approach for the Earth sciences. Earth and Planetary Science Letters 240, 539-558.

Steefel, C.I., MacQuarrie, K.T., 1996. Approaches to modeling of reactive transport in porous media. Reviews in Mineralogy and Geochemistry 34, 85-129.

Strang, G., 1968. On the construction and comparison of difference schemes. SIAM Journal on Numerical Analysis 5, 506-517.

Thouvenot, P., Bildstein, O., Munier, I., Cochepin, B., Poyet, S., Bourbon, X., Treille, E., 2013. Modeling of concrete carbonation in deep geological disposal of intermediate level waste, EPJ Web of Conferences. EDP Sciences, p. 05004.

Trotignon, L., Devallois, V., Peycelon, H., Tiffreau, C., Bourbon, X., 2007. Predicting the long term durability of concrete engineered barriers in a geological repository for radioactive waste. Physics and Chemistry of the Earth, Parts A/B/C 32, 259-274.

Valocchi, A.J., Malmstead, M., 1992. Accuracy of operator splitting for advection-dispersion-reaction problems. Water Resources Research 28, 1471-1476.

Van der Lee, J., 2002. CHESS Software for Geochemistry. Hydrology and Environmental Science, École des Mines de Paris, Fontainebleau, France.

van der Lee, J., De Windt, L., Lagneau, V., Goblet, P., 2003. Module-oriented modeling of reactive transport with HYTEC. Computers & Geosciences 29, 265-275.

Van Genuchten, M.T., Alves, W., 1982. Analytical solutions of the one-dimensional convective-dispersive solute transport equation. United States Department of Agriculture, Economic Research Service.

Wissmeier, L., Barry, D.A., 2011. Simulation tool for variably saturated flow with comprehensive geochemical reactions in two- and three-dimensional domains. Environmental Modelling & Software 26, 210-218.

Yeh, G.T., Tripathi, V.S., 1989. A critical evaluation of recent developments in hydrogeochemical transport models of reactive multichemical components. Water Resources Research 25, 93-108.

Zheng, C., Wang, P.P., 1999. MT3DMS: a modular three-dimensional multispecies transport model for simulation of advection, dispersion, and chemical reactions of contaminants in groundwater systems; documentation and user's guide. DTIC Document.

II.2 Additional benchmarks

In this section, additional benchmarks to the ones presented in the article are shown. This additional benchmarks and the previous benchmarks of section II.1 can be found in the code repository (https://github.com/TReacLab/TReacLab).

II.2.1 Benchmark 1: Transport validation

It is advisable to assess that the transport solvers work properly. To this end, a simple transport benchmark has been included to TReacLab. In a reactive transport simulation solved by a non-iterative operator splitting or an iterative splitting, usually the transport solver is coupled to a chemical solver. Here, since no reaction occurs, the transport operator is coupled to an identity class. The class outputs the inputted value without modification, namely $f(x) = x$. The benchmark is solved numerically using COMSOL, a finite difference scheme (FD script), the pdepe built-in function of MATLAB, and FVTool (Eftekhari). The numerical results are compared against an analytical solution (Lapidus and Amundson, 1952; Ogata and Banks, 1961). The analytical solution is described by:

$$c(x,t) = \begin{cases} C_i + (C_0 - C_i)\,A(x,t) & 0 < t < t_0 \\ C_i + (C_0 - C_i)\,A(x,t) - C_0\,A(x,t-t_0) & t > t_0 \end{cases}, \tag{II.1}$$

where A is:

$$A(x,t) = \frac{1}{2}\,erfc\left[\frac{Rx - vt}{2\sqrt{DRt}}\right] + \frac{1}{2}\,e^{(vx/D)}\,erfc\left[\frac{Rx + vt}{2\sqrt{DRt}}\right]. \tag{II.2}$$

Having as initial and boundary conditions:

$$c(x,0) = C_i, \tag{II.3}$$

$$c(0,t) = \begin{cases} C_0 & 0 < t < t_0 \\ 0 & t > t_0 \end{cases}, \tag{II.4}$$

$$\frac{\partial c(\infty,t)}{\partial x} = 0, \tag{II.5}$$

where $c(x,t)$ is the concentration at a point in the space x and time t, C_i and C_0 are initial and boundary constant values, v is the velocity, D the dispersion, and R makes reference to the retardation parameter which is here equal to 1. The parameters of the simulation can be seen in the sketch of Figure II.1.

$C_i = 3 \ 10^{-2}$ mol/L

$D = 7.84 \ 10^{-5}$ m^2/s $\Delta t = 20$ s

$v = 2.8 \ 10^{-3}$ m/s $C_0 = 0$ mol/L

$x_0 = 0$ m

$x_{max} = 5.6$ m

$\Delta x = 5.6 \ 10^{-2}$ m
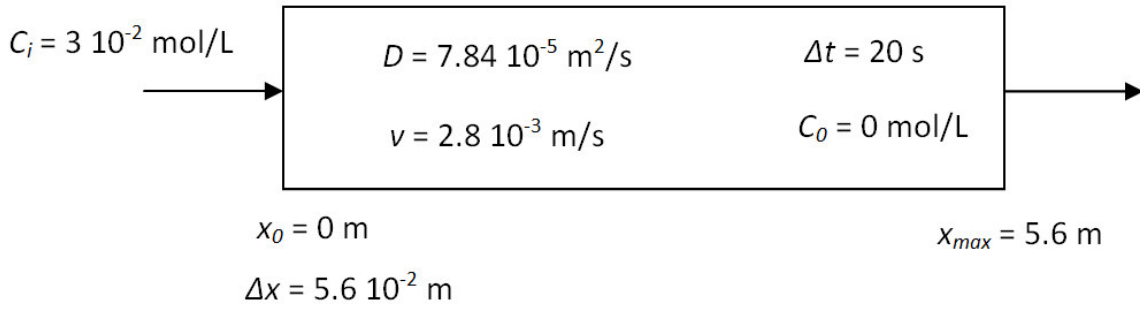
Figure II.1: Transport benchmark parameters and sketch. D is the dispersion coefficient, v is the velocity, C_o are the initial conditions in the 1D column, C_i is the Dirichlet boundary condition, x_{max} is the length of the column, Δt is the splitting time step and Δx is the spatial discretization step.

The simulation was run until $t = 400$ s, the result can be observed in Figure II.2. The results show a good agreement between the different codes. Additionally, a time comparison has been performed which is observable in Table II-2. The results indicate that pdepe and COMSOL are slower than the finite difference script (FD script) and FVTool. COMSOL and the function pdepe of MATLAB use high-order temporal schemes, whereas FVTool uses a backward Euler method and the FD script uses forward Euler method. Furthermore, COMSOL also communicates to MATLAB through a COMserver, since it is not possible to see the script of COMSOL, it becomes a black box and it is difficult to assess the reason of its slowness. However, high-order time integration schemes are more precise as Table II-2 indicates. The error of Table II-2 has been calculated by applying the Euclidian norm to the difference between the numerical and analytical results for each node, like in section II.1.

Software	Computational Time (s)
COMSOL	46
FD script	0.6
pdepe	20
FVTool	1.8

Table II-1: Time performance of the different software for the transport validation benchmark.
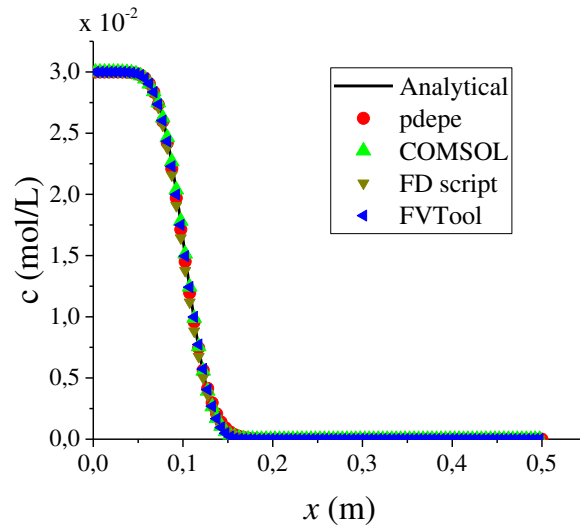
Figure II.2: Concentration vs. distance at t = 400 of the different software and analytical solution for the transport validation benchmark.

Software	error
COMSOL	$4.76 \ 10^{-4}$
FD script	$3 \ 10^{-3}$
pdepe	$8.24 \ 10^{-4}$
FVTool	$1.5 \ 10^{-3}$

Table II-2: Error comparison between software and analytical solution for the transport validation benchmark.

II.2.2 Benchmark 2: Cation exchange

This example presented first by Parkhurst and Appelo (1999b) has also been used by other researches as a validation benchmark and analysis of numerical methods and approaches (Amir and Kern, 2010; de Dieuleveult *et al.*, 2009). The problem has been solved numerically using the software coupling between FVTool and iPhreeqc, and also by PHREEQC alone in order to have reference results.

The exercise simulates a 1D column containing initially a sodium-potassium-nitrate solution in equilibrium with a cation exchanger. The column is flushed with a calcium-chloride solution, leading to a series of speciation reaction and exchange reactions. The mass balance of this exchange reactions is:

$$Ca^{2+} + 2X^- \rightleftharpoons CaX_2 \qquad \qquad \text{Log(K)} = 0.8 \qquad \text{(II.6)}$$

62

$$Na^+ + X^- \rightleftharpoons NaX \qquad\qquad Log(K) = 0 \qquad (II.7)$$

$$K^+ + X^- \rightleftharpoons KX \qquad\qquad Log(K) = 0.7 \qquad (II.8)$$

$$NH_4^+ + X^- \rightleftharpoons NH_4X \qquad\qquad Log(K) = 0.6 \qquad (II.9)$$

Calcium (Ca^{2+}) is more strongly bound to the exchanger than potassium (K^+) and sodium (Na^+). Hence, sodium and potassium are released to the solution from the surface of the solid matrix, leaving a free space which is occupied by calcium. Chloride is a tracer, hence the results of chloride can be calculated analytically such as in section II.2.1, using the equation (II.1). Nitrate acts almost like a tracer. Even though, the inputted nitrate might suffer redox reactions during speciation which might lead to ammonium (NH_4^+) and consequently react with the exchanger. During the simulation this values where around a magnitude of 10^{-60} mol/L, hence the cation exchange for ammonium (NH_4^+) is neglected. The nitrate component is not plotted because its curve is almost identical to chloride component. The transport parameters are given in Table II-3 and the initial and boundary values are given in Table II-4.

Parameter	Value
v [m/s]	$2.78 \ 10^{-6}$
D [m^2/s]	$5.56 \ 10^{-9}$
x_{max} [m]	6
Δx [m]	0.002
Δt [s]	90

Table II-3: Physical parameters for the cation exchange benchmark. v is the average velocity, D is the dispersion coefficient, xmax is the maximum length of the column, Δx is the grid size, and Δt is the time step.

Chemical Component and exchange capacity	Initial value	Boundary value at x=0
Ca [mol/L]	0	$6 \ 10^{-4}$
Cl [mol/L]	0	$1.2 \ 10^{-3}$
Na [mol/L]	10^{-3}	0
K [mol/L]	$2 \ 10^{-4}$	0
N [mol/L]	$1.2 \ 10^{-3}$	0
pH [-]	7	7
X [mol]	$1.1 \ 10^{-3}$	-

Table II-4: Cation exchange benchmark initial and boundary values for aqueous components. X indicates an exchange site with negative charge.

In Figure II.3a, we compare the result of PHREEQC, given by a solid line, against the results of FVTool-iPhreeqc coupling with a sequential splitting method, given by empty triangles. In general a good agreement exists between results, but a slight shift between both results is observable. This shift is attributable to the transport solver, since it also occurs in the tracer. Other methods (additive, alternating, Strang, SWS) have also been performed, their results match PHREEQC values as well. A similar comparison as in section II.1 for the "Ca" component taking as reference the Strang method with the smallest splitting time step was performed (Table II-5). The table shows independently of the method that smaller splitting time steps lead to results in better accordance with the reference results, therefore we conclude that the methods are consistent.

Figure II.3b shows the concentration of the components at the outflow. After one pore volume (8 h), the concentration of the tracer ("Cl") reaches the outflow of the column. The release of all the "K" component is delayed in comparison to "Na" , since "K" bounds stronger (because of larger log K in the exchange reaction). Once there is no more "Na" in the exchanger the amount of "Ca" that reaches the outflow starts to increase. Finally, once all the exchange sites have been occupied by "Ca", namely when "K" is out of the 1D column, "Ca" reaches its steady-state concentration equal as in the input side of the column.
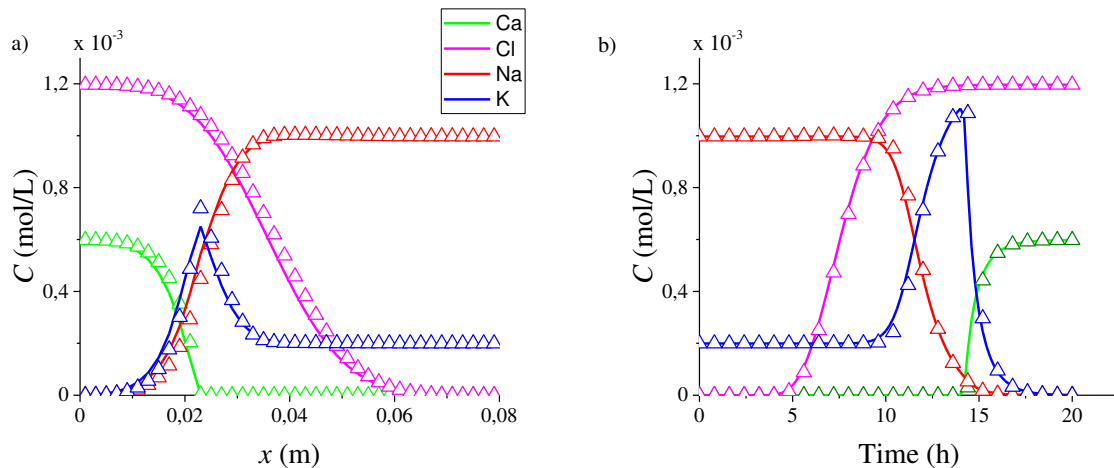
Figure II.3: a) Component concentration vs length at time t = 3.6 h, b) concentration at the end of the column vs time. The results of PHREEQC are represented by a solid line, while the results of the coupling between FVTool and iPhreeqc are given by empty triangles.

64

Δt (s)	1st order		2nd order		
	Additive	Sequential	Alternating OS	Strang	SWS
720	2.49 10^{-4}	2.18 10^{-4}	2,71 10^{-4}	1,35 10^{-4}	1,35 10^{-4}
360	1.23 10^{-4}	1.05 10^{-4}	1.47 10^{-4}	7,50 10^{-5}	6,07 10^{-5}
90	1.81 10^{-5}	1.74 10^{-5}	2,02 10^{-5}	0	3,16 10^{-6}

Table II-5: Error $\|e\|_2$ of equation (18 in section II.1) for the " Ca" component with different OS methods and splitting time steps for the cation exchange benchmark, taking Strang method with $\Delta t = 90$ s as reference.

II.2.3 Benchmark 3: Multispecies sorption and decay

The following benchmark is described in Clement *et al.* (1998). The system contains three species, c_2 is the daughter of c_1 and c_3 the daughter of c_2. Such system has been solved analytically by Cho (1971) in order to give an insight of the nitrification suffer by ammonium (NH_4^+) becoming nitrite (NO_2^-) and nitrate (NO_3^-). The system of equations is given by:

$$(1 + K_d)\frac{\partial c_1}{\partial t} = D\frac{\partial^2 c_1}{\partial x^2} - v\frac{\partial c_1}{\partial x} - k_1 c_1 \tag{II.10}$$

$$\frac{\partial c_2}{\partial t} = D\frac{\partial^2 c_2}{\partial x^2} - v\frac{\partial c_2}{\partial x} - k_2 c_2 + k_1 c_1 \tag{II.11}$$

$$\frac{\partial c_3}{\partial t} = D\frac{\partial^2 c_3}{\partial x^2} - v\frac{\partial c_3}{\partial x} - k_3 c_3 + k_2 c_2 \tag{II.12}$$

An analytical solution for the system has been derived by Lunn *et al.* (1996):

$$c_1 = C_{10}P_1, \tag{II.13}$$

$$c_2 = C_{20}P_2 + \frac{k_1 C_{10}}{(k_2 - k_1)}\left\{P_1 - P_2 + \exp\left(\frac{(k_2 - k_1)}{K_d}t\right)\left(P\left(D, \frac{\mu_2 - \mu^*}{D - D^*}\right) - P\left(D^*, \frac{\mu_2 - \mu^*}{D - D^*}\right)\right)\right\}, \tag{II.14}$$

$$c_3 = C_{30}P_3 + \frac{k_2 C_{20}}{(k_3 - k_2)}(P_2 - P_3) + \frac{k_1 k_2 C_{10}}{(k_2 - k_1)(k_3 - k_1)(k_3 - k_2)}\{(k_2 - k_1)P_3 + (k_1 - k_3)P_2 +$$

$$(k_3 - k_2)P_1\} + \frac{k_1 k_2 C_{10}}{(k_2 - k_1)(k_3 - k_2)}\exp\left(\frac{(k_2 - k_1)}{K_d}t\right)\left(P\left(D, \frac{\mu_2 - \mu^*}{D - D^*}\right) - P\left(D^*, \frac{\mu_2 - \mu^*}{D - D^*}\right)\right) - \tag{II.15}$$

$$\frac{k_1 k_2 C_{10}}{(k_3 - k_1)(k_3 - k_2)}\exp\left(\frac{(k_3 - k_1)}{K_d}t\right)\left(P\left(D, \frac{\mu_3 - \mu^*}{D - D^*}\right) - P\left(D^*, \frac{\mu_3 - \mu^*}{D - D^*}\right)\right)$$

where c_1, c_2, c_3 are the concentration at a point in the space x and time t, C_{10}, C_{20}, C_{30} are the values at the boundary, K_d is the adsorption coefficient, k_1, k_2, k_3 are the reaction rate coefficients, D is the dispersion, μ_i is a parameter given by:

$$\mu_i = \frac{v^2}{4D} + k_i, \qquad\qquad i = 1,2,3 \tag{II.16}$$

being v the velocity, the symbol * in D and μ indicates that these parameters are divided by $1/(1+K_d)$, and P_1, P_2, P_3 is a function such as:

$$P(A, \lambda) = \frac{1}{2}\left(\exp\left(\frac{vx}{2D} - x\sqrt{\lambda}\right)erfc\left(\frac{x}{\sqrt{4At}} - \sqrt{A\lambda t}\right) + \exp\left(\frac{vx}{2D} + x\sqrt{\lambda}\right)erfc\left(\frac{x}{\sqrt{4At}} + \sqrt{A\lambda t}\right)\right), \quad \text{(II.17)}$$

where A and λ for P_1 are D^* and μ^*/D^* respectively and for P_2, and P_3 are D and μ/D respectively. The parameters for the simulation are given in Table II-6. The boundary conditions of the 1D column are:

$$C_{10} = 1 \qquad C_{20} = 0 \qquad C_{30} = 0 \qquad\qquad \text{for x = 0} \qquad \text{(II.18)}$$

$$c_i = 0 \qquad\qquad i = 1,2,3 \qquad\qquad\qquad \text{for x}_{\text{max}} \qquad \text{(II.19)}$$

Parameter	Value
v [cm/h]	0.1
D [cm^2/h]	0.018
x_{max} [cm]	40
K_d	1
$k_1[\text{h}^{-1}]$	0.05
$k_2[\text{h}^{-1}]$	0.03
$k_3[\text{h}^{-1}]$	0.02
Δx [cm]	0.5
Δt [h]	0.5

Table II-6: Physical and chemical parameters for the multispecies sorption and decay benchmark. v is the average velocity, D is the dispersion coefficient, x_{max} is the maximum length of the column, Δx is the grid size, Δt is the time step, K_d is the adsorption coefficient, and k_i with i = 1,2, 3 are the reaction rates.

Figure II.4 shows the analytical solution and numerical solution at $t = 100$ h with an additive splitting and $t = 200$ h with a symmetrically weighted splitting. The numerical solution is obtained with the software coupling between a finite difference script for the transport operator and ode45 built-in function of MATLAB for the reaction operator. Other numerical splitting scheme (sequential, alternating, Strang) show similar trends. In Figure II.4a, it is observable that the numerical profiles of c_2 and c_3 are slightly advanced in comparison to the analytical profiles. After 100 h (Figure II.4b), the match between the numerical and analytical profiles is more accurate.
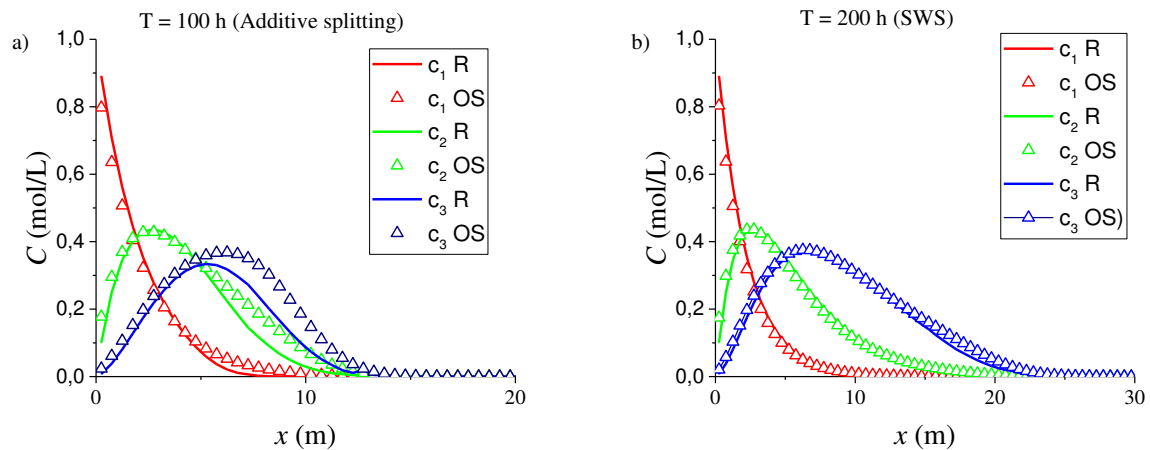
Figure II.4: Concentration vs length plots at a) t = 100 h and b) t = 200 h. The analytical solution is depicted by a solid line, in the legend it is accompanied by a R. The numerical solution is depicted by an empty triangle, in the legend accompanied by 'OS' (operator splitting). The numerical approach used is the additive splitting.

II.3   External transport and geochemical plugged codes

In order to do the simulations of this chapter of the thesis, several codes have been employed. Therefore, a section is dedicated to give an insight into these codes.

II.3.1 Transport codes

Three external transport codes have been used as transport operators: COMSOL, the pdepe built-in function of MATLAB and FVTool. Furthermore, a simple finite difference script has been developed.

II.3.1.1   COMSOL

COMSOL Multiphysics (COMSOL, 2012) is a commercial finite element method software used in various physics and engineering problems allowing several types of analyses: stationary, time-dependent, eigenfrequency, eigenvalue and also wide variety of customizable geometries. In COMSOL it is possible to introduce coupled systems of PDEs, but several add-on modules exist. The modules are categorized according to the application area. Every module incorporates the classical system of equations of their respective area.

COMSOL uses an interactive environment for the modelization of the problem. Nevertheless, it can be run by scripts programs written in MATLAB thanks to the Livelink for MATLAB (COMSOL, 2010). It is a client-server mode where MATLAB is the client and COMSOL the server which uses a TCP/ICP communication protocol.

There are three main ways to use COMSOL with MATLAB. The user can create the whole model in COMSOL, namely physical parameters, mesh and other pre-processing features, and then import the model into MATLAB for further use or just post-processing purposes. The user can also call MATLAB functions from COMSOL. Finally, the user can create the whole model from scratch in MATLAB by calling the suitable application interface program functions. In our case, since we use a simple geometry (1D) and just one physical module of COMSOL called solute transport, we have chosen to create the model from scratch, using only MATLAB and calling the interface program functions of COMSOL. The reason for that is that we want to keep a generic software which can handle different external software couplings and is not embedded with specific software. The equation of the solute transport physical module of COMSOL is:

$$\left(\theta_s + \rho_b k_p\right)\frac{\partial c}{\partial t} + \left(c - c_p \rho_p\right)\frac{\partial \theta_s}{\partial t} - \nabla\left((D_e - D_D)\nabla c + vc\right) = R + S, \qquad \text{(II.20)}$$

where θ_s is the porosity, ρ_b is the bulk density, c the concentration, k_p, c_p, and ρ_p are the rate constant, the solid concentration, and the density of the solid concentration respectively, related to one of the following sorption models: Langmuir, Freundlich or user-defined. D_e is the effective diffusion and D_D the dispersion tensor, v is the velocity, R stands for kinetic chemical reaction which might be added and S for the sink/source terms.

The COMSOL model allows changes of porosity due to sorption, but in this work we do not make use of this capability. Furthermore, no kinetic reaction module of COMSOL have been added to the transport equation. The reason resides on the fact that we separate the chemical operator from the transport operator, although the possibility might be considered in other projects.

II.3.1.2   FVTool

FVTool is an open-source objected-oriented toolbox written in MATLAB which solves mass conservative equations using finite volume methods. It was inspired by another

68

open-source code FiPy[1] and is written, developed and maintained by Dr. Eftekhari[2]. Our interest of the software stems from the simplicity of it, the fact that it is open-source, and is written in MATLAB, avoiding, therefore, the implementation of application programming interface (API). The general equation that the solver tackles is[3]:

$$\theta \frac{\partial c}{\partial t} + \nabla(D\nabla c + \ vc) = s, \tag{II.21}$$

with a general (Robin) boundary condition:

$$a\nabla c + bc = r, \tag{II.22}$$

where c is the concentration, θ is the volumetric content, D is the dispersion-diffusion tensor, v is the velocity, s is a sink/source term, a, b, and r are parameters related to the type of boundary condition. Since the toolbox is made by a set of classes, there is a flexibility on how you can combine the classes and which approach you can use to solve your problem of interest. For instance, it is possible to solve the scheme with a total variation diminishing approach and a flux limiter such as CHARM (Zhou, 1995) or Koren (Koren, 1993), or just with a classic finite volume discretization.

II.3.1.3 pdepe MATLAB

The pdepe built-in function of MATLAB or a modified version of it have been used. The function solves parabolic-elliptic PDEs in 1D, and has been used in various studies such as modeling brown stock washing problems (Kumar *et al.*, 2010), wound healing (Thackham *et al.*, 2009), and reactive transport (Torres *et al.*, 2015). The spatial discretization is obtained by applying a piecewise nonlinear Galerkin/Petrov-Galerkin method with second-order accuracy (Skeel and Berzins, 1990). The resulting ODE system is solved by ode15s, a built-in function of MATLAB which uses a variant of backward differentiation formulas called numerical differentiation formulas (Shampine and Reichelt, 1997; Shampine *et al.*, 1999). The spatial discretization is specified by the user, but the internal time step cannot be modified, although a maximum time step and a suggested initial step size can be imposed. The general formula is given by:

---

[1] http://www.ctcms.nist.gov/fipy/
[2] https://github.com/simulkade/FVTool
[3] http://fvt.simulkade.com/

$$c\left(x,t,u,\frac{\partial u}{\partial x}\right)\frac{\partial u}{\partial x} = x^{-m}\frac{\partial}{\partial x}\left(x^m f\left(x,t,u,\frac{\partial u}{\partial x}\right)\right) + s(x,t,u,\frac{\partial u}{\partial x}), \qquad (\text{II.23})$$

where x and t are the spatial and time variables respectively, and u is the dependent variable, which in our case is either the species or the component concentrations. The parameter m can vary from 0 to 2 in order to represent the symmetry of the problem (slab $(m = 0)$, cylindrical $(m = 1)$, or spherical symmetry $(m = 2)$) in our case it has kept to 0. To use the pdepe solver, 3 functions have to be defined: a) one giving the values of $c\left(x,t,u,\frac{\partial u}{\partial x}\right)$, $f\left(x,t,u,\frac{\partial u}{\partial x}\right)$ and $s(x,t,u,\frac{\partial u}{\partial x})$, b) another giving the initial conditions u_0, and finally c) one giving the boundary conditions by stating the values of $p(x,t,u)$ and $q(x,t)$ at the beginning and end of the 1D system. Table II-7 illustrates values of p and q according to the type of boundary conditions.

a)
$$c\left(x,t,u,\frac{\partial u}{\partial x}\right) = \theta,$$
$$f\left(x,t,u,\frac{\partial u}{\partial x}\right) = D\frac{\partial u}{\partial x} - vu, \qquad (\text{II.24})$$
$$s\left(x,t,u,\frac{\partial u}{\partial x}\right) = S.$$

b)
$$u(x,t_0) = u_0 \qquad (\text{II.25})$$

c)
$$p(x,t,u) + q(x,t)f\left(x,t,u,\frac{\partial u}{\partial x}\right) = 0 \qquad (\text{II.26})$$

Type	Formula	$p(x,t,u)$	$q(x,t)$
Dirichlet	$u = u_1$	$u - u_1$	0
Neumann	$\frac{\partial u}{\partial x} = J$	$vu - JD$	1
Cauchy or Robin	$D\frac{\partial u}{\partial x} - vu = J$	$-J$	1

Table II-7: Implementation of boundary conditions in the pdepe built-in function of MATLAB (Shafei, 2012).

In section II.2.1, we have employed the default time integration of the pdepe function, but in all the other benchmarks (section II.1) we have withdrawn the spatial discretization given by the MATLAB solver and applied a forward Euler scheme (first-order time explicit scheme). Consequently, it is usually less accurate than the default scheme which is a numerical differentiation formula scheme. Although, the application of forward Euler scheme results in

a well decoupled sequential non-iterative approach, if the system has only equilibrium reactions (de Dieuleveult *et al.*, 2009).

II.3.1.4   FD script

The finite difference scheme has been implemented considering that the advection and diffusion-dispersion terms are constant. We recall the advection-diffusion equation:

$$\theta \frac{\partial c}{\partial t} = L(c) \, . \tag{II.27}$$

The discretization of equation (II.27) using a forward Euler time scheme leads to:

$$c^{n+1} = c^n + \theta^{-1} \Delta t (L c^n + q). \tag{II.28}$$

where the superscript n indicates the current time level and $n + 1$ the next time level, θ is the constant volumetric content (it can also be porosity or retardation) represented by a diagonal matrix, q is a term given by the boundary conditions a vector of zeros except for the first and last values, and L is the linear transport operator given by the sum of the diffusion-dispersion term and the advection term, since we work in a 1D system the matrix is tridiagonal. The advection term has been discretized using a second-order central discretization (Hundsdorfer and Verwer, 2013) and by assuming that the velocity is constant on the positive direction. The diffusion-dispersion term has also been discretized using a second-order central discretization:

$$A_{advection} = \frac{v}{2\Delta x} \begin{pmatrix} 0 & -1 & & & \\ 1 & 0 & & & \\ & & \ddots & & \\ & & & 0 & -1 \\ & & & 1 & 0 \end{pmatrix} \tag{II.29}$$

$$A_{diffusion -dispersion} = \frac{D}{\Delta x^2} \begin{pmatrix} -2 & 1 & & & \\ 1 & -2 & & & \\ & & \ddots & & \\ & & & -2 & 1 \\ & & & 1 & -2 \end{pmatrix}. \tag{II.30}$$

$$L = A_{advection} + A_{diffusion -dispersion} \tag{II.31}$$

The advection and diffusion-dispersion term relied on two classes of TReacLab: Linear_Operator_Advection_FD_1D and Linear_Operator_Diffusion_FD_1D. Provided that the advection and diffusion-dispersion operators are linear, other discretizations can be called first-order upwind, second-order upwind biased, flux form (Hundsdorfer and Verwer, 2013).

Unfortunately, we have not applied any of these other discretizations in the presented benchmarks.

Since coupling methods can sometimes force the use of certain types of numerical schemes such as an implicit or explicit approach. When we applied the SIA CC scheme, we descritize the advection-diffusion equation with a backward Euler time discretization and add a source parameter R:

$$c^{n+1} = (I - \theta^{-1}\Delta t L)^{-1}(c^n + \Delta t q + R), \qquad (II.32)$$

where R is here a difference given by the fix components at initial and final state of each splitting time step, $R = F^n - F^{n+1}$.

II.3.2 Geochemical codes

Most of the geochemical system presented on the tests have been solved by applying codes based on PHREEQC: iPhreeqc and PhreeqcRM. Although, simple chemistry such as in section II.2.3 have been solved by analytical solutions, explicit or implicit first-order Euler scheme, or the ode45 function of MATLAB. In the following, we only described the PHREEQC's set solvers.

II.3.2.1 PHREEQC, iPhreeqc, and PhreeqcRM

PHREEQC (**pH**-**RE**dox-**EQ**uilibrium in **C** programming language) is a free, open-source state-of-art geochemical package of the USGS (Parkhurst and Appelo, 1999b). PHREEQC has several databases and allows to use user-defined database or modified previously existing databases. It can work with different aqueous models: Lawrence Livermore National Laboratory model, WATEQ4F model, Pitzer specific-ion-interaction aqueous model, and the specific ion interaction theory aqueous models. The software accounts for a series of geochemical equilibrium equations such aqueous solution interacting with minerals, gases, solid solutions, exchangers, and sorption surfaces. PHREEQC also includes kinetic reactions and 1D reactive transport.

PHREEQC formulation for every chemical equilibrium problem derives from a set of equations (Parkhurst and Appelo, 1999a):

f_{alk}	Mole balance alkalinity
f_e	Mole balance for exchange site
f_g	Mole balance gas
f_H	Mole balance of hydrogen
f_{H2O}	Activity of water
f_m	Mole balance of master species except H^+, e^-, H_2O, and the alkalinity
f_O	Mole balance of oxygen
f_{Ptotal}	Equilibrium with a fixed pressure multicomponent gas phase
f_p	Equilibrium with a pure phase
f_{pss}	Equilibrium with solid solution
f_{sk}	Mole balance for surface sites
f_z	Aqueous charge balance
$f_{z,s}$	Surface charge balance
f_μ	Ionic strength
$f_{\Psi s}$	Surface charge potential

Table II-8: PHREEQC main types of geochemical predefined equations.

The equations have been predefined in PHREEQC (hard coded), and, depending on the system, some of them will be presented or not. Consequently, a system without solid solutions phases will not present a solid solution function, or if in a system a pure phase (e.g. portlandite) disappears, its equation will also disappear.

In order to solve the system, PHREEQC uses a Newton-Raphson method for chemical equilibrium. To avoid singular matrix, PHREEQC combines the Newton-Rapshon method with an optimization algorithm (Barrodale and Roberts, 1978, 1980). Thus, in systems where no exact solution exists, PHREEQC gives a solution unless convergence has failed (Parkhurst and Appelo, 1999a).

PHREEQC has been coupled to other software by two main ways: a) loosely by creating an input file, run PHREEQC, and obtained results, b) tightly by embedding the PHREEQC source code (or required part of the code) into the other software. The first way is slow but non-intrusive, furthermore it leads to an error since it is not possible to define extremely sensitive data such as solution charge balance, total moles of hydrogen, and total moles of oxygen (Charlton and Parkhurst, 2011). The second is fast, but requires a high involvement with the implementation since it is intrusive. Also, for each software, the interface for the coupling must be created each time (Appelo and Rolle, 2010; Hoth *et al.*, 2000; Jacques and Šimůnek, 2005; Parkhurst *et al.*, 2004). In order to facilitate the coupling of PHREEQC with other modules and create a unique interface, the USGS released iPhreeqc (Charlton and Parkhurst, 2011). iPhreeqc is a set of free and open-source modules written in C++ that

implement all the capabilities of PHREEQC. They can interact with interpreted languages such as MATLAB or Python by a Microsoft component object model (or a dynamic library if the interpreter allows it), but also with compiled languages such as C++ or Fortran by a dynamic library. In Müller *et al.* (2011) a time performance comparison is carried out. The comparison is made between the old loose coupling of PHREEQC with Python, iPhreeqc as a COM and dynamic library with Python, C++ and the dynamic library of iPhreeqc and PHREEQC alone. In Figure II.5 is possible to observe the improvement in time performance brought by iPhreeqc.
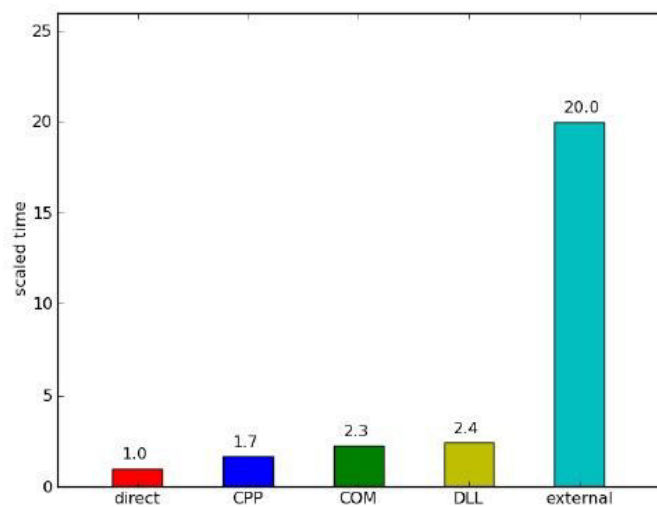
Figure II.5: Time performance comparison of different software coupling with PHREEQC. External stands for loose coupling between PHREEQC and Python, Dll stands for Python and iPhreeqc dynamic library, COM stands for Python and iPhreeqc Microsoft component object, CPP stands for C++ with the dynamic library, and direct stands for PHREEQC alone (Müller et al., 2011).

Since its release, PHREEQC has been widely used. It was first coupled with COMSOL in order to solve unsaturated flow with Richard's equation, expanding, therefore, the capabilities of PHREEQC (Wissmeier and Barry, 2011), and afterwards the same coupling was used to assess the possibility of plant growth in a system with bauxite residue sand (Wissmeier *et al.*, 2011). It has also used to simulate a closed circuit recycled board mill to study the problematic of scale deposits and generated sludge when biocide treatment occurs by coupling iPhreeqc with the mass flow balance simulator PS2000 (Huber *et al.*, 2013). Another COMSOL-iPhreeqc coupling was made in order to model large scale thermo-hydro-chemical

problems (Nardi *et al.*, 2014). In Jensen *et al.* (2014), iPhreeqc is coupled to a 1D finite element model where multi-species transport and the Poisson-Nernst-Plank equation are considered to model the leaching of a cement-based material. The same software coupling is also used to compare between two C-S-H descriptions : a solid-solution model (Kulik, 2011) and a surface complexation model (Nonat, 2004), as well as to model the ingress of chloride in mortar, a phenomena that occurs in mortar structures near see-water (Jensen, 2014). In Florez *et al.* (2015) iPhreeqc is coupled to a control volume radial basis function method that serves as a transport solver, the coupling uses a Richardson extrapolation in order to increase the order of the operator splitting approach. To exploit the parallelization capabilities offered by the operator splitting approaches and iPhreeqc, a coupling between iPhreeqc and OpenGeoSys for thermo-hydro-mechanical-chemical problems was undertaken (He et al., 2015). Other couplings between different software can be found in literature such as the coupling between UTCHEM-iPhreeq (Kazemi Nia Korrani et al., 2015, 2016b), UTCOMP-iPhreeq (Kazemi Nia Korrani et al., 2016a), and Feflow-iPhreeqc (de Sousa, 2012).

The iPhreeqc API has allowed to implement the interaction between different types of transport-hydro-mechanical codes and PHREEQC (Muniruzzaman and Rolle, 2016; Patel *et al.*, 2014; Perko *et al.*, 2015). Although iPhreeqc provides access to all the reaction capabilities of PHREEQC, it might require extensive coding, since the commands given to obtain the concentrations in mol/kgw and kg/L from PHREEQC are not the same and might require external calculations. In order to make iPhreeqc more generic and to avoid extensive coding, PhreeqcRM was released (Parkhurst and Wissmeier, 2015). PhreeqcRM is build upon iPhreeqc, hence the capabilities of iPhreeqc are retained. PhreeqcRM tries to simplify the coding between software by introducing some class methods that can be found in the different couplings between iPhreeqc and other software such as changing units, obtaining the values of O and H components in order to be transported, or getting the aqueous species for a multi-species approach (Masi *et al.*, 2017).

II.4 Insight into the operator spliting error and its combination with numerical methods

In section II.1, the different operator splitting methods in TReacLab have been categorized with a first or second temporal truncation order. Here we provide a more detailed

analysis in order to answer how the operator splitting error is obtained. To that purpose, we assume that all the reactions are differentiable kinetic functions. The first section addresses the error introduced by the sequential splitting using Taylor series, the same approach might be applied to other operator splitting methods. The second section builds upon the concepts developed in the first part to show a more practical use.

II.4.1 Error of the operator splitting methods

We consider an abstract initial value problem:

$$\frac{dc}{dt} = f(t, c(t)), \qquad c(t = 0) = c_0, \qquad 0 \le t \le T, \qquad \text{(II.33)}$$

In order to apply an operator scheme, the linear or non-linear function $f(t, c(t))$ is decomposed into the sum of two simpler operators: $f(t, c(t)) = f_1(t, c(t)) + f_2(t, c(t))$ which are assumed to be solved exactly. Usually, in reactive transport, the operators are transport (e.g. f_1) and chemistry (e.g. f_2), but different decompositions are possible (Clement et al., 1998). We analyze the local error of the sequential splitting for its first iteration, being τ the splitting time step (Geiser, 2009):

$$\frac{\partial c^1}{\partial t} = f_1(t, c(t)), \qquad c^1(0) = c_0, \qquad 0 \le t \le \tau, \qquad \text{(II.34)}$$

$$\frac{\partial c^2}{\partial t} = f_2(t, c(t)), \qquad c^2(0) = c^1(\tau), \qquad 0 \le t \le \tau \qquad \text{(II.35)}$$

$$c_{os}(\tau) = c^2(\tau). \qquad \text{(II.36)}$$

The local truncation error is defined by the difference between the exact solution and the split solution:

$$\varepsilon_n(\tau) = c(\tau) - c_{os}(\tau), \qquad \text{(II.37)}$$

where $\varepsilon_n(\tau)$ is the local truncation error, $c(\tau)$ is the exact solution after one splitting time step and $c_{os}(\tau)$ is the splitting solution after one splitting time step. The same convention as Csomós et al. (2005) is followed, namely:

$$\varepsilon_n(\tau) = \mathcal{O}(\tau^{p+1}), \qquad \text{(II.38)}$$

with some $p > 0$. Then, it is said that the splitting scheme is pth-order scheme. In order to prove that the sequential splitting has a first-order local error, we expand the exact solution around $t = 0$ using Taylor series:

$$c(\tau) = c_0 + \tau \frac{dc}{dt}\Big|_{t=0} + \frac{\tau^2}{2}\frac{d^2c}{dt^2}\Big|_{t=0} + \mathcal{O}(\tau^3),\tag{II.39}$$

combining equation (II.33), equation (II.39) and knowing that $f(t, c(t)) = f_1(t, c(t)) + f_2(t, c(t))$, leads to:

$$c(\tau) = c_0 + \tau(f_1 + f_2) + \frac{\tau^2}{2}\left(\frac{\partial f_1}{\partial t} + \frac{\partial f_1}{\partial c}(f_1 + f_2) + \frac{\partial f_2}{\partial t} + \frac{\partial f_2}{\partial c}(f_1 + f_2)\right) + \mathcal{O}(\tau^3)\tag{II.40}$$

The functions f_1, f_2 and theirs derivatives are evaluated at $(0, c_0)$. We now apply Taylor series at $t = 0$ to the sequential splitting method (equation (II.34)-(II.36)). Such that:

$$c^2(\tau) = c^2(0) + \tau \frac{dc^2}{dt}\Big|_{t=0} + \frac{d^2c^2}{dt^2}\Big|_{t=0} + \mathcal{O}(\tau^3) = c^1(\tau) + \tau f_2$$
$$+ \frac{\tau^2}{2}\left(\frac{\partial f_2}{\partial t} + \frac{\partial f_2}{\partial c}f_2\right) + \mathcal{O}(\tau^3)\tag{II.41}$$

Notice that in equation (II.41) in comparison to equation (II.40), f_2 and its derivatives are evaluated at $(0, c^1(\tau))$. Before calculating the error (equation (II.37)), since $c^2(0) = c^1(\tau)$ as stated in equation (II.35), the terms $c^1(\tau)$, $f_2(0, c^1(\tau))$, $\frac{\partial}{\partial t}f_2(0, c^1(\tau))$ and $\frac{\partial}{\partial c}f_2(0, c^1(\tau))$ must be expanded and substituted in equation (II.41). Now, we expand $c^1(\tau)$:

$$c^1(\tau) = c^1(0) + \tau \frac{dc^1}{dt}\Big|_{t=0} + \frac{d^2c^1}{dt^2}\Big|_{t=0} + \mathcal{O}(\tau^3) = c_0 + \tau f_1 + \frac{\tau^2}{2}\left(\frac{\partial f_1}{\partial t} + \frac{\partial f_1}{\partial c}f_1\right) + \mathcal{O}(\tau^3)\tag{II.42}$$

Here, f_1 and its derivatives are evaluated at $(0, c_0)$. Now, we should expand $f_2(0, c^1(\tau))$, $\frac{\partial}{\partial t}f_2(0, c^1(\tau))$ and $\frac{\partial}{\partial c}f_2(0, c^1(\tau))$. Since:

$$f(0, y_0 + a) = f(0, y_0) + a\frac{\partial f(0, y_0)}{\partial c} + \frac{a^2}{2}\frac{\partial^2 f(0, y_0)}{\partial c^2} + \mathcal{O}(\tau^3),\tag{II.43}$$

and with $c^1(\tau) = y_0 + a = c_0 + \mathcal{O}(\tau)$, we can extend $f_2(0, c^1(\tau))$, $\frac{\partial}{\partial t}f_2(0, c^1(\tau))$ and $\frac{\partial}{\partial c}f_2(0, c^1(\tau))$:

$$f_2(0, c^1(\tau)) = f_2 + \left[\tau f_1 + \frac{\tau^2}{2}\left(\frac{\partial f_1}{\partial t} + \frac{\partial f_1}{\partial c}f_1\right)\right]\frac{\partial f_2}{\partial c} + \frac{\tau^2 f_1^2}{2}\frac{\partial^2 f_2}{\partial c^2} + \mathcal{O}(\tau^3).\tag{II.44}$$

$$\frac{\partial}{\partial t}f_2\big(0, c^1(\tau)\big) = \frac{\partial f_2}{\partial t} + \left[\tau f_1 + \frac{\tau^2}{2}\left(\frac{\partial f_1}{\partial t} + \frac{\partial f_1}{\partial c}f_1\right)\right]\frac{\partial^2 f_2}{\partial t^2} + \frac{\tau^2 f_1^2}{2}\frac{\partial^3 f_2}{\partial t^3} + \mathcal{O}(\tau^3). \tag{II.45}$$

$$\frac{\partial}{\partial c}f_2\big(0, c^1(\tau)\big) = \frac{\partial f_2}{\partial c} + \left[\tau f_1 + \frac{\tau^2}{2}\left(\frac{\partial f_1}{\partial t} + \frac{\partial f_1}{\partial c}f_1\right)\right]\frac{\partial^2 f_2}{\partial c^2} + \frac{\tau^2 f_1^2}{2}\frac{\partial^3 f_2}{\partial c^3} + \mathcal{O}(\tau^3). \tag{II.46}$$

Notice that in equations (II.44-II.46), the evaluation point is $(0, c_0)$. Substituting equations (II.42) and (II.44-II.46) into equation (II.41) until the second-order terms of the Taylor expansion would lead to:

$$c^2(\tau) = c_0 + \tau\big(f_1 + f_2\big) + \frac{\tau^2}{2}\left(\frac{\partial f_1}{\partial t} + \frac{\partial f_1}{\partial c}f_1 + \frac{\partial f_2}{\partial t} + \frac{\partial f_2}{\partial c}\big(2 f_1 + f_2\big)\right) + \mathcal{O}(\tau^3). \tag{II.47}$$

hence, the local truncation error is:

$$\varepsilon_n(\tau) = c(\tau) - c_{os}(\tau) = \frac{\tau^2}{2}\left(\frac{\partial f_1}{\partial c}f_2 - \frac{\partial f_2}{\partial c}f_1\right) + \mathcal{O}(\tau^3), \tag{II.48}$$

Similar results are found in Hundsdorfer and Verwer (2013), and Simpson and Landman (2007). Equation (II.48) shows that in order to obtain a second order solution (equation (II.38)), the terms $\frac{\partial f_1}{\partial c}f_2$ and $\frac{\partial f_2}{\partial c}f_1$ must be equal. This equality is known in Lie-algebra by L-commutativity. The application of the Lie operator formalism and the Baker-Campbell-Hausdorff formula help to apply L-commutativity analysis (Lanser and Verwer, 1999). If all the operators show L-commutativity amongst them and each operator is solved exactly, the split solution must be equal to the exact solution. For the Strang and SWS methods, the commutation of some of the operators might increase the order of the scheme (Farago and Havasi, 2005). If a sequential or Strang method is applied, the solution depends on the order in which the operators are applied unless the operators commute (Holden *et al.*, 2010), such behavior is not given in the additive or SWS methods, since the order does not modify the error expression. The alternating splitting applies a sequential splitting changing the order of the operators after each time step, since the error for each order of operators is the same but with opposite sign, implying that the order can be reduced with small enough splitting time steps (Simpson and Landman, 2008).

The Taylor series analysis described here can be applied to other operator splitting approaches, such as Strang or additive, in order to obtained the local theoretical truncation error. Such analyses are cumbersome, therefore the application of Lie formalism to find the

error is usually more widespread in the literature (Lanser and Verwer, 1999; Sportisse, 2000). Such analyses may fail for stiff problems (Sportisse, 2000).

II.4.2 Operator splitting methods and numerical methods

In Simpson and Landman (2008), the functions f_1 and f_2 are substituted by a linear discretization of the transport operator using a Crank-Nicolson finite difference method represented by $f_1 = L(u) = Au + b$, where A is the spatial discretization, b is a term generated by the boundary conditions. The reaction operator is $f_2 = F$, which is solved either with analytical solution or with a Runge-Kutta algorithm. Then, the substitution of the operators into equation (II.48) gives:

$$E_i^{TR}(\tau) = \frac{\tau}{2}\left(\sum_{j=1}^m \frac{\partial F_i}{\partial u_j}\left(A_j u_j + b_j\right) - A_i F_1\right) + \mathcal{O}(\tau^2), \tag{II.49}$$

where i and j represent the number of components or species, and TR stands for sequence of operators transport-chemistry. This equation (II.49) might be separated in two parts: a boundary error part and an internal error part:

$$E_i^{TR}(\tau) = \frac{\tau}{2}\left(\sum_{j=1}^m \frac{\partial F_i}{\partial u_j} b_j\right) + \frac{\tau}{2}\left(\sum_{j=1}^m \frac{\partial F_i}{\partial u_j} A_j u_j - A_i F_1\right) + \mathcal{O}(\tau^2), \tag{II.50}$$

In equation (II.50), the first term of the right-hand side is related to the boundary error (Kaluarachchi and Morshed, 1995; Morshed and Kaluarachchi, 1995; Valocchi and Malmstead, 1992), and the second term is related to the internal error.

Such approaches can help to give a physical insight. Consider the following system:

$$\frac{\partial c_1}{\partial t} = D_1 \frac{\partial^2 c_1}{\partial x^2} - v_1 \frac{\partial c_1}{\partial x} + F_1(c_1), \tag{II.51}$$

$$\frac{\partial c_2}{\partial t} = D_2 \frac{\partial^2 c_2}{\partial x^2} - v_2 \frac{\partial c_2}{\partial x} + F_2(c_1, c_2), \tag{II.52}$$

where the advection and diffusion term are part of a linear transport operator and $F_1(c_1)$ and $F_2(c_1, c_2)$ are part of the chemistry operator. It is possible to calculate the operator splitting error of c_2 solved by a sequential splitting approach, applying equation (II.49):

$$E_{c_2}^{TR}(\tau) = \frac{\tau}{2}\left[\frac{\partial F_2}{\partial c_1} A_1 c_1 + \frac{\partial F_2}{\partial c_2} A_2 c_2 - A_2 F_2\right]. \tag{II.53}$$

To simplify the explanation, homogeneous boundary conditions are selected ($b_j = 0$), and A_i is a linear transport operator for two components or species (dependent variables). The development of the error is as follows:

$$E_{c_2}^{TR}(\tau) = \frac{\tau}{2}\left[\frac{\partial F_2}{\partial c_1}\left(D_1\frac{\partial^2 c_1}{\partial x^2} - v_1\frac{\partial c_1}{\partial x}\right) + \frac{\partial F_2}{\partial c_2}\left(D_2\frac{\partial^2 c_2}{\partial x^2} - v_2\frac{\partial c_2}{\partial x}\right) - D_2\frac{\partial^2 F_2}{\partial x^2} + v_2\frac{\partial F_2}{\partial x}\right]. \qquad \text{(II.54)}$$

We expand the terms $\frac{\partial^2 F_2}{\partial x^2}$ and $\frac{\partial F_2}{\partial x}$ using the chain rule and remove the terms that cancel each other such as the second term of the right-hand side equation (II.53), namely $\frac{\partial F_2}{\partial c_2}A_2c_2$:

$$E_{c_2}^{TR}(\tau) = \frac{\tau}{2}\left[(D_1 - D_2)\frac{\partial F_2}{\partial c_1}\frac{\partial^2 c_1}{\partial x^2} - D_2\left(\frac{\partial^2 F_2}{\partial c_1^2}\left(\frac{\partial c_1}{\partial x}\right)^2 + 2\frac{\partial^2 F_2}{\partial c_1 c_2}\frac{\partial c_1}{\partial x}\frac{\partial c_2}{\partial x} + \right.\right.$$
$$\left.\left. \frac{\partial^2 F_2}{\partial c_2^2}\left(\frac{\partial c_2}{\partial x}\right)^2\right) + (v_2 - v_1)\frac{\partial F_2}{\partial c_1}\frac{\partial c_1}{\partial x}\right], \qquad \text{(II.55)}$$

Now, we have a general expression for characterizing the local truncation error derived from a two species or components, we see that the internal error can be reduced if $D_1 = D_2$ and $v_2 = v_1$. Now, we can substitute the values of $F_1(c_1)$ and $F_2(c_1, c_2)$ for:

$$F_1(c_1) = -k_1 c_1, \qquad \text{and} \qquad F_2(c_1, c_2) = k_2 c_1 - k_3 c_2 \qquad \text{(II.56)}$$

The same values are used by Simpson and Landman (2008), which leads to:

$$E_{c_2}^{TR}(\tau) = \frac{\tau}{2}\left[(D_1 - D_2)\frac{\partial F_2}{\partial c_1}\frac{\partial^2 c_1}{\partial x^2} + (v_2 - v_1)\frac{\partial F_2}{\partial c_1}\frac{\partial c_1}{\partial x}\right], \qquad \text{(II.57)}$$

and $E_1^{TR}(\tau) = 0$, that implies that single species transport with a first-order decay reaction such as the first test of the submitted paper (section II.1) does not suffer from internal operator splitting in the case of applying a sequential splitting, but a splitting error will be introduced by the flux boundary condition (Equation (II.50)). Equation (II.55) shows that if a species is coupled to another through the chemical term $F_2(c_1, c_2)$ and a sequential splitting is applied, an internal error arises from the difference of velocity and diffusion. Such internal error is expected in systems which have two mobile phases and use multi-species diffusion.

The derivation of the splitting truncation error is cumbersome and can be tedious and complex for large coupled systems. Its use might be restricted to small problems in order to give a mathematical insight into the factors that can produce errors. For larger systems, symbolic computation might be a solution.

CHAPTER 3: ATMOSPHERIC CARBONATION

III ATMOSPHERIC CARBONATION

In section II.1, the main features of the carbonation concrete process, and the possible issues associated to the ILW-LL concrete over pack that can occur due to atmospheric carbonation, have been described. In this section we get into the details of atmospheric carbonation from a theoretical point of view and give some preliminary results.

III.1 Concrete conceptualization

III.1.1 Geometry

Figure III.1 shows the floor plan view of the concrete structure. The thickness of the concrete wall is 110 mm. The reinforcing bars of the concrete are placed in the middle of the 110 mm thickness concrete structure. Since we are only interested in the atmospheric carbonation over concrete, and considering that the intrusion of gaseous dioxide carbonate is given in both sides of the structure. The problem can be reduced to a half-wall (55 mm) of concrete by imposing a symmetry condition at the end where the reinforcing bars are placed, namely the flux for transport and flow continuum equations is zero. If we assume that the solid is an isotropic material, the half-wall of concrete can be simplified into a 1D Cartesian problem. Therefore, the modelization of the concrete structure is defined by a simple 1D interval with its correspondent initial and boundary conditions.
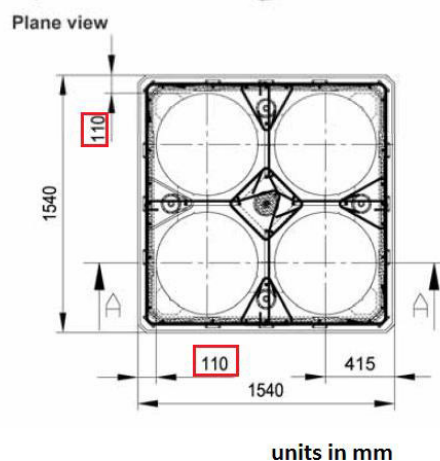

Figure III.1: Floor plan view of the concrete structure containing four primary ILW-LL (ANDRA, 2005).

III.1.2 Concrete composition

The concrete composition is a mix of aggregates (coarse gravel or crushed rocks such as limestone or granite), cement (commonly Portland cement), and water. After combining cement, water and aggregates, the hydration process starts (Bullard *et al.*, 2011). During the process, water and cement form a paste that binds together the aggregates until the paste hardens. The mixture and the hydration process determine the properties of the concrete (Taylor, 1997). The concrete planned to create the package is of type HPC CEM-I. HPC stands for high performance concrete, and CEM-I stands for Portland cement comprising portland and up to 5% of minor additional constituents according to the European EN 197 standard. The initial state of the chemical phases in the concrete is given by Table III-1.

Mineral	Volume fraction	Molar volume (cm^3/mol)
Portlandite	0.057	33.056
CSH 1.6	0.138	84.68
Ettringite	0.036	710.32
Hydrotalcite	0.003	227.36
C3FH6	0.021	154.50
Monocarboaluminate	0.024	261.96
Calcite	0,721	36.934

Table III-1: initial composition of the concrete package.

The initial composition is in equilibrium with a pore solution which components and associated primary species can be seen in Table III-2. The selection of the component name and the primary species is established by the Thermochimie version 8 database developed by Andra (https://www.thermochimie-tdb.com/).

Components	Na	K	Ca	S	C	Al	Si	Fe	Mg	Cl	H	O	E
Primary Species	Na^+	K^+	Ca^{2+}	SO_4^{2-}	CO_3^{2-}	Al^{3+}	$H_4(SiO_4)$	Fe^{2+}	Mg^{2+}	Cl^-	H^+	H_2O	e^-

Table III-2: Initial aqueous components and its associated primary species according to the thermochimie database version 8.

Once the concrete degradation starts caused by the carbonation process, the precipitation of secondary minerals will occur. Table III-3 shows possible secondary mineral phases.

Phase type	Phases
Oxides	Amorphous silica,
Hydroxides	Amorphous Gibbsite, Brucite, Iron Hydroxyde
Sheet silicates	Sepiolite
Other silicates	CSH 0.8, CSH 1.2, Katoite silicate, , Straetlingite
Sulfates, chlorides and other salts	Burkeite, Syngenite, Gypsum
Others	Hydrotalcite, Dawsonite, Ettringite

Table III-3: Mineral secondary phases.

III.1.3   Decoupling atmospheric carbonation processes

The atmospheric carbonation can be decoupled in three processes: fluid flow, mass transport and geochemical processes.

III.1.3.1   Fluid flow

The drying of the concrete is one of the main factors that take place during atmospheric carbonation. Drying will change the saturation levels affecting the diffusion of the gaseous species and aqueous species. The drying of the concrete is modeled through continuum flow equations. The single -phase fluid equation satisfies the following macroscopic continuity equation (Ewing, 1991):

$$\frac{\partial(\phi\rho)}{\partial t} + \nabla \cdot (\rho v) = \rho q, \tag{III.1}$$

where ϕ the porosity (-), ρ the density of the phase (ML^{-3}), v is the Darcy velocity (equation (I.9)) (LT^{-1}), and q is a source/sink term (ML^{-3}T^{-1}). Equation (III.1) can be extended to multiphase flow considering that the phases are immiscible (Lie, 2014):

$$\frac{\partial(S_\alpha\phi\rho_\alpha)}{\partial t} + \nabla \cdot (\rho_\alpha v_\alpha) = \rho_\alpha q, \tag{III.2}$$

where the subscript α denotes the phase of consideration (e.g. water phase, gaseous phase, NAPLs), and S_α is the saturation of the phase α. The saturation is a ratio between the volume occupied by the mobile phase and the volume of void space in the representative element volume. Consequently, the sum of the saturation of each phase is equal to 1. In order to calculate Darcy velocity of the phase α, the Darcy's law must also be extended:

$$v_\alpha = -\frac{K_\alpha}{\mu_\alpha}(\nabla p_\alpha - \rho_\alpha g). \tag{III.3}$$

The parameters are the same as that of equation (I.9) for the corresponding phase α, except for K_α which is the phase permeability:

$$K_\alpha = K_s\, K_{r\alpha}(S_\alpha), \tag{III.4}$$

where K_s is the intrinsic permeability that is affected by changes in the solid matrix such as dissolution and precipitation (Samson and Marchand, 2006), and $K_{r\alpha}$ is the relative permeability which depends on the saturation of the phase. The relative permeability accounts for the flow paths of the phase α when other phases are presented, it ranges from 0 (no phase α) to 1 (fully saturation). The simplest permeability models is Corey (Corey, 1954):

$$K_{rw} = \left(\hat{S}_w\right)^{n_w} k_w^0, \tag{III.5}$$

$$K_{rw} = \left(1 - \hat{S}_w\right)^{n_O} k_O^0, \tag{III.6}$$

where the terms k_O^0, k_w^0, n_w, n_O are fitting parameters and $\hat{S}_w$ is the normalized (or effective) water content:

$$\hat{S}_w = \frac{S_w - S_w^{min}}{S_w^{max} - S_w^{min}}. \tag{III.7}$$

Other common models for the relative permeability are the Brooks-Corey functions (Brooks and Corey, 1964):

$$K_{rw} = \left(\hat{S}_w\right)^{n_1 + n_2 n_3}, \tag{III.8}$$

$$K_{rw} = \left(1 - \hat{S}_w\right)^{n_1}\left[1 - \left(\hat{S}_w\right)^{n_2}\right]^{n_3}, \tag{III.9}$$

and the van Genuchten-Mualem model (Van Genuchten, 1980):

$$K_{rw} = \hat{S}_w\left[1 - (1 - \left(\hat{S}_w\right)^{1/m})^m\right]^2, \tag{III.10}$$

$$K_{rw} = \left(1 - \hat{S}_w\right)^{\kappa}\left[1 - \left(\hat{S}_w\right)^{1/m}\right]^{2m}, \tag{III.11}$$

where the parameters n_1, n_2, n_3, m, and κ depend on the soil properties.

In a carbonation problem, we face a system made up of two mobile phases: gaseous and liquid (water). Then, If we coupled equation (III.2) and (III.3), the system is described by:

$$\frac{\partial (S_l \phi \rho_l)}{\partial t} + \nabla \cdot \left(-\rho_l \frac{K_l}{\mu_l} (\nabla p_l - \rho_l g) \right) = \rho_l q, \tag{III.12}$$

$$\frac{\partial (S_g \phi \rho_g)}{\partial t} + \nabla \cdot \left(-\rho_g \frac{K_g}{\mu_g} (\nabla p_g - \rho_g g) \right) = \rho_g q. \tag{III.13}$$

The subscript l stands for liquid and the subscript g for gas. The system counts with four dependent variables S_l, S_g, p_l, and p_g. In order two work with just two variables, two constitutive relationships are needed. The relationship between saturations have been already commented:

$$S_l + S_g = 1. \tag{III.14}$$

The other arises from the interface between the liquid and the gaseous phase, known as capillary force (Miller *et al.*, 1998). On a molecular level, when two fluids are present in a pore space, the molecules of one fluid are attracted to the solid by adhesive forces, such fluid is known as the wetting phase fluid. The molecules of the other fluid are attracted to the wetting fluid by cohesive forces, such fluid is known as the non-wetting phase fluid. In a hydrophilic porous media like concrete, water is the wetting phase (Szymkiewicz, 2012). The difference of pressure at the fluid-fluid interface gives rise to the capillary pressure:

$$p_c = p_g - p_l. \tag{III.15}$$

The capillary pressure is assumed to be function of the liquid saturation, $p_c(S_l)$ (Chen *et al.*, 1994). The relationship between the capillary pressure and the water saturation shows hysteresis (Figure III.2), the hysteresis might be explained by the different value of the wetting angle when the fluid advances or recedes, the pore-scale trapping of air and by the ink-bottle effect (Pinder and Gray, 2008). An example of hysteresis models are the Parlange (1976) model, the Likos and Lu (2004) model, or Zhou (2015). In this work we do not use hysteric models and will work only with the capillary curve which are monotonic functions. The most common curves are the Brooks and Corey (1964):

$$\hat{S}_w = \begin{cases} (p_c/p_e)^{-n_b}, & \text{if } p_c > p_e \\ 1, & p_c \leq p_e \end{cases} \tag{III.16}$$

and the Van Genuchten (1980):

$$\hat{S}_w = \left(1 + \left(\beta_g p_c\right)^{n_g}\right)^{-m_g}, \tag{III.17}$$

where p_e is the entry pressure of air, $n_b \in [0.2, 5]$, n_g and m_g are related to the pore-size distribution and β_g is a scaling parameter.
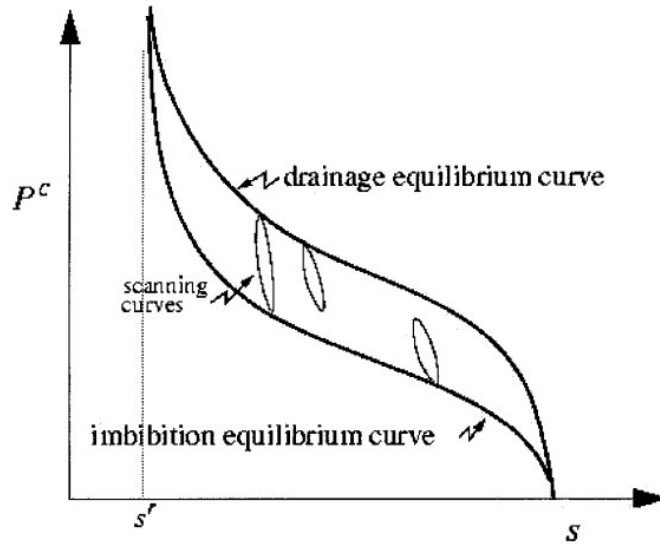
Figure III.2: Typical capillary pressure-water saturation curve (Hassanizadeh et al., 2002).

The capillary pressure can also be related to the air relative humidity by Kelvin equation (Or and Wraith, 2002):

$$p_c = \frac{RT\rho}{M} \ln(H_r). \tag{III.18}$$

where R is the universal gas constant ($L^2MN^{-1}\Theta^{-1}T^{-1}$), T is the temperature (T), ρ the density of the water (ML^{-3}), M is the mole mass of water (N), and H_r is the relative air humidity (-).

The two-phases system can be solved by the use of equations (III.12)-(III.15) comprised by two PDEs and two algebraic relationships, we assume that functions for the capillary pressure, and permeability relative are known (They are discussed later in this section). The selection of the primary variables lead to different formulations that affect the behavior of numerical simulations. Furthermore, artificial variables are usually used, since they have better mathematical properties (Bastian, 1999; Douglas *et al.*, 1959).

The two-phases model can be simplified by assuming that the gaseous phase is continuous in the pore space and connected to the atmosphere (Szymkiewicz, 2012). Therefore, the pressure of the gaseous phase can be considered constant. Hence, the capillary pressure depends only in the liquid pressure, therefore usually the gaseous pressure is set to 0, namely $p_g = p_{atm} = 0$, thus:

$$p_c = -p_l. \tag{III.19}$$

Such approach implies that liquid saturation and also relative permeability can be defined by water pressure. The liquid saturation and relative permeability of equation (III.12) depend now on the water pressure, and the gaseous equation (III.13) is removed from the system since $p_g = 0$:

$$\frac{\partial (S_l(p_l)\phi\rho_l)}{\partial t} + \nabla \cdot \left(-\rho_l \frac{K_l(p_l)}{\mu_l}(\nabla p_l - \rho_l g) \right) = \rho_l q, \tag{III.20}$$

The accumulation term can be expanded by the chain rule. Furthermore we assume that there is no porosity change, we use the fact that liquid saturation and density are functions of liquid pressure, and that the volumetric content (θ) is defined by the porosity times the l:

$$
\begin{aligned}
\frac{\partial (S_l\phi\rho_l)}{\partial t} &= \rho_l\phi\frac{\partial S_l}{\partial t} + \rho_l S_l\frac{\partial \phi}{\partial t} + \phi S_l\frac{\partial \rho_l}{\partial t} = \rho_l\phi\frac{\partial S_l}{\partial p_l}\frac{\partial p_l}{\partial t} + \phi S_l\frac{\partial \rho_l}{\partial p_l}\frac{\partial p_l}{\partial t} = \\
&\rho_l\frac{\partial \theta_l}{\partial p_l}\frac{\partial p_l}{\partial t} + \theta_l\frac{\partial \rho_l}{\partial p_l}\frac{\partial p_l}{\partial t} = \left(\rho_l\frac{\partial \theta_l}{\partial p_l} + \theta_l\frac{\partial \rho_l}{\partial p_l} \right)\frac{\partial p_l}{\partial t}
\end{aligned}
\tag{III.21}
$$

The term in parenthesis of equation (III.21) is the storage coefficient, usually denote by C_{lp}. Equation (III.21) can be introduced into (III.20) and the new equation can be divided by the density, leading to the generalized Richards' equation (Lie, 2014):

$$C'_{lp}\frac{\partial (\rho_l)}{\partial t} - \nabla \cdot \left(\frac{K_l(p_l)}{\mu_l}(\nabla p_l - \rho_l g) \right) = q, \tag{III.22}$$

where $C'_{lp} = C_{lp}/\rho_l$. If we use the pressure head ($h = p_l/\rho_l g$) as dependent variable instead of the liquid pressure, and neglect the liquid compressibility $\frac{\partial \rho_l}{\partial p_l}$. We obtain the classical h-based form of Richards' equation (Richards, 1931):

$$C\frac{\partial (h)}{\partial t} - \nabla \cdot \left(\boldsymbol{K}(h)(\nabla h - 1) \right) = q, \tag{III.23}$$

where $C = \frac{\partial \theta_l}{\partial h}$ is the specific moisture capacity function (L^{-1}) and $\mathbf{K}(h)$ is the unsaturated hydraulic conductivity (LT^{-1}). The Brooks and Corey model (equation (III.16)) is now given by:

$$\hat{S}_w = \begin{cases} \dfrac{1}{|\alpha h|^n}, & if\ h < 0 \\ 1, & h \geq 1 \end{cases} \qquad \text{(III.24)}$$

and the Van Genuchten by:

$$\hat{S}_w = \begin{cases} \dfrac{1}{[1 + |\alpha h|^n]^m}, & if\ h < 0 \\ 1, & h \geq 1 \end{cases} \qquad \text{(III.25)}$$

where n, α and m are parameters related to the medium.

In order to solve the fluid flow for the atmospheric carbonation we might rely on one of the different formulations of the two-phase equations or in the Richards' equation. Richards' equation have been criticized for neglecting the role of preferential paths which increase the speed of infiltration (Beven and Germann, 2013; Nimmo, 2012), although the implementation of Richards' equations in models such as dual permeability or porosity tries to account for preferential paths (Gerke and van Genuchten, 1993; Šimůnek *et al.*, 2003). In our case, since we assume that there are not cracks on the concrete and that the intrinsic permeability is homogeneous and low, we do not expect preferential paths. Moreover, it has been also criticized for neglecting the capillary pressure (Niessner and Hassanizadeh, 2008), but in the case of drying for weakly permeable materials such as a concrete type: HPC CEM-I, Richard's equation considering only the liquid phase might be even better than a multiphase approach (Mainguy *et al.*, 2001).

III.1.3.2   Multicomponent Transport

Following equation (7) of section II.1, the multicomponent equation in a case of concrete atmospheric where gas, solid, and aqueous phase coexist can be written as (Zilberbrand, 2011):

$$\frac{\partial \theta_l u_l}{\partial t} + \frac{\partial \theta_g u_g}{\partial t} + \frac{\partial \theta_s u_s}{\partial t} = L(u_l) + L(u_g) + US\,_k^t r_k + UQ, \qquad \text{(III.26)}$$

where u_l, u_g, u_s are the component concentration for the liquid, gas or solid (ML^{-3}), $\theta_l, \theta_g, \theta_s$ are the volumetric content of each phase (-), $L(*)$ is the transport operator which is applied only to the mobile components (liquid and gas phases) (ML^{-3}T^{-1}), S_k^t is the transposed stoichiometric matrix for kinetic reactions, r_k is the reaction rate (ML^{-3}T^{-1}), U is the component matrix, and Q is a source/sink term. The total component concentration is given by the sum of the liquid, gas and solid component concentration vectors, $u = u_l + u_g + u_s$, and equation (5) of section II.1 relates component concentration with species concentration $u = Uc$.

III.1.3.3 Geochemical reactions

The atmospheric carbonation process involves homogeneous and heterogeneous reactions. We consider only homogeneous reactions in the aqueous phase, and as heterogeneous reactions we choose the reactions involved in the transfer of mass between gas and liquid, and liquid and solid.

The homogeneous equations considered here, are those that are included in PHREEQC database Thermochimie version 8 such as dissociation, or acid-base reaction. The transfer of mass between the solid matrix and the aqueous solution is modeled by precipitation and dissolution reactions. The minerals are modeled as pure phase, namely not solid solution conceptualization is used. If precipitation/dissolution processes are treated as equilibrium reactions, their equation is given by the mass action law combined with the saturation index (Parkhurst and Appelo, 1999):

$$SI \, K_J = \prod_{i=1}^{N_{aq}} \langle c_i \rangle^{s_{ij}} \tag{III.27}$$

where N_{aq} stands for the aqueous species involved in the reaction, $\langle c_i \rangle$ is the activity of the species i, K_J is the equilibrium constant of the reaction j, s_{ij} is the stoichiometric coefficient, and SI is the saturation index. The saturation index states the relationship between solution and solid, it can be supersaturated ($SI > 0$), in equilibrium ($SI = 0$) or undersaturated ($SI < 0$). The pure phase minerals have a constant activity, hence the activity of the pure phase is equal to 1 by convention (Appelo and Postma, 2004). The saturation index, the

logarithm of the quotient of the ion-activity product and the solubility constant, are set to zero, in order to force equilibrium between the different mineral phases and the aqueous solution.

If a kinetic approach is chosen, the precipitation/dissolution processes are modeled by the transition state theory which states that the reactants are in equilibrium with another species of higher Gibbs free energy known as transition state complex. The rate equation is described by (Lasaga *et al.*, 1994):

$$r_j = \pm k_j A_j \left| 1 - SI_j^n \right|^\eta, \tag{III.28}$$

where r_j is the rate, positive values represent dissolution processes and negatives precipitation processes, k_j is the kinetic constant, A_j is the reactive surface per mass of water, SI_j is the saturation index, and n and η are empirical parameters, and the subscript j stand for the reaction j.

The gas-liquid interactions are assumed to be in equilibrium and are modeled by the Henry's law (Steefel *et al.*, 2015):

$$f_j = K_{Hj}^{-1} \prod_i^{N_{aq}} \langle c_i \rangle^{s_{ij}}, \tag{III.29}$$

where f_j is the fugacity of the gas species j, K_{Hj} is the Henry constant of the gas species j, $\langle c_i \rangle$ is the activity of the aqueous component i, and s_{ij} the stoichiometric value of the gas species j and the aqueous component i. The fugacity is related to the partial pressure of the water by:

$$f_j = p_j \delta_j, \tag{III.30}$$

where δ_j is the fugacity coefficient of the gas j, and p_j is the partial pressure of the gas j. Ideal gases have a fugacity coefficient equal to 1, therefore its fugacity is equal to its partial pressure. PHREEQC uses or ideal gases or gases under the Peng-Robinson model (Peng and Robinson, 1976).

III.2 First modeling approach to the atmospheric carbonation problem

In this section we detail our first approaches to model the atmospheric carbonation problem. We document the approach and expose some preliminary results.

III.2.1   Constant saturation test

III.2.1.1   Coupling procedure and hydraulic properties

In this test, it is assumed that all reactions are in equilibrium, there are no external sink/source, saturation is constant, diffusion is the only transport mechanism, and the amount of water released from the dissolution of hydrated products is ignored. The component mass balance for a component in 1D is given by:

$$\frac{\theta_l \partial c_l}{\partial t} + \frac{\theta_g \partial c_g}{\partial t} + \frac{\theta_s \partial c_s}{\partial t} = \frac{\partial}{\partial x} \cdot \left(D_l \frac{\partial}{\partial x}(c_l) + D_g \frac{\partial}{\partial x}(c_g) \right), \qquad \text{(III.31)}$$

where θ_l, θ_g, θ_s, c_l, c_g and c_s are the volumetric content and component concentration for liquid, gas and solid respectively. The diffusion values D_l, and D_g are calculated from the Millington-Quirk equation (Millington, 1959):

$$D_{\beta,i} = d_{o,\beta,i} \emptyset^{a+1} S_\beta^b, \qquad \text{(III.32)}$$

where $D_{\beta,i}$ is the effective diffusion of the component i in the phase β, $d_{o,\beta,i}$ is the molecular diffusion coefficient of the component i in the phase β, $\emptyset$ is the porosity and S_β is the saturation of the phase β, a and b are parameters specific to the material. The value of a and b for this experience are 2 and 4.2 (Richet *et al.*, 2004; Thiery, 2006; Thiery *et al.*, 2007).

We will use a sequential non-iterative approach. The transport step draws the spatial discretization from the pdepe built-in function of MATLAB and integrates the spatial discretization in time using a forward Euler method. Then, the new values of the aqueous components and gas species (H_2O, CO_2) are introduced in PHREEQC to obtain the new mass balance between the different phases. The physical parameters for the problem are listed in Table III-4.

Parameter	Value
d_{g,CO_2} [m^2/s]	$1.6\ 10^{-5}$
d_{g,H_2O} [m^2/s]	$2.4\ 10^{-5}$
d_l [m^2/s]	$1.9\ 10^{-9}$
S_l [-]	0.802/ 0.602
$\emptyset$ [-]	0.08
a[-]	2
b [-]	4.2

Table III-4: Physical parameters used in the constant saturation test.

PHREEQC applies two models for gas phases during gas-water interactions, either the pressure is fixed or the volume is fixed. A preliminary test has shown that for this specific case, the amount of evaporated water after each reaction using the fixed pressure approach was unrealistic. Therefore, it has been opted to work with a fixed volume model.

III.2.1.2 Initial values and boundary conditions

The initial concentration of concrete are calculated by using the data from Table III-1, supposing that the control volume is 1 liter, the porosity is 0.08, and running a batch simulation in PhreeqcRM where secondary minerals are in equilibrium for two constant liquid saturations (0.802 and 0.602). The mass of the minerals in the 1 liter control volume has been reduced until a dissolution front of Portlandite is observable in our simulations for a sensible time simulation (no more than 4 hours), but always keeping the same initial ratio between the different initial minerals (Table III-1). The initial concentration for the components in solution are listed in Table III-5. Notice that the values of the components O and H must be summed to the artificial component H_2O in order to have the exact concentration of O and H. It has been reported that transporting H_2O and the excess of O and H is more robust than transporting total O and H (Parkhurst and Wissmeier, 2015). The initial values for the mineral are listed in Table III-6.

Chemical Component	Initial concentration
Al [mol/L]	$5.218 \ 10^{-6}$
C [mol/L]	$1.146 \ 10^{-6}$
Ca [mol/L]	$0.15 \ 10^{-2}$
Cl [mol/L]	$7.2478 \ 10^{-7}$
Fe [mol/L]	$5.9799 \ 10^{-7}$
K [mol/L]	$8.73 \ 10^{-2}$
Mg [mol/L]	$1.2235 \ 10^{-9}$
Na [mol/L]	0.1688
S [mol/L]	$6.2267 \ 10^{-4}$
Si [mol/L]	$1.0375 \ 10^{-6}$
O [mol/L]	0.261
H [mol/L]	0.258
H_2O [mol/L]	55.3434
Charge [eq/L]	$5.7516 \ 10^{-15}$
$CO_2(g)$ [mol]	0
$H_2O(g)$ [mol]	$1.2813 \ 10^{-4}$
pH [-]	13.251
pe [-]	-1.2268

Table III-5: Components initial concentration, plus pH and pe, for the constant saturation test.

Mineral phase	Initial value [mol/L]
Portlandite	$2.0941 \ 10^{-4}$
CSH1.6	$2.2962 \ 10^{-4}$
Ettringite	0
Hydrotalcite	$1.9138 \ 10^{-6}$
C3FH6	$1.9684 \ 10^{-5}$
Monocarboaluminate	$1.3851 \ 10^{-4}$
Calcite	0.0028
CSH0.8	0
CSH1.2	0
Gibbsite	0
Gypsum	0
Ferrihydrate(am)	0
Katoite	0
$SiO_2(am)$	0
Stratlingite	0
Analcime	0
Anhydrite	0
Arcanite	0
Brucite	0
Burkeite	0

Table III-6: Mineral phases initial values for the constant saturation test.

The boundary condition are no flux on the left and right side of the 1D column for all the aqueous components (Figure III.3). The gaseous species CO_2 and H_2O have a constant

boundary value at the left side of the 1D column domain. The value is calculated by applying the law of ideal gases, being the atmospheric CO_2 partial pressure equal to $3.9 \ 10^{-4}$ atm and the atmospheric H_2O partial pressure equal to $3.13 \ 10^{-2}$ atm with a temperature of 25°C. The units of $CO_2(g)$ and $H_2O(g)$ are given in mol/L.

$$D_l \nabla C_{l,i} = 0 \qquad\qquad D_l \nabla C_{l,i} + D_{g,i} \nabla C_{g,i} = 0$$

$$C_{g,CO_2} = 1.2925 \ 10^{-5}$$
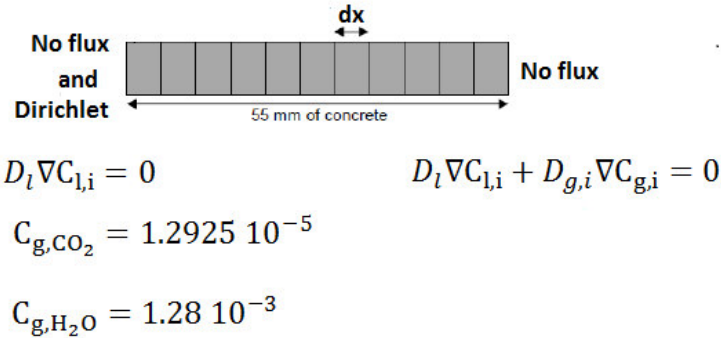
$$C_{g,H_2O} = 1.28 \ 10^{-3}$$

Figure III.3: 1D domain sketch and boundary conditions for the constant saturation test.

III.2.1.3   Discretization and Von Neumann number

In order to avoid instabilities in the transport explicit scheme, the Von Neumann number is respected:

$$\frac{\Delta t \, D}{(\Delta x)^2} = \frac{1}{2} \tag{III.33}$$

The main problem of respecting the Von Neumann number is that we are compelled to use small time steps. If we divide the 55 mm into 11 mesh cells, namely $\Delta x = 5 \ 10^{-3} m$, and calculate D_g as the effective gaseous diffusion coefficient using equation (III.32) for vapor and use the data of Table III-4

S_l	D_{g,H_2O} (m^2/s)	Δt (s)
0.802	$1.36 \ 10^{-11}$	915029
0.602	$2.56 \ 10^{-10}$	48744

Table III-7: Splitting time step due to Von Neumann criteria.

S_l is the liquid saturation, D_{g,H_2O} is the effective diffusion of vapor and Δt is the splitting time step.

III.2.1.4 Preliminary results for the constant saturation test, case $S_l = 0.802$

The simulation is run for a duration of 150 years. Figure III.4 displays the precipitation and dissolution of the primary minerals for the case where saturation is 0.802. No secondary mineral are formed during the simulation. In this first case, the carbonation front does not reach a profound depth along the x axis, portlandite dissolves only in the first node.

The precipitation of calcite is mainly explained by the dissolution of portlandite and $CO_2(g)$ dissolving into the porous solution. Also, minerals like CSH1.6 and monocarboaluminate might play a role since they release Ca^{2+} ions. The variations of hydrotalcite might be neglected since they are of the order of 10^{-10} mol/L. Variations of C3FH6 are low being around 10^{-6} mol/L. The dissolution of CSH1.6 leads to an increase of the Si component in the solution (Figure III.5a). The formation of hydrotalcite even small leads to a decrease in the Mg component (Figure III.5c), since its value is around 10^{-9} mol/L, therefore it is affected by the variations of hydrotalcite. Hydrotalcite also contains Al^{+3}, but its precipitation decrease only marginally the value of the Al component in the solution. Al increase is due to the dissolution of monocarboaluminate (Figure III.5b). The pH decreases but not significantly, as it was expected (Figure III.5d), the reason of the small decrease might be linked to the fact that there are still minerals, like CSH1.6, in the first node that are able to buffer the increase of acidity owing to carbonation.
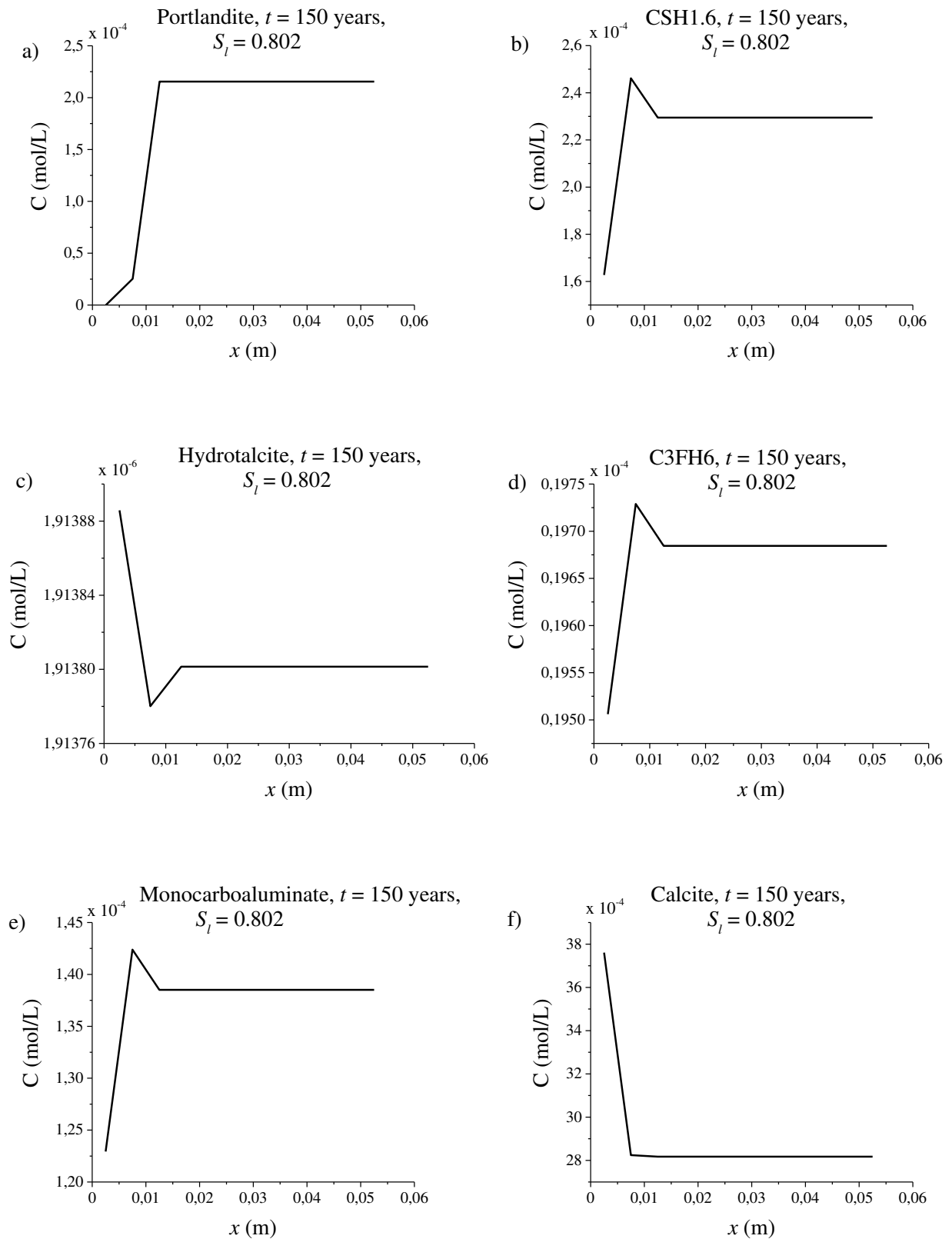
Figure III.4: Dissolution and precipitation fronts due to carbonation for the initial minerals, test with constant saturation, $S_l = 0.802$.
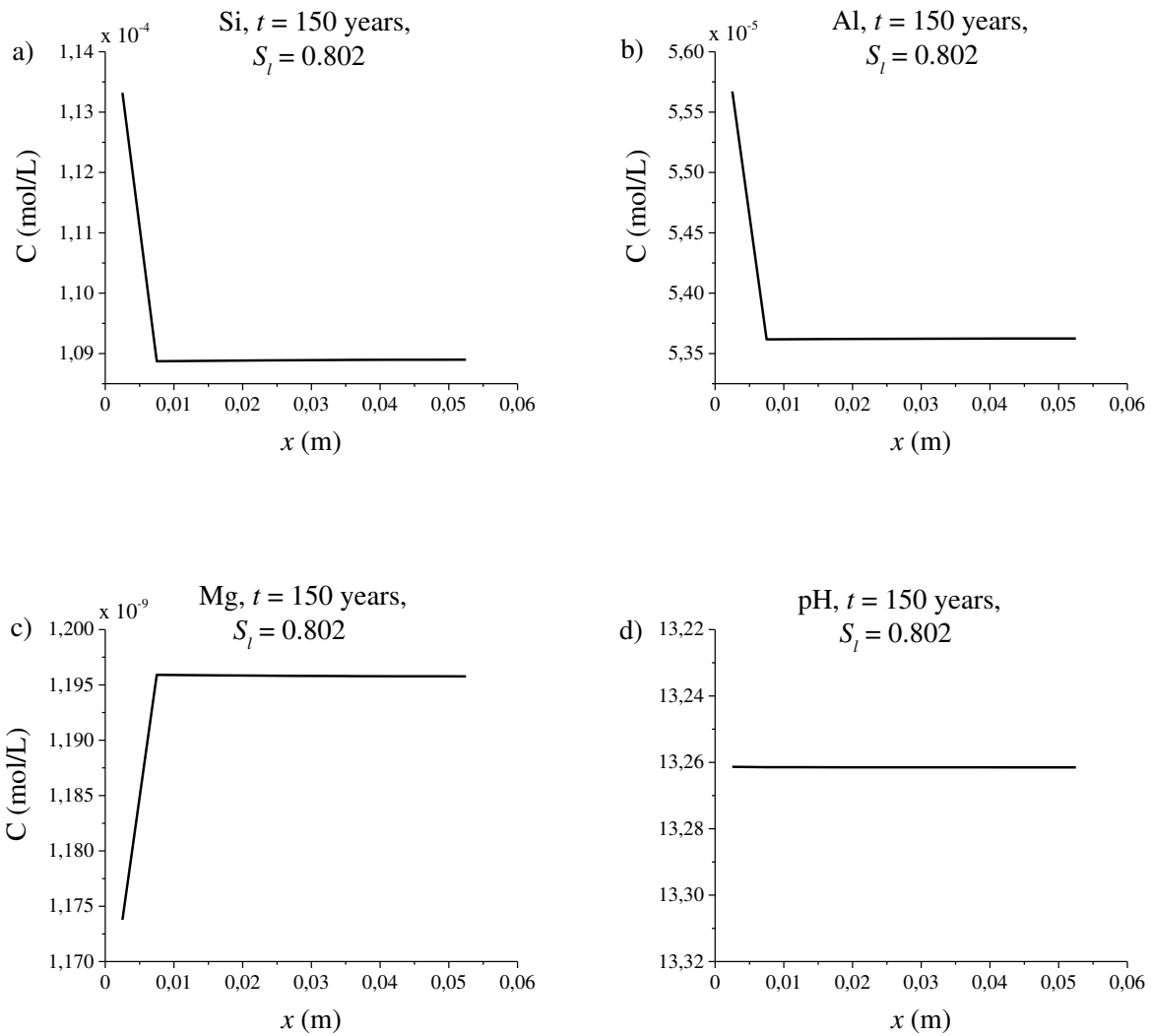
Figure III.5: Aqueous components concentrations and pH, test with constant saturation, $S_l=0.802$.

III.2.1.5 Preliminary results for the constant saturation test, case $S_l = 0.602$

In Figure III.6 is possible to observe the precipitation and dissolution of the initial minerals. In contrast to the test with constant liquid saturation at 0.802 (Figure III.4), we can observe that the dissolution front of portlandite is deeper, around $x = 2.75$ meters. The dissolution front of portlandite is followed by the dissolution of C3FH6, CSH1.6 and monocarboaluminate. This four minerals release Ca^{2+} which combined with CO_3^{2-} leads to the precipitation of calcite. Since the liquid saturation is lower than the previous case ($S_l = 0.802$), the volumetric volume of gaseous components (or species) is larger, hence at each iteration

more mass of $CO_2(g)$ dissolves into the system causing higher changes of mass in the minerals.

In contrast to the previous simulation the dissolution of C3FH6 is more pronounced, but the variations of hydrotalcite are still mild. The reason is due to the fact that the concentration Mg^{2+} in the porous solution is rather small 10^{-9} and it can be found only in hydrotalcite, therefore its dissolution or precipitation is bounded by the amount of Mg^{2+} in the porous solution.

The only secondary mineral that is formed in the simulated composition of the concrete is amorphous ferrihydrate Figure III.7a. The formation of ferrihydrate is attributable to the dissolution of C3FH6. To our surprise the pH has not reaches the levels expected in a carbonated zone (around 9) (Figure III.7b). The formation of ferrihydrate does not explain the almost constant pH level, since this formation of ferrihydrate consumes hydroxyl ions which should lead to a decrease in pH. This abnormal behavior might be a consequence of ignoring the changes of water in order to keep constant the level of saturation.
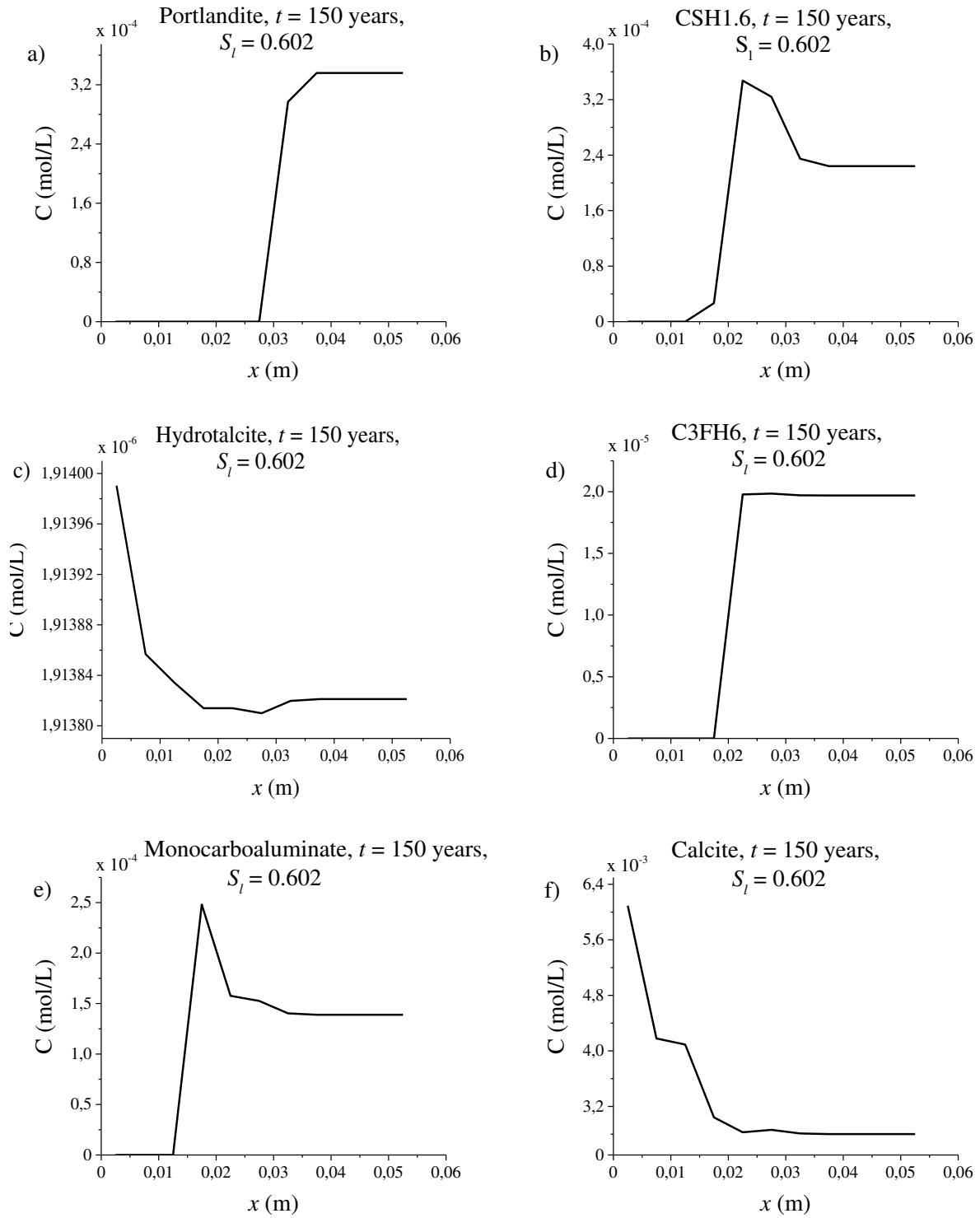
Figure III.6: Dissolution and precipitation fronts due to carbonation for the initial minerals, test with constant saturation, $S_l = 0.602$.
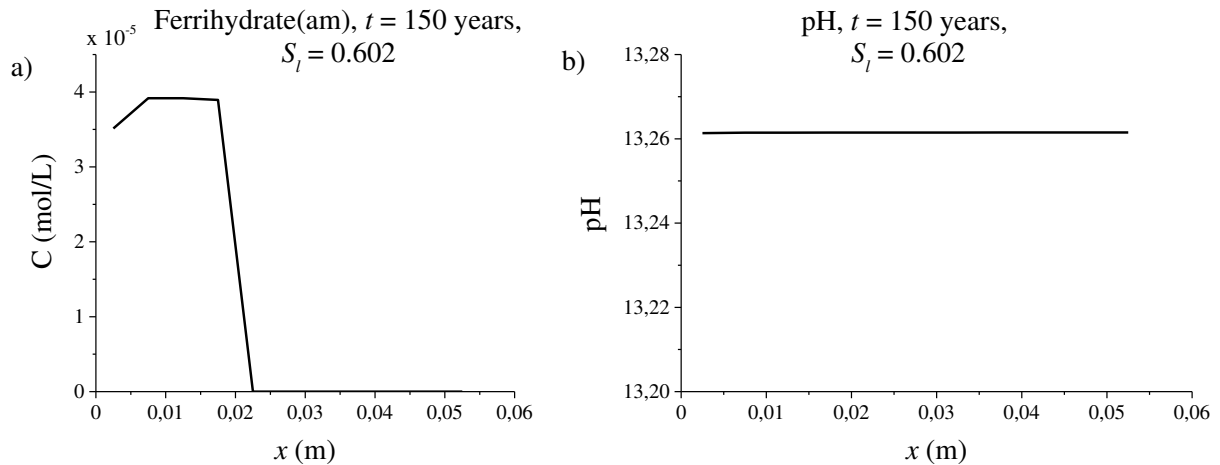
Figure III.7: a) amorphous ferrihydrate precipitation, b) pH in the solution.

III.3 Discussion and perspectives

One of the main problems of simulations presented in this section is the lack of experimental data for the chosen composition, therefore code intercomparison might be useful to assess the validity of the simulated results. Moreover, the mass of the minerals has been significantly reduced in our simulations in order to observe the dissolution front of portlandite within an acceptable computation time frame (hours). Simulating realistic amounts of minerals might be unpractical, with simulation reported to last from 1 to 6 months (Trotignon *et al.*, 2011). A parallelized script would probably not be more efficient, since the amount of nodes in the problem is small. Therefore, we opt to reduce the mass of minerals, although it can have an impact on the results.

Assuming that the results are correct (the pH values tend to indicate the opposite), the following step would be to simulate the mass transport of the phase by means of the Richard's equation (Mainguy *et al.*, 2001) or a multiphase approach. The saturation values and fluxes values (velocity) of such simulations can be imposed directly into the transport-reaction operator splitting approach, however such approaches still neglect water changes due to dissolution and precipitation of hydrated minerals. In order to take into account the changes in liquid saturation due to dissolution and precipitation, the calculation of the Richard's or multiphase flow equation can be included into the operator splitting time loop by following a three processes sequential approach, such approach can be founded in Wissmeier and Barry

101

(2011). This property update is considered as evaluated in lagged time (Nardi *et al.*, 2014), and in decoupled processes software it is not only applicable to water changes due to chemistry, but also porosity changes (Radu *et al.*, 2013). In principle, such approach is considered to be applicable when changes are not significant, but the numerical error introduced by such approaches is unclear. The application of Taylor series for simple chemistry systems on the H_2O component might be helpful.

Therefore, if accuracy and separation of processes are desired, a fixed-point iteration approach has to be used. It is considered that a two fixed-point iterations should be applied, one for transport and flow, and the other for the first coupling (transport+flow) and the reaction operator. If PHREEQC software is used, a new implementation for the iterative approach must be considered. iPhreeqc does not allow to copy iPhreeqc objects into new variables, but the exact amount of each component, minerals and other chemical entities can be dumped into an external file, which can be reused later to see invariant values of the iterative process. We do not know the consequences of using two fixed-point iteration approaches, but we hypothesize that the already existing convergence and performance time problems of iterative approaches might be enhanced in a case where two fixed-point iteration methods are used.

Another weak point of our simulation is assuming that all aqueous species have the same diffusion-dispersion coefficient. Since we are not dealing with advection-dominanted transport, such approach is not less realistic but it is functional for first approaches, giving an understanding of the evolution of the system. Different values of the diffusion coefficient can also imply a contribution in the operator splitting error, as seen in section II.4.2.

CHAPTER 4: CONCLUSION

IV CONCLUSION

This thesis explores the application of operator splitting approaches in the field of reactive transport modeling, aiming to solve each part of the decoupled problem with a suitable solver, and to apply the developed work into the atmospheric carbonation problematic which arises in the storage concrete packages of intermediate-level long-lived waste of a nuclear repository.

An object-oriented programming paradigm has been used to develop a fully segmented implementation of a general expression of the operator splitting approaches. The object-oriented paradigm has provided a satisfactory set of characteristics such as encapsulation of data and methods, reusability, and extensibility. Other works in reactive transport modeling have acknowledged the advantages of such programming paradigm (Gamazo *et al.*, 2016; Kolditz and Bauer, 2004). We also underline that although we work only with transport and chemical operators the generic approach used here allows to separate the operators in different processes, e.g. advection-reaction and diffusion (Liu and Ewing, 2005) and to implement easily other methods such as the one presented in Gasda *et al.* (2011). Amongst the generic operator splitting approaches that have been implemented into the present code named TReacLab, it is possible to find sequential, additive, alternating, Strang, and symmetrically weighted splitting methods (Csomós and Faragó, 2008; Faragó *et al.*, 2008; Simpson *et al.*, 2005; Strang, 1968). Furthermore, a fixed-point (or Picard iteration) approach for two classical formulations in the field of reactive transport have been implemented: SIA CC, and SIA TC (de Dieuleveult *et al.*, 2009). It has been corroborated by the applied practical cases that all the operator splitting approaches are consistent and valid. Moreover, if we consider well-posed PDEs with a consistent decomposition of each operator which are accurate enough and stable, we should expect better results using second-order accurate operator splitting approaches. The iterative approaches have not been able to reach convergence in all the cases which makes us rethink about how general our iterative implementation is, since initially it was crafted to work only for cases dealing with speciation and precipitation/dissolution at equilibrium.

The operators splitting introduces an error associated with the separation of processes (Valocchi and Malmstead, 1992). The error has usually been limited to single species (Barry *et al.*, 1996) and sometimes have been understood heuristically (Jacques *et al.*, 2006). In order

to understand better the error, which might help to understand results and better design operator splitting approaches, the temporal truncation error is studied. If only chemical kinetics equations are considered, it is possible to assess the error for each species or component by means of Taylor series (Csomós and Faragó, 2008; Csomós *et al.*, 2005; Simpson and Landman, 2008) or Lie formalism (Lanser and Verwer, 1999). These calculations can be tedious, therefore symbolic computation might play a role in order to identify the sources of error.

Several external transport solvers (COMSOL, pdepe MATLAB, FVTool, and FD scripts) and geochemical codes (iPhreeqc, PhreeqcRM) have been plugged with good results. The combination of the external codes with the operator splitting methodes (iterative and non-iterative) must be always assessed. For instance, solvers that use first-order time integration scheme might cause a reduction in the order of the truncation error when they are combined with a second-order operator splitting such as Strang method (Csomós and Faragó, 2008). Also, some implemented algorithms work only with implicit or explicit schemes, such as the SIA CC. Moreover, we have notice that COMSOL suffers from a time penalization each time that is called from MATLAB. That fact makes COMSOL, not the best tool for problems with a low number of grids. Although, COMSOL performs better than other software. The use of black boxes for research is questionable, black boxes might be a problem when transparence is search.

The carbonation simulations are not mature enough to draw general conclusions. The main problem currently faced is to find acceptable concrete mineral compositions that can be simulated in a reasonable time. Additionally, we notice that if we want to take into account the influence of mineral dissolution into the flow process an iterative approach must be implemented. Comparison of non-iterative approaches against the iterative approach can show how relevant is the mineral dissolution into the flow process.

REFERENCES

Abriola, L.M., Pinder, G.F., 1985. A Multiphase Approach to the Modeling of Porous Media Contamination by Organic Compounds: 1. Equation Development. Water Resources Research 21, 11-18.

Amir, L., Kern, M., 2010. A global method for coupling transport with chemistry in heterogeneous porous media. Computational Geosciences 14, 465-481.

Amos, R.T., Mayer, K.U., Blowes, D.W., Ptacek, C.J., 2004. Reactive Transport Modeling of Column Experiments for the Remediation of Acid Mine Drainage. Environmental Science & Technology 38, 3131-3138.

ANDRA, D., 2005a. Andra Research on the Geological Disposal of Highlevel Long-lived Radioactive Waste–Results and Perspectives, Chatenay-Malabry, France., p. 40.

ANDRA, S.A., 2005b. Evaluation of the feasibility of a geological repository in an argillaceous formation. Andra, Chatenay-Malabry, France.

Appelo, C., Rolle, M., 2010. PHT3D: A reactive multicomponent transport model for saturated porous media. Groundwater 48, 627-632.

Appelo, C.A.J., Postma, D., 2004. Geochemistry, groundwater and pollution. CRC press.

ASN, 2008. Guide de sûreté relatif au stockage définitif des déchets radioactifs en formation géologique profonde, 32 p.

Barrodale, I., Roberts, F.D.K., 1978. An Efficient Algorithm for Discrete L1 Linear Approximation with Linear Constraints. SIAM Journal on Numerical Analysis 15, 603-611.

Barrodale, I., Roberts, F.D.K., 1980. Algorithm 552: Solution of the Constrained L1 Linear Approximation Problem. ACM Trans. Math. Softw. 6, 231-235.

Barry, D.A., Miller, C.T., Culligan-Hensley, P.J., 1996. Temporal discretisation errors in non-iterative split-operator approaches to solving chemical reaction/groundwater transport models. Journal of Contaminant Hydrology 22, 1-17.

Bary, B., Mügler, C., 2006. Simplified modelling and numerical simulations of concrete carbonation in unsaturated conditions. Revue européenne de génie civil 10, 1049-1072.

Bary, B., Sellier, A., 2004. Coupled moisture—carbon dioxide–calcium transfer model for carbonation of concrete. Cement and Concrete Research 34, 1859-1872.

Bastian, P., 1999. Numerical computation of multiphase flows in porous media. habilitationsschrift Univeristät Kiel.

Bear, J., 1972. Dynamics of fluids in porous media. Elsevier, New York.

Besnard, K., 2004. Modélisation du transport réactif dans les milieux poreux hétérogènes. Application aux processus d'adsorption cinétique non linéaire, Geosciences Rennes. Universite de Rennes I, France.

Beven, K., Germann, P., 2013. Macropores and water flow in soils revisited. Water Resources Research 49, 3071-3092.

Bjerrum, N., 1926. I. Influence of ionic association on the activity of ions at moderate degrees of association. K. Dan. Vidensk. Selsk 7, 1-48.

Bozau, E., van Berk, W., 2013. Hydrogeochemical Modeling of Deep Formation Water Applied to Geothermal Energy Production. Procedia Earth and Planetary Science 7, 97-100.

Brinkley , S.R., 1947. Calculation of the equilibrium composition of systems of many constituents. The Journal of Chemical Physics 15, 107-110.

Brooks, R.H., Corey, A.T., 1964. Hydraulic Properties of Porous Media. Colorado State University.

Bullard, J.W., Jennings, H.M., Livingston, R.A., Nonat, A., Scherer, G.W., Schweitzer, J.S., Scrivener, K.L., Thomas, J.J., 2011. Mechanisms of cement hydration. Cement and Concrete Research 41, 1208-1223.

Burnett, R.D., Frind, E.O., 1987. Simulation of contaminant transport in three dimensions: 2. Dimensionality effects. Water Resources Research 23, 695-705.

Carrayrou, J., Hoffmann, J., Knabner, P., Kräutle, S., de Dieuleveult, C., Erhel, J., Van der Lee, J., Lagneau, V., Mayer, K.U., MacQuarrie, K.T.B., 2010. Comparison of numerical methods for simulating strongly nonlinear and heterogeneous reactive transport problems—the MoMaS benchmark case. Computational Geosciences 14, 483-502.

Carrayrou, J., Mosé, R., Behra, P., 2004. Operator-splitting procedures for reactive transport and comparison of mass balance errors. Journal of Contaminant Hydrology 68, 239-268.

Charlton, S.R., Parkhurst, D.L., 2011. Modules based on the geochemical model PHREEQC for use in scripting and programming languages. Computers & Geosciences 37, 1653-1663.

Chen, X., Thornton, S.F., Small, J., 2015. Influence of Hyper-Alkaline pH Leachate on Mineral and Porosity Evolution in the Chemically Disturbed Zone Developed in the Near-Field Host Rock for a Nuclear Waste Repository. Transport in Porous Media 107, 489-505.

Chen, Z., Ewing, R., Espedal, M., 1994. Multiphase flow simulation with various boundary conditions. Computational Methods in Water Resources, 925-932.

Cho, C., 1971. Convective transport of ammonium with nitrification in soil. Canadian Journal of Soil Science 51, 339-350.

Clement, T.P., Sun, Y., Hooker, B.S., Petersen, J.N., 1998. Modeling Multispecies Reactive Transport in Ground Water. Ground Water Monitoring & Remediation 18, 79-92.

Cochepin, B., Trotignon, L., Bildstein, O., Steefel, C.I., Lagneau, V., Van der lee, J., 2008. Approaches to modelling coupled flow and reaction in a 2D cementation experiment. Advances in Water Resources 31, 1540-1551.

COMSOL, A., 2010. COMSOL Multiphysics-LiveLink for Matlab User's Guide, comsol 4.1 edition.

COMSOL, A., 2012. 4.3 User's Guide. Comsol.

Corey, A.T., 1954. The interrelation between gas and oil relative permeabilities. Producers monthly 19, 38-41.

Csomós, P., Faragó, I., 2008. Error analysis of the numerical solution of split differential equations. Mathematical and Computer Modelling 48, 1090-1106.

Csomós, P., Faragó, I., Havasi, Á., 2005. Weighted sequential splittings and their analysis. Computers & Mathematics with Applications 50, 1017-1031.

Darcy, H., 1856. Les fontaines publiques de la ville de Dijon: exposition et application. Victor Dalmont.

de Dieuleveult, C., Erhel, J., 2010. A global approach to reactive transport: application to the MoMas benchmark. Computational Geosciences 14, 451-464.

de Dieuleveult, C., Erhel, J., Kern, M., 2009. A global strategy for solving reactive transport equations. Journal of Computational Physics 228, 6395-6410.

de Sousa, E.R., 2012. Groundwater modelling meets geochemistry: Building the bridge between FEFLOW and PHREEQC with IFMPhreeqc, In: Association, I.M.W. (Ed.), Annual Conference.

Debure, M., De Windt, L., Frugier, P., Gin, S., 2013. HLW glass dissolution in the presence of magnesium carbonate: Diffusion cell experiment and coupled modeling of diffusion and geochemical interactions. Journal of Nuclear Materials 443, 507-521.

Dentz, M., Le Borgne, T., Englert, A., Bijeljic, B., 2011. Mixing, spreading and reaction in heterogeneous media: A brief review. Journal of Contaminant Hydrology 120, 1-17.

Dittrich, T.M., Reimus, P.W., 2015. Uranium transport in a crushed granodiorite: Experiments and reactive transport modeling. Journal of Contaminant Hydrology 175–176, 44-59.

Dobson, P.F., Kneafsey, T.J., Sonnenthal, E.L., Spycher, N., Apps, J.A., 2003. Experimental and numerical simulation of dissolution and precipitation: implications for fracture sealing at Yucca Mountain, Nevada. Journal of Contaminant Hydrology 62–63, 459-476.

Douglas, J., Jr., Peaceman, D.W., Rachford, H.H., Jr., 1959. A Method for Calculating Multi-Dimensional Immiscible Displacement. Society of Petroleum Engineers.

Duprat, F., Vu, N.T., Sellier, A., 2014. Accelerated carbonation tests for the probabilistic prediction of the durability of concrete structures. Construction and Building Materials 66, 597-605.

Dupuis, M.-C., Gonnot, F.-M., 2013. The Cigeo project: Meuse/Haute-Marne reversible geological disposal facility for radioactive waste. Andra, Chatenay-Malabry, France., p. 104.

Eftekhari, A.A., 2016. https://zenodo.org/record/18156#.WK63llXhCUk.

Ekolu, S.O., 2016. A review on effects of curing, sheltering, and CO2 concentration upon natural carbonation of concrete. Construction and Building Materials 127, 306-320.

Engesgaard, P., Kipp, K.L., 1992. A geochemical transport model for redox-controlled movement of mineral fronts in groundwater flow systems: A case of nitrate removal by oxidation of pyrite. Water Resources Research 28, 2829-2843.

Ewing, R.E., 1991. Simulation of multiphase flows in porous media, Mathematical Modeling for Flow and Transport Through Porous Media. Springer, pp. 479-499.

Fahs, M., Carrayrou, J., Younes, A., Ackerer, P., 2008. On the Efficiency of the Direct Substitution Approach for Reactive Transport Problems in Porous Media. Water, Air, and Soil Pollution 193, 299-308.

Faragó, I., Gnandt, B., Havasi, Á., 2008a. Additive and iterative operator splitting methods and their numerical investigation. Computers & Mathematics with Applications 55, 2266-2279.

Farago, I., Havasi, A., 2005. On the convergence and local splitting error of different splitting schemes. Progress in Computational Fluid Dynamics, an International Journal 5, 495-504.

Faragó, I., Thomsen, P.G., Zlatev, Z., 2008b. On the additive splitting procedures and their computer realization. Applied Mathematical Modelling 32, 1552-1569.

Fick, A., 1855. V. On liquid diffusion. The London, Edinburgh, and Dublin Philosophical Magazine and Journal of Science 10, 30-39.

Florez, W.F., Portapila, M., Hill, A.F., Power, H., Orsini, P., Bustamante, C.A., 2015. The control volume radial basis function method CV-RBF with Richardson extrapolation in geochemical problems. Computers & Geosciences 76, 151-163.

Frippiat, C.C., Holeyman, A.E., 2008. A comparative review of upscaling methods for solute transport in heterogeneous porous media. Journal of Hydrology 362, 150-176.

Gamazo, P., Slooten, L.J., Carrera, J., Saaltink, M.W., Bea, S., Soler, J., 2016. PROOST: object-oriented approach to multiphase reactive transport modeling in porous media. Journal of Hydroinformatics 18, 310-328.

Gasda, S.E., Farthing, M.W., Kees, C.E., Miller, C.T., 2011. Adaptive split-operator methods for modeling transport phenomena in porous medium systems. Advances in Water Resources 34, 1268-1282.

Geiser, J., 2009. Decomposition methods for differential equations: theory and applications. CRC Press.

Gerke, H.H., van Genuchten, M.T., 1993. A dual-porosity model for simulating the preferential movement of water and solutes in structured porous media. Water Resources Research 29, 305-319.

Glasser, F.P., Marchand, J., Samson, E., 2008. Durability of concrete — Degradation phenomena involving detrimental chemical reactions. Cement and Concrete Research 38, 226-246.

Glenn, H., Peter, L., Chuan, L., 2007. Subsurface multiphase flow and multicomponent reactive transport modeling using high-performance computing. Journal of Physics: Conference Series 78, 012025.

Gramling, C.M., Harvey, C.F., Meigs, L.C., 2002. Reactive transport in porous media: A comparison of model prediction with laboratory visualization. Environmental Science & Technology 36, 2508-2514.

Hammond, G.E., Valocchi, A.J., Lichtner, P.C., 2005. Application of Jacobian-free Newton–Krylov with physics-based preconditioning to biogeochemical transport. Advances in Water Resources 28, 359-376.

Hassan, A.E., 2004. Validation of numerical ground water models used to guide decision making. Ground Water 42, 277-290.

Hassanizadeh, S.M., Celia, M.A., Dahle, H.K., 2002. Dynamic effect in the capillary pressure–saturation relationship and its impacts on unsaturated flow. Vadose Zone Journal 1, 38-57.

He, W., Beyer, C., Fleckenstein, J.H., Jang, E., Kolditz, O., Naumov, D., Kalbacher, T., 2015. A parallelization scheme to simulate reactive transport in the subsurface environment with OGS#IPhreeqc 5.5.7-3.1.2. Geosci. Model Dev. 8, 3333-3348.

Hoffmann, J., Kräutle, S., Knabner, P., 2010. A parallel global-implicit 2-D solver for reactive transport problems in porous media based on a reduction scheme and its application to the MoMaS benchmark problem. Computational Geosciences 14, 421-433.

Hoffmann, J., Kräutle, S., Knabner, P., 2012. A general reduction scheme for reactive transport in porous media. Computational Geosciences 16, 1081-1099.

Holden, H., Karlsen, K.H., Lie, K.-A., Risebro, N.H., 2010. Splitting methods for partial differential equations with rough solutions: Analysis and MATLAB programs. European Mathematical Society.

Hoth, N., Kornjaev, A., Hafner, F., 2000. Reactive transport modelling with simulator MODCALIF-CHEM: prediction of the environmental impact of lignite dump waters. IAHS PUBLICATION, 481-488.

Hubbert, M.K., 1957. Darcy's law and the field equations of the flow of underground fluids. Hydrological Sciences Journal 2, 23-59.

Huber, P., Nivelon, S., Ottenio, P., Nortier, P., 2013. Coupling a Chemical Reaction Engine with a Mass Flow Balance Process Simulation for Scaling Management in Papermaking Process Waters. Industrial & Engineering Chemistry Research 52, 421-429.

Hundsdorfer, W., Verwer, J.G., 2013. Numerical solution of time-dependent advection-diffusion-reaction equations. Springer Science & Business Media.

Jacques, D., Šimůnek, J., 2005. User manual of the multicomponent variably-saturated flow and transport model HP1. Description, Verification and Examples, Version 1, 79.

Jacques, D., Šimůnek, J., Mallants, D., Van Genuchten, M.T., 2006. Operator-splitting errors in coupled reactive transport codes for transient variably saturated flow and contaminant transport in layered soil profiles. Journal of Contaminant Hydrology 88, 197-218.

Jensen, M.M., 2014. A Coupled Transport and Chemical Model for Durability Predictions of Cement Based Materials. Technical University of DenmarkDanmarks Tekniske

Universitet, Department of Structural Engineering and MaterialsInstitut for Bærende Konstruktioner og Materialer.

Jensen, M.M., Johannesson, B., Geiker, M.R., 2014. Framework for reactive mass transport: Phase change modeling of concrete by a coupled mass transport and chemical equilibrium model. Computational Materials Science 92, 213-223.

Kaluarachchi, J.J., Morshed, J., 1995. Critical assessment of the operator-splitting technique in solving the advection-dispersion-reaction equation: 1. First-order reaction. Advances in Water Resources 18, 89-100.

Kazemi Nia Korrani, A., Jerauld, G.R., Sepehrnoori, K., 2016a. Mechanistic Modeling of Low-Salinity Waterflooding Through Coupling a Geochemical Package With a Compositional Reservoir Simulator. SPE Reservoir Evaluation & Engineering.

Kazemi Nia Korrani, A., Sepehrnoori, K., Delshad, M., 2015. Coupling IPhreeqc with UTCHEM to model reactive flow and transport. Computers & Geosciences 82, 152-169.

Kazemi Nia Korrani, A., Sepehrnoori, K., Delshad, M., 2016b. A Mechanistic Integrated Geochemical and Chemical-Flooding Tool for Alkaline/Surfactant/Polymer Floods. SPE Journal 21, 32-54.

Kolditz, O., Bauer, S., 2004. A process-oriented approach to computing multi-field problems in porous media. Journal of Hydroinformatics 6, 225-244.

Kolditz, O., Bauer, S., Bilke, L., Böttcher, N., Delfs, J.-O., Fischer, T., Görke, U.J., Kalbacher, T., Kosakowski, G., McDermott, C., 2012. OpenGeoSys: an open-source initiative for numerical simulation of thermo-hydro-mechanical/chemical (THM/C) processes in porous media. Environmental Earth Sciences 67, 589-599.

Koren, B., 1993. A robust upwind discretization method for advection, diffusion and source terms. Centrum voor Wiskunde en Informatica Amsterdam.

Kulik, D.A., 2011. Improving the structural consistency of C-S-H solid solution thermodynamic models. Cement and Concrete Research 41, 477-495.

Kumar, D., Kumar, V., Singh, V.P., 2010. Mathematical modeling of brown stock washing problems and their numerical solution using MATLAB. Computers & Chemical Engineering 34, 9-16.

Langergraber, G., Šimůnek, J., 2012. Reactive transport modeling of subsurface flow constructed wetlands using the HYDRUS wetland module. Vadose Zone Journal 11.

Lanser, D., Verwer, J.G., 1999. Analysis of operator splitting for advection–diffusion–reaction problems from air pollution modelling. Journal of Computational and Applied Mathematics 111, 201-216.

Lapidus, L., Amundson, N.R., 1952. Mathematics of adsorption in beds. VI. The effect of longitudinal diffusion in ion exchange and chromatographic columns. The Journal of Physical Chemistry 56, 984-988.

Lasaga, A.C., Soler, J.M., Ganor, J., Burch, T.E., Nagy, K.L., 1994. Chemical weathering rate laws and global geochemical cycles. Geochimica et Cosmochimica Acta 58, 2361-2386.

Lee, J.H., Siegel, M.D., Arguello Jr, J.G., Webb, S.W., Dewers, T.A., Mariner, P.E., Edwards, H.C., Fuller, T.J., Freeze, G.A., Jove-Colon, C.F., 2011. Nuclear Energy Advanced Modeling and Simulation (NEAMS) waste Integrated Performance and Safety Codes (IPSC): gap analysis for high fidelity and performance assessment code development. Sandia National Laboratories.

Lichtner , P.C., Hammond, G.E., Lu, C., Karra, S., Bisht, G., Andre, B., Mills, R., Kumar, J., 2015. PFLOTRAN User Manual.

Lie, K., 2014. An introduction to reservoir simulation using MATLAB: User guide for the Matlab reservoir simulation toolbox (MRST), SINTEF ICT, Department of Applied Mathematics, Oslo, Norway.

Likos, W.J., Lu, N., 2004. Hysteresis of capillary stress in unsaturated granular soil. Journal of engineering mechanics 130, 646-655.

Liu, J., Ewing, R.E., 2005. An operator splitting method for nonlinear reactive transport equations and its implementation based on dll and com, Current Trends in High Performance Computing and Its Applications. Springer, pp. 93-102.

Lunn, M., Lunn, R.J., Mackayb, R., 1996. Determining analytic solutions of multiple species contaminant transport, with sorption and decay. Journal of Hydrology 180, 195-210.

Mainguy, M., Coussy, O., Baroghel-Bouny, V., 2001. Role of air pressure in drying of weakly permeable materials. Journal of engineering mechanics 127, 582-592.

Martin, L.H.J., Leemann, A., Milodowski, A.E., Mäder, U.K., Münch, B., Giroud, N., 2016. A natural cement analogue study to understand the long-term behaviour of cements in nuclear waste repositories: Maqarin (Jordan). Applied Geochemistry 71, 20-34.

Marty, N.C.M., Bildstein, O., Blanc, P., Claret, F., Cochepin, B., Gaucher, E.C., Jacques, D., Lartigue, J.-E., Liu, S., Mayer, K.U., Meeussen, J.C.L., Munier, I., Pointeau, I., Su, D., Steefel, C.I., 2015. Benchmarks for multicomponent reactive transport across a cement/clay interface. Computational Geosciences 19, 635-653.

Masi, M., Ceccarini, A., Iannelli, R., 2017. Multispecies reactive transport modelling of electrokinetic remediation of harbour sediments. Journal of Hazardous Materials 326, 187-196.

Mayer, K., 2000. MIN3P V1. 0 User Guide. University of Waterloo, Department of Earth Sciences 26.

Mayer, K.U., 1999. A numerical model for multicomponent reactive transport in variably saturated porous media. University of Waterloo.

Merkel, B.J., Planer-Friedrich, B., Nordstrom, D., 2005. Groundwater geochemistry. A Practical Guide to Modeling of Natural and Contaminated Aquatic Systems 2.

Miller, C.T., Christakos, G., Imhoff, P.T., McBride, J.F., Pedit, J.A., Trangenstein, J.A., 1998. Multiphase flow and transport modeling in heterogeneous porous media: challenges and approaches. Advances in Water Resources 21, 77-120.

Millington, R., 1959. Gas diffusion in porous media. Science 130, 100-102.

Molins, S., Carrera, J., Ayora, C., Saaltink, M.W., 2004. A formulation for decoupling components in reactive transport problems. Water Resources Research 40, W10301.

Morel, F., Morgan, J., 1972. Numerical method for computing equilibriums in aqueous chemical systems. Environmental Science & Technology 6, 58-67.

Morshed, J., Kaluarachchi, J.J., 1995. Critical assessment of the operator-splitting technique in solving the advection-dispersion-reaction equation: 2. Monod kinetics and coupled transport. Advances in Water Resources 18, 101-110.

Mosé, R., Siegel, P., Ackerer, P., Chavent, G., 1994. Application of the mixed hybrid finite element approximation in a groundwater flow model: Luxury or necessity? Water Resources Research 30, 3001-3012.

Müller, M., Parkhurst, D.L., Charlton, S.R., 2011. Programming PHREEQC Calculations with C++ and Python A Comparative Study. EXCHANGE 1, 632-636.

Muniruzzaman, M., Rolle, M., 2016. Modeling multicomponent ionic transport in groundwater with IPhreeqc coupling: Electrostatic interactions and geochemical reactions in homogeneous and heterogeneous domains. Advances in Water Resources 98, 1-15.

Nardi, A., Idiart, A., Trinchero, P., de Vries, L.M., Molinero, J., 2014. Interface COMSOL-PHREEQC (iCP), an efficient numerical framework for the solution of coupled multiphysics and geochemistry. Computers & Geosciences 69, 10-21.

Nasir, O., Fall, M., Evgin, E., 2014. A simulator for modeling of porosity and permeability changes in near field sedimentary host rocks for nuclear waste under climate change influences. Tunnelling and Underground Space Technology 42, 122-135.

Ngo, V.V., Delalande, M., Clément, A., Michau, N., Fritz, B., 2014. Coupled transport-reaction modeling of the long-term interaction between iron, bentonite and Callovo-Oxfordian claystone in radioactive waste confinement systems. Applied Clay Science 101, 430-443.

Niessner, J., Hassanizadeh, S.M., 2008. A model for two-phase flow in porous media including fluid-fluid interfacial area. Water Resources Research 44.

Nimmo, J.R., 2012. Preferential flow occurs in unsaturated conditions. Hydrological Processes 26, 786-789.

Nonat, A., 2004. The structure and stoichiometry of C-S-H. Cement and Concrete Research 34, 1521-1528.

Nordstrom, 2004. Modelling Lowtemperature Geochemical Processes.–Treatise on Geochemistry, 5: pp. 37—72. Elsevier.

Ogata, A., Banks, R.B., 1961. A solution of the differential equation of longitudinal dispersion in porous media: fluid movement in earth materials. US Government Printing Office.

Or, D., Wraith, J.M., 2002. Soil water content and water potential relationships. Soil physics companion 1, 49-84.

Parkhurst, D.L., Appelo, C., 1999a. User's guide to PHREEQC (Version 2) (Equations on which the program is based).

Parkhurst, D.L., Appelo, C., 1999b. User's guide to PHREEQC (Version 2): A computer program for speciation, batch-reaction, one-dimensional transport, and inverse geochemical calculations.

Parkhurst, D.L., Kipp, K.L., Engesgaard, P., Charlton, S.R., 2004. PHAST, a program for simulating ground-waterflow, solute transport, and multicomponent geochemical reactions. USGS Techniques and Methods 6, A8.

Parkhurst, D.L., Wissmeier, L., 2015. PhreeqcRM: A reaction module for transport simulators based on the geochemical model PHREEQC. Advances in Water Resources 83, 176-189.

Parlange, J.Y., 1976. Capillary hysteresis and the relationship between drying and wetting curves. Water Resources Research 12, 224-228.

Patel, R.A., Perko, J., Jacques, D., De Schutter, G., Van Breugel, K., Ye, G., 2014. A versatile pore-scale multicomponent reactive transport approach based on lattice Boltzmann method: Application to portlandite dissolution. Physics and Chemistry of the Earth, Parts A/B/C 70–71, 127-137.

Peng, D.-Y., Robinson, D.B., 1976. A new two-constant equation of state. Ind. Eng. Chem. Fundam 15, 59-64.

Perko, J., Mayer, K.U., Kosakowski, G., De Windt, L., Govaerts, J., Jacques, D., Su, D., Meeussen, J.C.L., 2015. Decalcification of cracked cement structures. Computational Geosciences 19, 673-693.

Pfingsten, W., 2014. The influence of stable element inventory on the migration of radionuclides in the vicinity of a high level nuclear waste repository exemplified for 59Ni. Applied Geochemistry 49, 103-115.

Pinder, G.F., Gray, W.G., 2008. Essentials of multiphase flow in porous media. John Wiley & Sons.

Poonoosamy, J., Kosakowski, G., Van Loon, L.R., Mäder, U., 2015. Dissolution–precipitation processes in tank experiments for testing numerical models for reactive transport calculations: Experiments and modelling. Journal of Contaminant Hydrology 177–178, 1-17.

Press, W.H., Teukolsky, S.A., Vetterling, W.T., Flannery, B.P., 2007. Numerical Recipes 3rd Edition: The Art of Scientific Computing. Cambridge University Press.

Prickett, T.A., Lonnquist, C.G., Naymik, T.G., 1981. A" random-walk" solute transport model for selected groundwater quality evaluations. Bulletin/Illinois State Water Survey; no. 65.

Radu, F.A., Muntean, A., Pop, I.S., Suciu, N., Kolditz, O., 2013. A mixed finite element discretization scheme for a concrete carbonation model with concentration-dependent porosity. Journal of Computational and Applied Mathematics 246, 74-85.

Reilly, P.J., Wood, R.H., Robinson, R.A., 1971. Prediction of osmotic and activity coefficients in mixed-electrolyte solutions. The Journal of Physical Chemistry 75, 1305-1315.

Richards, L.A., 1931. Capillary conduction of liquids through porous mediums. Physics 1, 318-333.

Richet, C., Galle, C., Le Bescop, P., Peycelon, H., Bejaoui, S., Tovena, I., Pointeau, I., L'hostis, V., Lovera, P., 2004. Synthèse des connaissances sur le comportement à long terme des bétons applications aux colis cimentés. CEA Saclay Direction de l'Énergie Nucléaire France, 16-18.

Ruan, X., Pan, Z., 2012. Mesoscopic simulation method of concrete carbonation process. Structure and Infrastructure Engineering 8, 99-110.

Rubin, J., 1983. Transport of reacting solutes in porous media: Relation between mathematical nature of problem formulation and chemical nature of reactions. Water Resources Research 19, 1231-1252.

Russell, T.F., Wheeler, M.F., 1983. Finite element and finite difference methods for continuous flows in porous media. The mathematics of reservoir simulation 1, 35-106.

Saaltink, M.W., Carrera, J., Ayora, C., 2000. A comparison of two approaches for reactive transport modelling. Journal of Geochemical Exploration 69–70, 97-101.

Saaltink, M.W., Carrera, J., Ayora, C., 2001. On the behavior of approaches to simulate reactive transport. Journal of Contaminant Hydrology 48, 213-235.

Samper, J., Juncosa, R., Delgado, J., Montenegro, L., 2000. Core 2D. A code for non-isothermal water flow and reactive solute transport. Users manual version 2. Empresa Nacional de Residuos Radiactivos.

Samper, J., Xu, T., Yang, C., 2009. A sequential partly iterative approach for multicomponent reactive transport with CORE2D. Computational Geosciences 13, 301-316.

Samson, E., Marchand, J., 2006. Multiionic approaches to model chloride binding in cementitious materials, R. Gagné M. Jolin F. Paradis J. Marchand, B. Bissonnette, éditeur: Proc. 2nd Int. RILEM symp. on Advances in concrete through science and engineering, pp. 101-122.

Scheidegger, A.E., 1954. Statistical hydrodynamics in porous media. Journal of Applied Physics 25, 994-1001.

Sedighi, M., 2011. An investigation of hydro-geochemical processes in coupled thermal, hydraulic, chemical and mechanical behaviours of unsaturated soils. Cardiff University.

Shafei, B., 2012. Reactive transport in natural porous media: Contaminant sorption and pore-scale heterogeneity. Georgia Institute of Technology.

Shampine, L.F., Reichelt, M.W., 1997. The matlab ode suite. SIAM journal on scientific computing 18, 1-22.

Shampine, L.F., Reichelt, M.W., Kierzenka, J.A., 1999. Solving index-1 DAEs in MATLAB and Simulink. SIAM review 41, 538-552.

Shi, Z., Lothenbach, B., Geiker, M.R., Kaufmann, J., Leemann, A., Ferreiro, S., Skibsted, J., 2016. Experimental studies and thermodynamic modeling of the carbonation of Portland cement, metakaolin and limestone mortars. Cement and Concrete Research 88, 60-72.

Simpson, M.J., Landman, K.A., 2007. Analysis of split operator methods applied to reactive transport with Monod kinetics. Advances in Water Resources 30, 2026-2033.

Simpson, M.J., Landman, K.A., 2008. Theoretical analysis and physical interpretation of temporal truncation errors in operator split algorithms. Mathematics and Computers in Simulation 77, 9-21.

Simpson, M.J., Landman, K.A., Clement, T.P., 2005. Assessment of a non-traditional operator split algorithm for simulation of reactive transport. Mathematics and Computers in Simulation 70, 44-60.

Šimůnek, J., Jarvis, N.J., van Genuchten, M.T., Gärdenäs, A., 2003. Review and comparison of models for describing non-equilibrium and preferential flow and transport in the vadose zone. Journal of Hydrology 272, 14-35.

Skeel, R.D., Berzins, M., 1990. A Method for the Spatial Discretization of Parabolic Equations in One Space Variable. SIAM journal on scientific and statistical computing 11, 1-32.

Sportisse, B., 2000. An Analysis of Operator Splitting Techniques in the Stiff Case. Journal of Computational Physics 161, 140-168.

Spycher, N.F., Sonnenthal, E.L., Apps, J.A., 2003. Fluid flow and reactive transport around potential nuclear waste emplacement tunnels at Yucca Mountain, Nevada. Journal of Contaminant Hydrology 62–63, 653-673.

Steefel, C., 2009. CrunchFlow software for modeling multicomponent reactive flow and transport. User's manual. Earth Sciences Division. Lawrence Berkeley, National Laboratory, Berkeley, CA. October, 12-91.

Steefel, C., Appelo, C., Arora, B., Jacques, D., Kalbacher, T., Kolditz, O., Lagneau, V., Lichtner, P., Mayer, K.U., Meeussen, J., 2015a. Reactive transport codes for subsurface environmental simulation. Computational Geosciences 19, 445-478.

Steefel, C.I., Appelo, C.A.J., Arora, B., Jacques, D., Kalbacher, T., Kolditz, O., Lagneau, V., Lichtner, P.C., Mayer, K.U., Meeussen, J.C.L., Molins, S., Moulton, D., Shao, H., Šimůnek, J., Spycher, N., Yabusaki, S.B., Yeh, G.T., 2015b. Reactive transport codes for subsurface environmental simulation. Computational Geosciences 19, 445-478.

Steefel, C.I., DePaolo, D.J., Lichtner, P.C., 2005. Reactive transport modeling: An essential tool and a new research approach for the Earth sciences. Earth and Planetary Science Letters 240, 539-558.

Steefel, C.I., MacQuarrie, K.T., 1996. Approaches to modeling of reactive transport in porous media. Reviews in Mineralogy and Geochemistry 34, 85-129.

Steefel, C.I., Maher, K., 2009. Fluid-Rock Interaction: A Reactive Transport Approach. Reviews in Mineralogy and Geochemistry 70, 485-532.

Strang, G., 1968. On the construction and comparison of difference schemes. SIAM Journal on Numerical Analysis 5, 506-517.

Sun, N.-Z., Sun, A., 2013. Mathematical modeling of groundwater pollution. Springer Science & Business Media.

Szymkiewicz, A., 2012. Modelling water flow in unsaturated porous media: accounting for nonlinear permeability and material heterogeneity. Springer Science & Business Media.

Ta, V.-L., Bonnet, S., Senga Kiesse, T., Ventura, A., 2016. A new meta-model to calculate carbonation front depth within concrete structures. Construction and Building Materials 129, 172-181.

Taylor, H.F., 1997. Cement chemistry. Thomas Telford.

Thackham, J.A., Sean McElwain, D.L., Turner, I.W., 2009. Computational Approaches to Solving Equations Arising from Wound Healing. Bulletin of Mathematical Biology 71, 211-246.

Thiery, M., 2006. Modélisation de la carbonatation atmosphérique des matériaux cimentaires(prise en compte des effets cinétiques et des modifications microstructurales et hydriques). Etudes et recherches des Laboratoires des ponts et chaussées. Série Ouvrages d'art.

Thiery, M., Baroghel-Bouny, V., Bourneton, N., Villain, G., Stéfani, C., 2007a. Modélisation du séchage des bétons: analyse des différents modes de transfert hydrique. Revue européenne de génie civil 11, 541-577.

Thiery, M., Villain, G., Dangla, P., Platret, G., 2007b. Investigation of the carbonation front shape on cementitious materials: Effects of the chemical kinetics. Cement and Concrete Research 37, 1047-1058.

Thompson, J.B., 1959. Local Equilibrium in Metasomatic Processes. In: Research in Geochemistry (P.H. Abelson, ed.), John Wiley.

Thouvenot, P., Bildstein, O., Munier, I., Cochepin, B., Poyet, S., Bourbon, X., Treille, E., 2013. Modeling of concrete carbonation in deep geological disposal of intermediate level waste, EPJ Web of Conferences. EDP Sciences, p. 05004.

Torres, E., Couture, R.M., Shafei, B., Nardi, A., Ayora, C., Van Cappellen, P., 2015. Reactive transport modeling of early diagenesis in a reservoir lake affected by acid mine drainage: Trace metals, lake overturn, benthic fluxes and remediation. Chemical Geology 419, 75-91.

Trotignon, L., Devallois, V., Peycelon, H., Tiffreau, C., Bourbon, X., 2007. Predicting the long term durability of concrete engineered barriers in a geological repository for radioactive waste. Physics and Chemistry of the Earth, Parts A/B/C 32, 259-274.

Trotignon, L., Thouvenot, P., Munier, I., Cochepin, B., Piault, E., Treille, E., Bourbon, X., Mimid, S., 2011. Numerical Simulation of Atmospheric Carbonation of Concrete Components in a Deep Geological Radwaste Disposal Site During Operating Period. Nuclear Technology 174, 424-437.

Valocchi, A.J., Malmstead, M., 1992. Accuracy of operator splitting for advection-dispersion-reaction problems. Water Resources Research 28, 1471-1476.

van der Lee, J., De Windt, L., Lagneau, V., Goblet, P., 2003. Module-oriented modeling of reactive transport with HYTEC. Computers & Geosciences 29, 265-275.

Van Genuchten, M.T., 1980. A closed-form equation for predicting the hydraulic conductivity of unsaturated soils. Soil science society of America journal 44, 892-898.

Van Zeggeren, F., Storey, S.H., 2011. The computation of chemical equilibria. Cambridge University Press.

Veyskarami, M., Hassani, A.H., Ghazanfari, M.H., 2016. Modeling of non-Darcy flow through anisotropic porous media: Role of pore space profiles. Chemical Engineering Science 151, 93-104.

Waage, P., Guldberg, C.M., 1986. Studies concerning affinity. J Chem Educ 63, 1044.

Whitaker, S., 1986. Flow in porous media I: A theoretical derivation of Darcy's law. Transport in Porous Media 1, 3-25.

White, W.B., Johnson, S.M., Dantzig, G.B., 1958. Chemical equilibrium in complex mixtures. The Journal of Chemical Physics 28, 751-755.

Wissmeier, L., Barry, D.A., 2008. Reactive transport in unsaturated soil: Comprehensive modelling of the dynamic spatial and temporal mass balance of water and chemical components. Advances in Water Resources 31, 858-875.

Wissmeier, L., Barry, D.A., 2011. Simulation tool for variably saturated flow with comprehensive geochemical reactions in two- and three-dimensional domains. Environmental Modelling & Software 26, 210-218.

Wissmeier, L., Barry, D.A., Phillips, I.R., 2011. Predictive hydrogeochemical modelling of bauxite residue sand in field conditions. Journal of Hazardous Materials 191, 306-324.

Xie, M., Mayer, K.U., Claret, F., Alt-Epping, P., Jacques, D., Steefel, C., Chiaberge, C., Simunek, J., 2015. Implementation and evaluation of permeability-porosity and

tortuosity-porosity relationships linked to mineral dissolution-precipitation. Computational Geosciences 19, 655-671.

Xiong, Q., Joseph, C., Schmeide, K., Jivkov, A.P., 2015. Measurement and modelling of reactive transport in geological barriers for nuclear waste containment. Physical Chemistry Chemical Physics 17, 30577-30589.

Xu, T., Spycher, N., Sonnenthal, E., Zhang, G., Zheng, L., Pruess, K., 2011. TOUGHREACT Version 2.0: A simulator for subsurface reactive transport under non-isothermal multiphase flow conditions. Computers & Geosciences 37, 763-774.

Yang, C., Samper, J., Montenegro, L., 2008. A coupled non-isothermal reactive transport model for long-term geochemical evolution of a HLW repository in clay. Environmental Geology 53, 1627-1638.

Yeh, G.T., Tripathi, V.S., 1989. A critical evaluation of recent developments in hydrogeochemical transport models of reactive multichemical components. Water Resources Research 25, 93-108.

Zhang, Q., 2016. Mathematical modeling and numerical study of carbonation in porous concrete materials. Applied Mathematics and Computation 281, 16-27.

Zhou, A., 2015. A non-linear hysteresis model for soil-water retention behaviour, Unsaturated Soil Mechanics-from Theory to Practice: Proceedings of the 6th Asia Pacific Conference on Unsaturated Soils (Guilin, China, 23-26 October 2015). CRC Press, p. 329.

Zhou, G., 1995. Numerical simulations of physical discontinuities in single and multi-fluid flows for arbitrary Mach numbers. Chalmers University of Technology.

Zilberbrand, M., 2011. Geochemical modeling of groundwater, vadose and geothermal systems. CRC Press.

Zoua, S., Ma, J., Koussis, A.D., 1996. Analytical solutions to non-Fickian subsurface dispersion in uniform groundwater flow. Journal of Hydrology 179, 237-258.